Max-Planck-Institut für Polymerforschung

Max Planck Institute for Polymer Research

JOHANNES GUTENBERG UNIVERSITÄT MAINZ

LIGHT-CONTROLLED SELF-ASSEMBLY AND SELF-SORTING OF MAMMALIAN CELLS

Dissertation

zur Erlangung des Grades

Doktor der Naturwissenschaften

Am Fachbereich Biologie

Der Johannes Gutenberg-Universität Mainz

vorgelegt von

Marc Müller

Mainz, 2019

The thesis was carried out from November 2016 until December 2019 at the Max Planck Institute for Polymer Research, Mainz.

Dekan: Prof.

Gutachter 1:

Gutachter 2:

Date of oral examination:

I hereby declare that I wrote the dissertation submitted without any unauthorized external assistance and used only sources acknowledged in this work. All textual passages which are appropriate verbatim or paraphrased from published and unpublished texts, as well as all information obtained from oral sources, are duly indicated and listed in accordance with bibliographical rules. In carrying out this research, I complied with the rules of standard scientific practice as formulated in the statutes of Johannes Gutenberg-University Mainz to ensure standard scientific practice.

_____ _____

Marc Müller

Table of contents

List of abbreviations

As	*Avena stativa*
azo	azobenzene
BSA	bovine serum albumin
CAM	cell adhesion molecules
CRY2	cryptochrome 2
DAH	differential adhesion hypothesis
DNA	desoxyribonucleic acid
DLCA	diffusion limited cluster aggregation
DMEM	Dulbecco's modified eagle medium
DMSO	dimethyl sulfoxide
EC	extracellular
EDTA	ethylenediaminetetraacetic acid
EMT	epithelial mesenchymal transition
FAD	flavin adenine dinucleotide
FBS	fetal bovine serum
FMN	flavin mononucleotide
GFP	green fluorescence protein
IC	intracellular
Ig	Iummunoglobulin
iLID	improved light induced dimer
IMB	Institute of Molecular Biology
LB	Luria-Bertani
LID	light induced dimer
LOV	light oxygen voltage sensing
LOV2	light oxygen voltage sensing 2
MESF	molecules of equivalent soluble fluorochrome

OD	optical density
ORF	open reading frame
PAS	per-arnt-sim
PBS	phosphat buffered saline
PCR	polymerase chain reaction
PDGFR	platelet derived growth factor receptor
PGA	polyglycolic acid
PS	penicillin streptomycin
PFA	paraformaldehyd
PHYB	phytochrome B
PIF6	phytochrome interaction factor 6
RLCA	reaction limited cluster aggregation
PEG	polyethylene glycol
ssDNA	single strand desoxyribonucleic acid
synNotch	synthetic notch
TM	transmembrane
UV	ultraviolet

Abstract

Building tissue from cells as the basic building block based on principles of self-assembly is a challenging and promising approach. Understanding how far principles of self-assembly and self-sorting known for colloidal particles apply to cells remains unanswered. In this thesis, I demonstrate that not just controlling the cell-cell interactions but also their dynamics is a crucial factor that determines the formed multicellular structure, using photoswitchable interactions between cells that are activated with blue light and reverse in the dark. Tuning dynamics of the cell-cell interactions by pulsed light activation, results in multicellular architectures with different sizes and shapes. When the interactions between cells are dynamic compact and round multicellular clusters under thermodynamic control form, while otherwise branched and lose aggregates under kinetic control assemble. These structures parallel what is known for colloidal assemblies under reaction and diffusion limited cluster aggregation, respectively. Similarly, dynamic interactions between cells are essential for cells to self-sort into distinct groups. Using four different cell types, which expressed two orthogonal cell-cell interaction pairs, the cells sorted into two separate assemblies. Bringing concepts of colloidal self-assembly to bottom-up tissue engineering provides a new theoretical framework and will help in the design of more predictable tissue-like structures.

Zusammenfassung

Der Aufbau von künstlichem Gewebe durch eine modulare Zusammensetzung von Zellen ist eine vielversprechende Herausforderung. Dabei organisieren sich die Zellen selbst und bilden komplexere Strukturen. Die Prinzipien der Selbstorganisation, die von kolloidalen Systemen bekannt sind, sind noch ungeklärt für Zellen. In dieser Doktorarbeit beschäftige ich mich mit kontrollierten Zell-Zellkontakten und deren Dynamik, die die Form der multizellularen Strukturen maßgeblich bestimmen. Für den Ansatz der kontrollierten Zell-Zellkontakten sollen lichtschaltbare Proteine eingesetzt werden, die unter blauem Licht aktiviert und wieder im Dunklen inaktiviert werden können. Das blaue Licht als Aktivator bieten die Möglichkeit, mit unterschiedlichen Lichtpulsen die Dynamik der Zell-Zell Kontakte aktiv zu beeinflussen. Dieses pulsierende Licht und die damit veränderte Dynamik der Zell-Zellkontakte wirkt sich auf die Größe und Struktur der multizellularen Strukturen aus. Durch dynamische Interaktionen zwischen den Zellen entstehen kompakte und runde Aggregate, die thermodynamisch kontrolliert werden. Sind im Gegensatz die Zellaggregate kinetisch kontrolliert, entstehen verzweigte baumartige Strukturen. Die unterschiedlichen Strukturen, die durch unterschiedliche Dynamiken der Zell-Zellkontakte entstehen können, sind schon aus der kolloidalen Aggregation unter dem Namen der Reaktions- und Diffusions-limitierten Cluster-Aggregation bekannt. Durch den Einsatz von ähnlichen Dynamiken und der Expression von orthogonal bindenden lichtschaltbaren Proteinen auf der Oberfläche von Zellen ist es mir gelungen, vier unterschiedlichen Zellen mit blauem Licht zu beleuchten, die sich daraufhin selbst in zwei vorgegebene Familien sortieren. Dieser Ansatz bietet das Potential, zusammen mit den Konzepten der kolloidalen Aggregation Vorhersagen sowie ein neues Design für künstlichen Geweben zu entwickeln.

List of publications

Accepted:

The importance of cell-cell interaction dynamics in bottom-up tissue engineering: Concepts of colloidal self-assembly in the fabrication of multicellular architectures.

Authors: **Mueller M.,** Rasoulinejad S., Garg S., Wegner, S. V. (2019).

Nano Letter

Blue Light Switchable Cell–Cell Interactions Provide Reversible and Spatiotemporal Control Towards Bottom-Up Tissue Engineering

Authors Yüz S. G., Rasoulinejad S., **Mueller M.,** Wegner A. E., and Wegner, S. V. (2019)

Advanced Biosystems. doi: 10.1002/adbi.201800310

Submitted:

Independent and Reversible Blue and Red Light Controlled Self-sorting Multicellular Structures

Authors: Rasoulinejad S., **Mueller M**., Wegner S. V. (2019).

1 Introduction

1.1 Tissue engineering

Tissue engineering aims to restore, maintain, and/or improve tissue function by creating functional biological substitutes at the intersection of biology, engineering and materials science.[1] In order to achieve autonomous organization of tissue structures, it is necessary for the engineered tissue to interact with its natural or synthetic environment such that it can perform analogous functions to the native tissue.[2] To achieve this goal tissue engineering can be categorized into two different approaches, top-down and bottom up-tissue engineering.

1.1.1 Top-down tissue engineering

The traditional top-down approach of tissue engineering is described as seeding cells with soluble growth factors into an artificial extracellular matrix (ECM) called scaffold, where the cells can adhere, proliferate and differentiate.[3] Beside the soluble signals, the adhesion of the cells to the scaffold is an important determinant of how it behaves. Therefore, scaffolds have been biofunctionalized with natural ECM proteins including collagen, fibronectin and laminin as well as synthetic adhesion peptides (e.g. RGD), which support cell-matrix adhesions to the materials.[4,5] In these cases cells primarily adhere to the ECM through a family of cell surface receptors named integrins detailed below.[5]

The scaffold materials play an important role as they provide a skeleton for the developing tissue and a certain mechanical stability at the beginning.[3] The physical characteristics of the scaffold like stiffness, elasticity and the size of the pores are important parameters, which determine the final tissue.[4,6,7] For example, scaffolds with varying stiffness alter how stem cells differentiate; where they prefer to differentiate into keratinocyte on soft matrix and osteogenic cells on stiff materials.[8,9] The stiffness and

elasticity of the scaffold can be influenced by using different materials like polyacrylamide gels or polymer polyglycolic acid (PGA).[4]

When the cells are seeded and adhere to a scaffold, the cells proliferate and can alter the scaffold properties by producing their own ECM. Ideally, after the cells have built up their own ECM and the scaffold is not needed anymore, it should be degraded. An example for a widely used degradable material is PGA, which can be degraded by cells through the hydrolysis of the ester bonds.[10] Using different scaffold materials, the top-down approach to tissue engineering has been successful in producing tissues for skin,[11] cartilage,[12] bone,[13] nerve [14] and corneal reconstruction.[15]

The top-down approach to tissue engineering has not been able to overcome certain challenges. Tissues such as lung, liver and kidney are more difficult to engineer because of their complex architectures and intricate metabolic activities. Moreover, these cell rich and ECM poor tissues are difficult to achieve with scaffolds as the material occupies too much space and reduces the adhesions between cells. The scaffold material can also limit the diffusion of oxygen, nutrients and grow factors.[16] Additional challenges are the refill of the open spaces after the scaffold is degrading and the side effect of the degrading scaffold that can produce toxic degradation products.[17]

1.1.2 Bottom up tissue engineering

The complementary approach to top-down tissue engineering is the bottom-up approach. Bottom-up tissue engineering starts from single cells and allow them to arrange and proliferate in a scaffold-independent manner.[18] Without a scaffold to adhere to, the adhesions between the cells are the principle initial driving force to build up the tissues and cells can produce their own ECM in the process. Therefore, the bottom up approach allows the cells to grow and behave in their natural form and relies on the intrinsic capacity of cells to form modular tissues that mimic their natural conterparts.[19]

Building functional tissues from the bottom-up requires interactions between single units i.e. cells. Assembly of cells into multicellular structures is not limited to mixing cells together, it also involves inducing contacts and communications between the cells, that results in an organization of building blocks into hierarchical structures, which are crucial for function.[20,21]

One motivation behind this approach is to take advantage of the natural ability of cells to arrange into tissues, resembling their tissue of origin. Different techniques to create a scaffold-free tissues include bioprinting, cell sheets and cell aggregation.[18,22,23] In bioprinting cells or cell clusters are used as ink and are printed into 3D stuctures.[24,25] While having a high potential to assemble complex tissues with multiple cell types, this method still faces unresolved limitations like damaging the cells during the process and the lack of mechanical stability.[22] By using cell sheets, cells will be grown in layers and stacked together or the sheets can fused on the opposite ends to create tubular tissues or fused side by side to create layered tissue.[23] Another possibility is to rely on the self-assembly of cells to build up three dimensional cell aggregates.[18] For this purpose, cells are seeded in a non-adherent environment, and the cells aggregate, relying on cell-cell adhesions.[3] Such cell aggregates or bioprinted subunits can be used as modular building blocks, which can be fused together to build up bigger and more complex structures.[19]

The scaffold-free approach has been shown to be advantageous in several aspects. Firstly, the assemble of cells without a scaffold allows to build fine structures at the micrometer scale.[19] Secondly, the assembly overcomes the limitations of nutrient perfusion and oxygen diffusion to create vascularity.[26] Thirdly, extracellular mechanical stresses originating from the scaffolds are reduced in scaffold free constructs.[27] Moreover, the natural microenvironment without artificial scaffold allows better cell-cell communication and allows cells to produce a fully functional ECM on their own.[3] On the other side, the self-assembly of cells without scaffold can be limited by the requirement

for cell-cell adhesions between different cells types, the formation of large scale structures and the ability of cells to produce the needed amount of ECM by themselves.[2]

The top-down and bottom-up approach to tissue engineering are not contrary to each other but complement each other's strengths and weaknesses. The top-down approach enables the more robust tissues on a scaffold at a larger scale that can be inserted into the human body and degraded afterwards. On the other hand, the bottom-up approach that allows producing more precise fine structures, which are important for tissue functions, without the limitation of nutrient perfusion and oxygen diffusion. Therefore, a combined approach of the top-down and bottom-up approaches would allow assembling self-assembled microtissues into larger scale scaffolds and achieve bigger tissues with more precise structure.[19]

1.2 Cell adhesion

The interaction of cells with their environment is a fundamental step in cell biology and understanding the adhesive interactions of adhesions is crucial for both top-down and bottom-up tissue engineering. Cell adhesions can be divided into the adhesions between the cell and its ECM and the adhesions between a cell and neighboring cells. In both cases the adhesion is formed by molecules that are localized on the cell surface and called cell adhesion molecules (CAM).[28] These CAM can transmit an adhesion between single cells and the adhesion between the cell and their environment.

1.2.1 Cell matrix adhesion

The interaction of cells with the extracellular matrix are mediated though integrins.[29] Integrins are heterodimeric transmembrane receptors consists of an α- and β-subunit. The extracellular part of integrins can interacts with binding sites in the ECM and can recognize specific peptide sequences such as the RGD (arginine, glycine and aspartate)

motif that is part of typical extracellular matrix proteins like collagen and fibronectin. The binding the integrins with the extracellular matrix leads to a conformational change in the integrins and transmits the extracellular signal to the inside of the cytosol of the cell. As a result, adaptor proteins like talin, paxillin, vinculin and a focal adhesion kinase are recruited to the cytosolic domain and are connected with the actin cytoskeleton. In turn, this leads to more integrin recruitment to the binding site and result in the formation of focal adhesions.[30,31] Through this mechanism the signal from the ECM is transduced to the inside of the cell and translated into a signal cascade.[32] This signal cascade can result in diverse outputs in the cell, for example the disassembly of the adhesion,[32] cell migration, differentiation or the proliferation of the cell.[31]

1.2.2 Cell-cell interaction

Cells can also interact with each other by using CAM. The most important class of proteins that are involved in cell-cell adhesions are cadherins. Cadherins are expressed on the cell surface, similar to integrins, and are able to bind to cadherins on the neighboring cells. Different cell types express different types of cadherins, leading to several subfamilies, the classical cadherins type I and type II only being found in vertebrates.[33] The classical cadherins (e.g. E-cadherin, N-cadherin, P-cadherin etc.) consists of five extracellular domains, including a calcium binding sides between each of the extracellular domains, a single pass transmembrane domain, followed by a cytosolic domain (Figure 1).

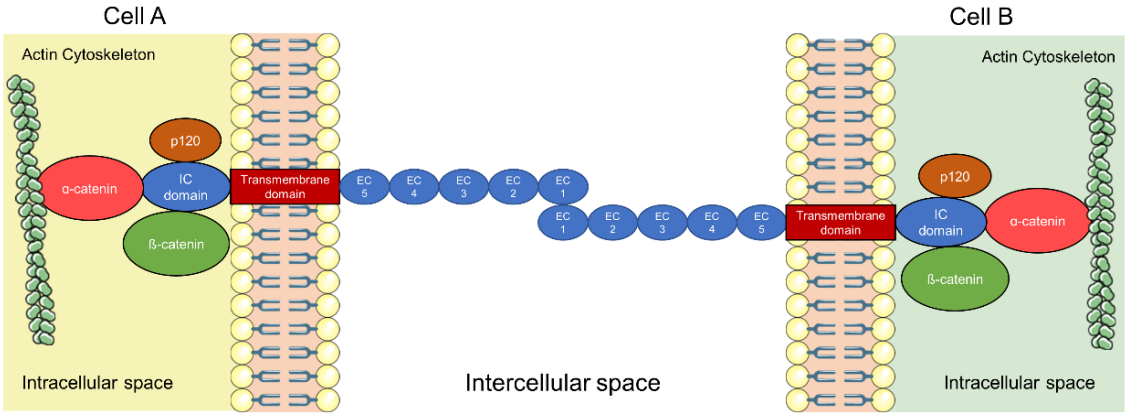

Figure 1: E-cadherin dependent cell-cell adhesion. The E-cadherin consists of five extracellular (EC) domains, one transmembrane (TM) domain and an intracellular (IC) domain. During binding of two E-cadherin molecules the proteins p120, β-catenin and α-catenin get recruited to the IC domain and α-catenin interact with the actin cytoskeleton. Adapted from Gall et al 2013.[34]

The classical cadherins form preferentially homophillic interactions with cadherins expressed on the neighboring cell though an exchange of β-strands between the first extracellular domains.[35] This interaction leads to signal transduction to the cytosolic domain of the cadherin. Upon cadherin-cadherin binding, the proteins p120, β-catenin and α-catenin are recruited to the cytosolic domain and form a link to the actin cytosekeleton.[34] Similar to the signaling of integrins, the cadherins are enriched at the point of cell-cell adhesions.[36] The formation of cell-cell adhesions is of fundamental importance to the cell and plays a central role in many processes including the epithelial-mesenchymal transition (EMT), cell-sorting, and collective cell migration.[37]

1.3 Differential adhesion hypothesis

Driesch described in 1908 a blastula from a sea urchin that was cut in half and formed afterwards two complete gastrula in half size.[38] This observation shows the ability of a mixture of different cell types to reorganize and self-assemble in distinct structures without the need of a template. Holtfreter later described the sorting behavior of cells of endoderm, mesoderm and ectoderm origin in a structured way that resembles their

original spatial organization in the original tissue and named it *"tissue affinities"*.[39] Observations as listed above showing the capacity of cells to self-organize were the driving force for formulation of the differential adhesion hypothesis (DAH).

In 1963, Steinberg described the DAH, where he compares the cell sorting behavior of cells to the behavior of liquid mixtures, where the components (liquids or cells) arrange so that the internal free energy is reduced to a minimum and structures at thermodynamic equilibrium form.[40–43] The active or passive motility of cells in a tissue provides the analogy to liquids where the basic subunits can rearrange with respect to each other.[44] Other aspects in which mixtures of different cells behave similar to mixtures of liquids are their ability to rounding up to minimize their surface area, the spreading of one cell type over another, the fusion of two cellular aggregates, the sorting out behavior of mixed cell populations and the hierarchy of the layering of two cell types, which is in accordance to the surface tension of the tissue.[44] These analogy of multicellular assemblies to liquids explains the organization of cells with respect to each other and comes down to the ability of the different cell types to adhere within the mixture.[45] In multicellular assemblies the cells strive to reach the lowest free energy configuration and keep rearranging until this minimum is reached. This occurs when the adhesion between the cells are maximized and requires the cell-cell adhesions to be dynamic to allow for rearrangement. Differently organized multicellular assemblies of cells can be described by Steinberg based on the work of adhesion between cells of different types, which is defined as the work that must be done to separate two cells of different types from each other. In comparison, the work of cohesion describes the work that has to be done to separate two cells of the same type. For a mixture of cells of type a and type b, the work of adhesion can be defined as W_{ab} and is a result of heterophilic cell-cell adhesions. The work of cohesion between one cell type can described as W_a for cell type a and W_b for cell type b and is a result of the homophilic cell-cell interactions. Using these definitions the DAH describes three

different cases of multicellular assemblies in a mixture of two cell types; intermixed, enveloped and self-isolated (Figure 2).[43]

1) Intermixed: The cells of type a and type b stay intermixed when the work of adhesion between the two cell populations is higher than the work of cohesion of each cell type as this results in the maximal adhesion. Therefore, intermixed multicellular assemblies of two cell types form when $W_{ab} > (W_a+W_b)/2$.

2) Enveloped: An enveloped arrangement of cell, where one cell type is in the center and the second one at its periphery, forms when the average work of cohesion of cell type a and cell type b is bigger than the work of adhesion between the two cell types and the work of cohesion of once cell type is smaller than the work of adhesion between the cell types. Herein, the cell type with the stronger cohesion, type a, forms the core and the less cohesive cell type, type b, surrounds this core. Therefore, the enveloped multicellular assemblies form when $(W_a+W_b)/2 > W_{ab} > W_b$.

3) Self-isolated: The two cell types form separate assemblies when the work of adhesion between the cell types is smaller than the work of cohesion of either population. In this case each cell type will self-isolate with no intermixing. Therefore, the self-isolated multicellular assemblies of two cell types form when $W_a > W_b > W_{ab}$.

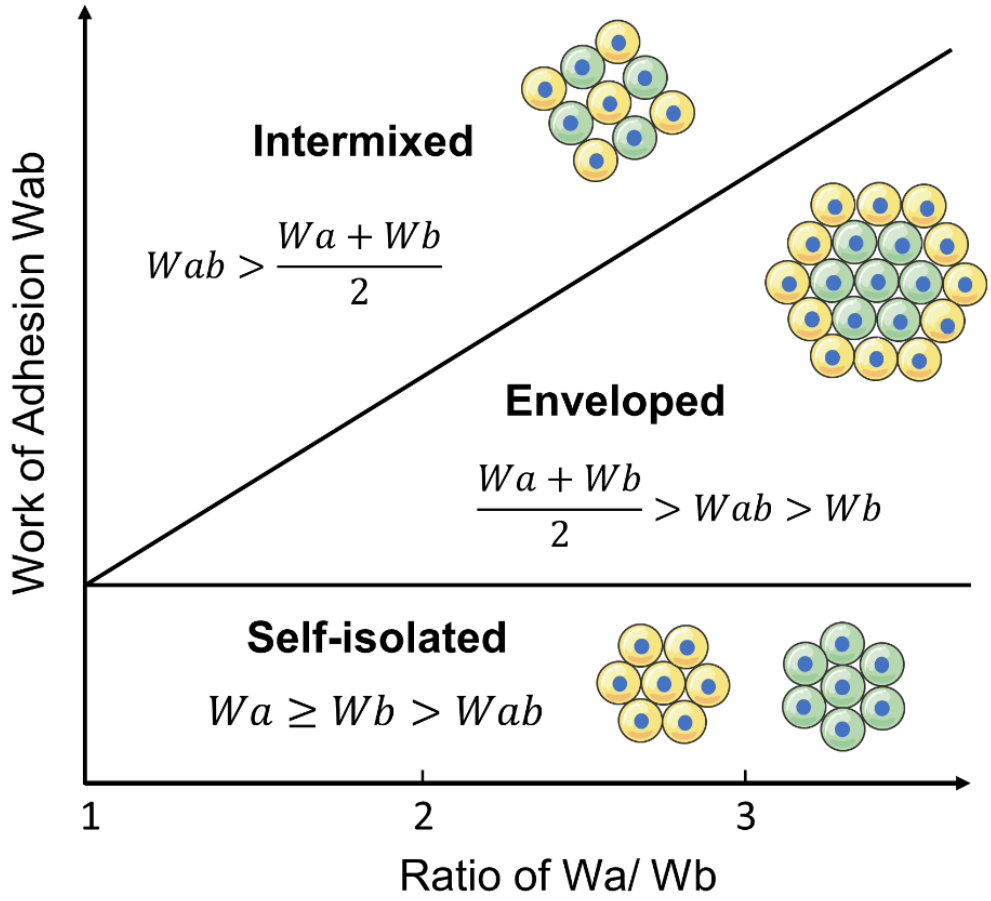

Figure 2: Differential adhesion hypothesis (DAH). Two different populations of cells arrange depending on their work of cohesion and adhesion in the cell formation of intermixed, enveloped and self-isolated. The cells are intermixed if the work of adhesion W_{ab} is stronger than the average individual work of cohesion W_a and W_b. Cells form an enveloped shape when the average work of cohesion $(W_a + W_b)/2$ of both cells is higher than the work of adhesion of both and the single cohesion. Self-isolation is formed when the work of cohesion of the single cells is dominating. The Figure is adapted from Steinberg et al. 1963.[43]

The differential adhesion hypothesis has been tested *in silico* and *in vitro* experiments. *In silico* a balance of attraction and repulsion forces between cells, which are simulated as spherical units, are able to self-assembly in different shapes predicted by DAH as well as additional shapes such as ring and disk structure.[46] In cell culture experiments cells expressing different types and amounts of cadherins at their surfaces were used to test the DAH.[47] For example, when two cell populations expressing E- and P-cadherin on their surfaces are able to assemble into multicellular structures[48] and the two cell types remained intermixed, which can be explained by the similar binding strength of E- and

P-cadherins to each other.[49] When examining binary mixtures of cells expressing N-cadherin, E-cadherin and cadherin-6b different multicellular assemblies form depending on the adhesions between the cadherins (Figure 3).[47] These cadherins showed different works of adhesion and cohesion ($W_{(\text{E-cadherin})} > W_{(\text{N-cadherin})} \approx W_{(\text{N-cadherin, E-cadherin})} > W_{\text{cadherin-6b}}$ and $W_{(\text{N-cadherin, cadherin-6b})} \approx W_{(\text{E-cadherin, cadherin-6b})} \approx 0$).[47] Each cell type was able to aggregate when cultured alone and populations labeled with different fluorescent markers intermixes. When cell types expressing cadherins that do not interact were mixed, e.g. N-cadherin and cadherin-6b expressing cells, self-isolated cell clusters assembled. On the other hand, when cells with similar homo- and hetero-adhesion, i.e. E-cadherin and N-cadherin expressing cells, coaggregation with domain formation was observed.[47]

The DAH only requires differences in homo- and heterophilic interaction to obtain different relative arrangements of the different cell types, yet does not require these adhesions to be originating from a certain type of cell-cell interaction. Therefore, not just different types of adhesion molecules but also differences in expression levels can lead to cell sorting behavior. For instance, two cell types with different expression levels of P-cadherin showed an enveloped arrangement with the cell type with the higher expression levels at the core and the cell type with the lower expression of the P-cadherin enveloping it.[43,50]

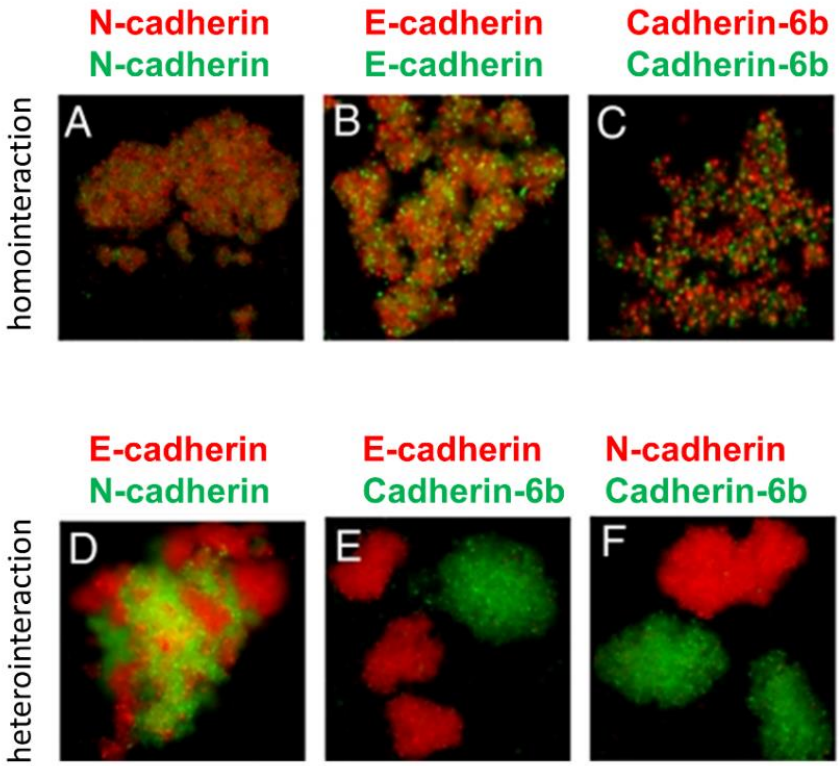

Figure 3: Aggregation assay of different cadherin expressing in Chinese ovarian hamster cells. (A-C) The homointeractions between three different cadherins from two different families of cadherins showed an intermix behavior. (D-F) By mixing different families of cadherins, N- and E-cadherin that belongs to the cadherin-I subfamily, the cells showing subdomains in a cell aggregate. The cadherins from two different families showed an asocial sorting within the own family of cadherins (D-F). Adopted from Katsamba et al. 2009.[47]

In summary, the DAH provides a conceptual framework for the self-assembly of cellular building blocks into multicellular structures under thermodynamic control. To achieve this thermodynamic control, the cell-cell interactions have to be dynamic enough such that this state can be achieved. The DAH also predicts different arrangements of cells depending on the differences in adhesions between different cell types in the mixture, i.e. intermixed, envelope and self-isolated cell types. Experiments with dissociated tissues and cell cultures support this hypothesis.

1.4 Colloidal principles as inspiration for multicellular assemblies

1.4.1 Self-assembly of colloidal particles

Colloids are widely used as model system to study the fundamental principles of self-assembly of nano and micrometer sized objects.[51,52] Therefore, principles established for self-assembly of particles are a good framework to look at the assembly of cells into tissues.[53] As in the case of bottom-up tissue assembly, the interactions between individual colloids drive the self-assembly process. The specificity of the interactions between colloids is one important parameter for the controlled self-assembly. Here, single stranded deoxyribonucleic acid (DNA) has been widely used for the self-assembly of both micro and nano-meter sized particles.[54–56] In most cases, DNA strands are covalent coupled to gold or polymer-based particles with complementary DNA regions.[57,58] These specific interactions between DNA base pairs and the large variety of possible DNA sequences offer great specificity and diversity.[59] Moreover, the DNA strands with varying the annealing temperatures can be used to adjust the self-assembly dynamics.[60] One drawback yet is that the change in temperature that is required to drive the assembly is missing spatial control and in some cases high temperatures, which are not compatible with biological systems, are required. [54]

The second aspect to consider in self-assembly is their control in space and time. As mentioned above, controlling self-assembly with temperature only provides limited spatial control. In this respect, light triggered assembly of colloidal particles brings the advantages of a high spatial and temporal control, which also be detailed on below in section 1.6. Therefore, colloidal particles have been decorated with light responsive functional groups like azobenzenes[61,62] and spiropyrans.[63,64] In particular, the host-guest interaction between cyclodextrins (α-, β-, ɣ-cyclodextrin) and azobenzenes in the dark, which can be disrupted with UV-light, has been used to control the self-assembly of

colloidal particles.[65–67] Using different cyclodextrins and azobenzenes the self-assembly of particles was controlled in space and time as well as triggered for specific sets of colloids using specific orthogonal interaction.[65,66,68] While this approach has many desired merits such as spatiotemporal control, reversibility and specificity, the use of cell toxic UV-light limits its transfer into cellular systems.

One approach that overcomes the problems associated with the use of UV-light is using photoswitchable proteins as interaction mediators between particles to drive self-assembly.[69,70] For this purpose, the proteins iLID and Nano, which bind to each other under blue light and dissociate from each other in the dark, were immobilized onto two populations of polystyrene beads. Upon blue light illumination, the mixture of these two beads aggregated and this was reversible in the dark. Similarly, the photoswitchable interaction between the protein nMagHigh and pMagHigh has been used to bring two populations of beads together.[69] In a similar approach, the light triggered homodimerization of VVDHigh under blue light and Cph1 under red light has been used to assemble polystyrene particles with different colors of light.

1.4.2 Dynamics in colloidal self-assembly

Besides the interactions between the particles that drive the self-assembly, the dynamics between the interaction partners are important. As a consequence of the dynamics, particles in solution can attach to each other by either dictated by their random collision or with a certain probability.[71] The collision of particles and their sticking probability can leads to an aggregation of particles.[72] Two regimes are identified for aggregation and are called diffusion limited cluster aggregation (DLCA) and reaction limited cluster aggregation (RLCA).[73] The DLCA described particles that stick together when the particles meet upon collision and irreversibly attach.[74] This happen when between the particles negligible repulsive forces are present and dominated by attraction forces.[72] In this scenario the thermodynamic equilibrium, where the interactions between particles are maximized is not attained and branched clusters that are kinetically trapped form.[75,76] In comparison, RLCA shows repulsing forces between the particles that are present and the colloidal particles can interact multiple times until they aggregate.[72] During RLCA the particles can rearrange and find the most thermodynamically stable position that's lead to round and compact structures compare to branched cluster aggregation at the DLCA.[74]

Aggregates with RLCA and DLCA were obtained using DNA coated particles where the attractive and repulsive forces could be changed systematically.[77] This was possible using two populations of particles with complementary strands of DNA of controlled lengths of the complementary und non-complementary DNA regions to build up defined aggregates.[77] In this design complementary ssDNA strands hybridize and connect the two particles together, while the non-complementary strands create repulsive forces between the particles. Depending on the proportion of non-complementary ssDNA and complementary linker ssDNA functionalized particles, the mixture showed a different assembly. Large clusters formed when the interactions were mostly attractive, the

clusters became smaller when attractive and repulsive forces were matched and the particles remained as single particles when the interactions were repulsive.[77] Another possibility with this setup is to control if the aggregates form under thermodynamic or kinetic control. Kinetically trapped aggregates under DLCA form when the ssDNA coated particles are quickly cooled below their annealing temperatures. When these kinetically trapped structures were activated by increasing the temperatures to overcome the kinetically trapped arrangements a more thermodynamically controlled arrangement were obtained with RLCA.

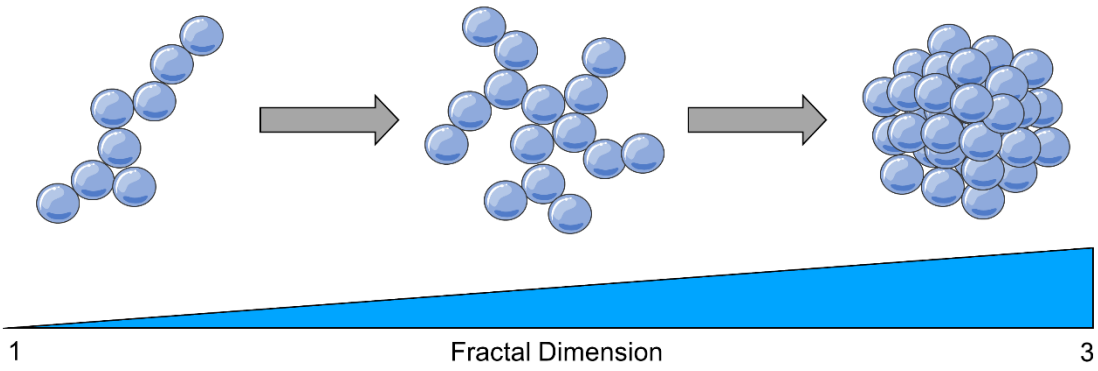

Figure 4: Fractal dimension of different aggregates depending on their conditions and mechanism. The spectrum is shown from fractal dimension from 1 to 3. Adapted from Lazzari et al 2016.[78]

The shape of the aggregates can describe through their fractal dimension and gives an insight into the regimes that are built by DLCA or RLCA. (Figure 4).[78] Fractal dimension described the complexity of an object by the change in detail to the change in scale.[79] The fractal dimension of an object can be calculated using the box counting method by there the fractal dimension (*D*) is estimated as the relationship between different boxes that are able to cover the object and the size of this boxes that corresponds to the number of parts (*N*) and the scale (ε).[80] These can be described by the following equation:

$$D = \lim_{\varepsilon \to 0} \frac{\log N_\varepsilon}{\log \varepsilon}$$

The more branched aggregates that are resulting from DLCA have a smaller fractal dimension compare to the more compact aggregates that are resulting from RLCA.[78] [73,81] Describing aggregates by using fractal dimension has been used in the aggregation of DNA functionalized colloids by changing the temperature.[82] The concept of fractal dimension has been used to classify aggregate across different scales to identify objects with higher complexity in their morphologies like marine snow or bacterial aggregates.[83]

1.4.3 Self-sorting of colloidal particles

The self-sorting of different types of colloids into subassemblies is another important aspect to consider in achieving more complexity. Self-sorting described the assembly of at least two components into self-isolated or intermixed structures, illustrating the ability to distinguish between self and non self.[66,84]

These self-sorting behavior can be assigned in different types depending on the interactions between the colloidal particles, as exemplified with four different colloids (Figure 5).[66,84,85]

- 1) Indiscriminate self-sorting describes the unspecific assembly of all four colloids into one type of aggregate, which can be the result of unspecific interactions such as hydrophobic, hydrophilic or van der Waals interactions.[66,86,87]

- 2) Asocial self-sorting behavior (also called narcissistic self-sorting) is based on self-complementary interactions between particles of the same type such that each type of particle forms separate assemblies. This requires specific self-complementary interactions between the same type of particles.

- 3) Social self-sorting describes that in a four-component mixture of colloids, these self-sort into two distinct families of colloidal aggregates based on two orthogonal

heterophilic interactions. This can be achieved by the specific recognition of the partner particle and no interaction with particles of other types in this mixture.[84]

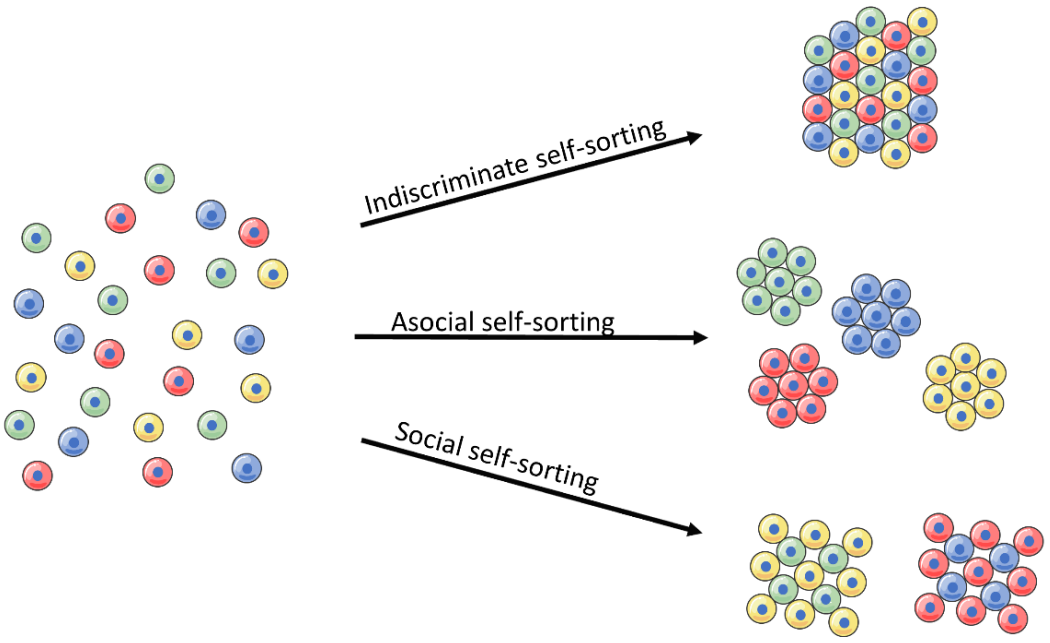

Figure 5: Conceptual structures of colloidal self-assembly. Four different colloidal components of identical size can be self-sorted into different types of assembly. They can assemble independently from different families, so called indiscriminate self-assembly. The components can interact only with their own kind, asocial self-sorting. The last case would be if a component interacts with another family and builds a social self-assembly. Adapted from Han et al. 2017.[66]

These different modes of self-sorting observed in colloidal mixtures can transferred to the assembly and sorting of cells. In fact, these different modes of self-sorting are parallel to what is formulated in the DAH, where also homophilic and heterophilic interactions between cells control self-sorting behavior for cells.

The above described light controlled colloidal assembly systems based on photoswitchable proteins were also used to obtain different self-sorting modes.[69,70] In a mixture of Chp1 and VVDHigh decorated particles, which specifically homodimerize under red and blue light, asocial self-sorting was observed under light.[69] Likewise, the iLID and Nano as well as nMagHigh and pMagHigh decorated particles were used to achieve social self-sorting upon blue light illumination.[70]

1.5 Controlling of cell-cell interactions

Cell-cell interactions are of fundamental importance to create multicellular structures that can be used in bottom up tissue engineering. Besides the natural occurring cadherin based adhesions described above, cell-cell interactions can also be controlled by introducing chemical functionalities on cells or engineering cells to self-organize using new genetic circuits towards the aim of building up multicellular structures.[3]

1.5.1 Chemical modification of the cell surface for the assembly of multicellular structures

Cell-cell interactions can be controlled through the introduction of reactive functional groups on the cell surface.[88] These cell-cell interactions can be based on covalent and non-covalent bonds.

Different click reactions were used to form cell-cell contracts between cells through covalent bonds. For this purpose, the cells were functionalized with different functional groups via lipid fusion or metabolic labeling with non-natural sugars. With these methods complementary ketone and oxamine groups as well as alkyne and azide groups were introduced at the cell surfaces.[89] The reaction between these functional groups through click chemistry has allowed to assemble different cells in a biorthogonal fashion in various combinations of cell types to achieve a wide variety of structures and robust cellular assemblies.[90,91] Even through those covalent cell-cell interactions provide a crucial step in the assembly of multicellular structures, these cell-cell interactions are not reversible and essential glue cells together.

The dynamics of interaction between cells is an important feature of natural cell-cell interactions and as also postulated by the DAH of central importance in rebuilding tissues from cells as building blocks.[92] In this respect, synthetic cell-cell interactions based on noncovalent bonds between cells are also of relevance. In early examples, the

modification of cell surfaces with biotin has been used to obtain cell aggregates in the presence of streptavidin.[93–95] While being noncovalent, these interactions are very strong and still lack the desired reversibility or dynamics and also provide limited flexibility in combining different cells with each other. The modification of cell surfaces with DNA strands opens the possibility to form more flexible and diverse structures out of different cell types with specific interactions and cellular connectivity, similar to what has been achieved in DNA based the colloidal assembly described before.[96] Moreover, the modification of cell surfaces with DNA aptamers opens a possibility to target specific cells types with certain surface receptors.[97] These methods add more flexibility to the range of cell-cell interactions with different binding partners but show limitation in the controlled reversibility of these interactions.

Reversibility was achieved for cell-cell interactions by using light as an external trigger, similarly to what has been shown for colloids before.[92 92,98] Specifically, two reports have shown the temporal and spatial control of cell-cell interactions by using light as an external trigger. Luo et al. modified the cell surface with a photo-oxime-group, which can react with keto groups presented on neighboring cells and be cleaved afterwards by the illumination with UV-light (Figure 6a).[98] This setup enables both the controlled formation of cell-cell interactions and their reversion at a desired time in a desired location. Peng Shi et al. later developed cell-cell interactions that can be reversed multiple times achieving a truly switchable cell-cell interactions.[92] For this purpose, the cell membranes were engineered to contain β-cyclodextrin functionalities using click chemistry. In the presence of a divalent photoswitchable azobenzene (azo) linker (azo-PEG-azo) the azobenzene groups can bind to the cyclodextrin moieties in the dark and lead to cell-cell interactions. (Figure 6b). Upon UV-light illumination the azobenzene undergoes a *trans* to a *cis* isomerization, which results in the dissociation from the cyclodextrin and the disruption of the cell-cell interactions. The azobenzene isomerization can be reversed

from *cis* to *trans* upon blue light, which allows reforming new cell-cell interactions. This reversible conformational change in the azobenzene enables a specific and switchable interaction between the azobenzene linker and the engineered surface of two cells, which is controlled by blue and UV-light. Although, these two approaches to control cell-cell interaction by using light as an external trigger are powerful in answering fundamental questions on cell biology there are still a number of limitations. The used UV-light can be damaging the cells, the chemical modifications are difficult to maintain over long periods of time and the flexibility of addressing different cell types independently is limited.

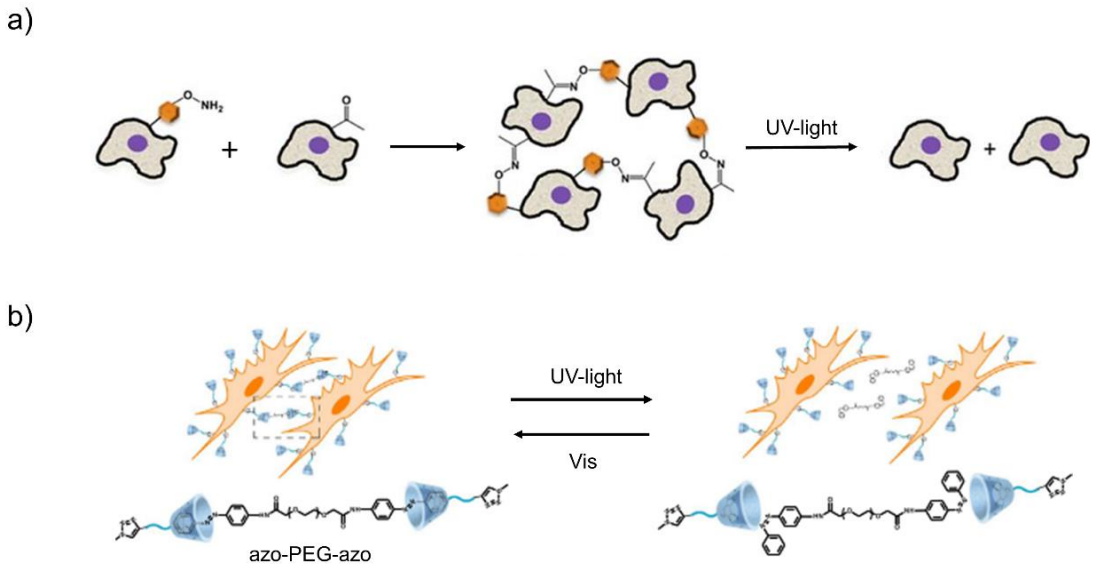

Figure 6: Examples of light induced reversible cell-cell interactions. a) Modification of the cell membrane by incorporating a photocleavable oxime group as cell-cell contact, which can be cleaved by UV-light. Figure is adopted from Luo et al. 2015.[98] b) The cells are engineered with a β-cyclodextrin on the cell surface that can bind to the azo-PEG-azo linker to connect two cells with each other. The conformation of the azobenzene changes from *trans*- to *cis*- by illumination with UV-light. This change of the linker results in a reversible binding of the cells. This Figure is adapted from Shi et al. 2016.[92]

While these chemical based cell-cell interactions are reversible, in most of the cases kinetically controlled structures form due to the strong interactions between the molecules. Yet, to achieve self-sorting in multicellular mixtures as was described in the DAH, the cell-cell interactions must be dynamic enough to avoid kinetically trapped

structures. Moreover, multiple reversible cell-cell interactions that are orthogonal to each other are required to obtain self-sorting, a challenge that is not met by current systems.

1.5.2 Genetically programing self-organization in multicellular structures

One way to control the arrangement and self-sorting of cells is to use principles stated by the DAH, which relies on differences in the adhesions between cells.[44]The self-sorting of cells can by this principle be obtained by changing the expression levels of natural adhesion molecules like cadherins. The different expression of proteins has been controlled by regulating their transcription levels inside the cell.[99] For example, using a tetracycline inducible promotor for induce E-cadherin und P-cadherin expression in two cell types, the de novo patterning could be induced in two and three dimensional cell culture.[100]

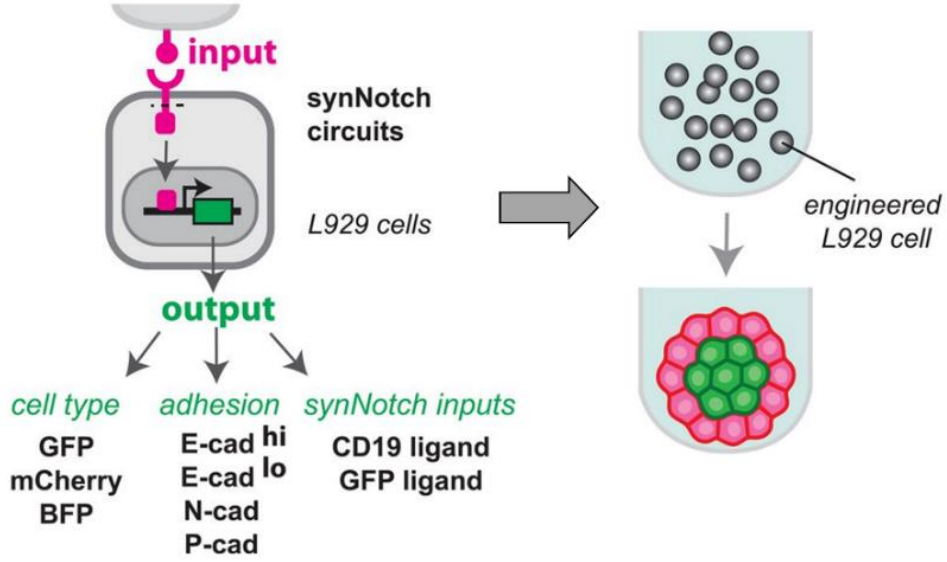

Figure 7: Examples of cadherin-controlled cell-cell contacts that based on a genetic expression by a synNotch circuit. By expressing of different cadherins in different amount different morphologies can be achieved. The output of the synNotch receptor can be divided into cell type, adhesion properties and other synNotch inputs. Figure is adopted from Toda et al 2018.[101]

Instead of externally controlling the expression of cadherins, the self-sorting of cells could also be programmed using a synthetic Notch (synNotch) receptor. The synNotch

receptor relies on the recognition of a ligand expressed on one cell by its receptor on a neighboring cell, which leads to transmission of a signal to the inside of the cell and the activation of gene expression.[102] This synNotch receptor was used to design a genetically engineered circuit to control multicellular organized structures based on cell to cell signaling (Figure 7). In this design, there are three categories of gene expression output: a fluorescence protein to identify the cell type, adhesion molecules with different adhesion properties in terms of type of cadherin and expression levels (E-, N- or P-cadherin with different expression levels) and the ligand for a downstream synNotch receptor which will serve as input signal for further steps (CD19- and GFP-ligand). The different expression levels of cadherins on the cell surfaces regulated through the synNotch receptors and the ability of the cells to be recognized with respect to by each other allowed creating different arrangements of cells, from single aggregates to a three layer envelop shell or asymmetric assemblies.[101] Overall, this approach makes it possible to use minimal intercellular communication as the driver of self-organization in multicellular structures. The next step would be to achieve spatial and temporal over the activation such that the cell fate and the structure of the assemblies is not predetermined by their genetic code but can be controlled externally as desired.

In summary, different approaches have been developed to control self-assembly of cells into multicellular structures. On one side these rely on the chemical modification of cell surfaces with covalent and noncovalent binding partners and have been developed to be light responsive to obtain high spatial temporal control. Here the biggest challenges are the use of UV-light, which can be damaging to cells and maintaining the chemical functionalities over a long time. On the other side, the self-assembly of cells has also been driven by the natural ability of cells to self-sort using natural adhesion molecules like cadherins. These adhesion molecules have been implemented into inducible promoters for controlled activation and integrated into synthetic gene circuits. While

multicellular assemblies obtained using the chemical interactions are mostly kinetically controlled, cadherin-based interactions being very dynamic are mostly thermodynamically controlled, meaning the cells rearrange and maximize the adhesions to their neighbors.

1.6 **Photoswitchable proteins**

In recent years the field of optogenetics provided new tools to control diverse cellular functions using light.[103,104] The integration of photoswitchable proteins into cells has enabled the control and investigation of processes including but not limited to gene expression,[105] enzyme activity,[106] protein localization,[107] cell migration,[108] liquid-liquid phase separation,[109] gene editing[110] and numerous signaling pathways.[111]

Controlling any system with light as an external trigger compare to other stimuli like chemical inputs, temperature, redox etc., comes with unique advantages. First, light provides high spatial control as it can be delivered a specific time point with a focused beam of light down to a diffraction limited spot. Secondly, light allows also high control in time as it can be turned on instantly and is delivered to the point of activation instantly. The combination of these two features, i.e. the high spatiotemporal control, that light offers for any light regulated processes is of great importance to study biological functions, where spatiotemporal control is of central importance to function. At the same time, the photoactivation can also be used to create patterns with a subcellular resolution using photomasks and is still a very scalable stimulus.

Another important feature of biological systems is the reversibility of processes and their dynamics. Also, in this respect light is unique as a stimulus as it be turned off immediately, i.e. removed immediately and can be delivered in pulses or at different doses/intensities, which provides the possibility of modulation and tuning.[112] The large variety in photoswitchable proteins that respond to different wavelengths also open the

possibility to address different functions with different colors of light Moreover, visible light is non-invasive, meaning the impact of light to the organism is minimal, which is a concern for other stimuli. Not only the toxicity is minimal by using light, it is also bioorthogonal and does not influence other biological processes.[113] Light responsive proteins can be grouped into light activated channel proteins and light dependent protein-protein interactions. Here we focus on the different photoswitchable protein-protein interactions, which can be distinguished as homodimerizing and heterodimerizing protein pairs. Examples of photoswitchable proteins that bind to a protein of the same under light kind are the UV-light responsive UVR8 from *Arabidopsis thaliana*,[114] blue light responsive Vivid protein from *Neurospora crassa,*[115] CRY2oligo from *Arabidopsis thaliana,*[116] EL222 from *Erythrobacter litoralis* that results in DNA binding[117] and the red light responsive protein Cph1 from *Synechocystis sp. PCC6803.*[118] Photoswitchable proteins with heterodimerize under light are the blue light responsive proteins like Cryptochrome 2 (CRY2) from *Arabidopsis thaliana,* which binds to CIBN,[119] others detailed below and the red light activated protein Phytochrome B (PhyB) from *Arabidopsis thaliana* that binds to PIF3 and 6.[120] All these interactions are reversible in the dark and the red light triggered ones also reverse under far-red light.

As part of this thesis, the blue light switchable heterodimerizing proteins iLID and Nano as well as nMag and pMag were used and are discussed here in more detail.

1.6.1 iLID and Nano protein pair

The photoswitchable protein improved light induced dimer (iLID) is based on the light oxygen voltage 2 (LOV2) domain of the phototropin 1 from *Avena Sativa* (*As)*, (Figure 8).[107] The domain consists of a per-arnt-sim (PAS) domain flanked with α-helices on the N- and C-termini.[121] The C-terminal α-helix, called the Jα-helix, consists of 20 amino acids with alternating patterns of hydrophobic and hydrophilic residues.[122] Under blue light, the cofactor flavin mononucleotide (FMN) is excited from a single into a triplet

state.[123] This step enables the formation of a covalent bond between a cysteine in the LOV2 domain and the cofactor FMN.[122] The formation of this bond alters the conformation of the entire protein and results in the unwinding of the C-terminal Jα-helix.[124–126] The unfolding of the Jα-helix in iLID can be separated into a two-step process: First, the covalent bond formation of FMN to the cystein 450 (Cys450) and the breaking of the hydrogen bonds formed by glutamine 513 (Gln513) within 10 µs. Secondly, the unwinding of the Jα-helix which takes another 240 µs and makes it available for other interactions.[127] When blue light illumination is stopped, the covalent bond breaks within seconds and the Jα-helix rewinds.[125,128] It was shown that different protein domains can be fused to the end of the Jα-helix[129] and the illumination with blue light will reveals the fused protein domains.[129] In the engineered photoswitchable protein iLID the seven amino acid bacterial peptide SsrA from *Escherichia coli* has been introduced into the Jα-helix. In the dark, the SsrA peptide integrated in iLID is hidden in the Jα-helix such that it cannot bind to, that can bind to its binding partner SspB. Upon blue light illumination, SsrA in iLID gets exposed due to the unwinding of the Jα-helix and enables the binding of SspB.

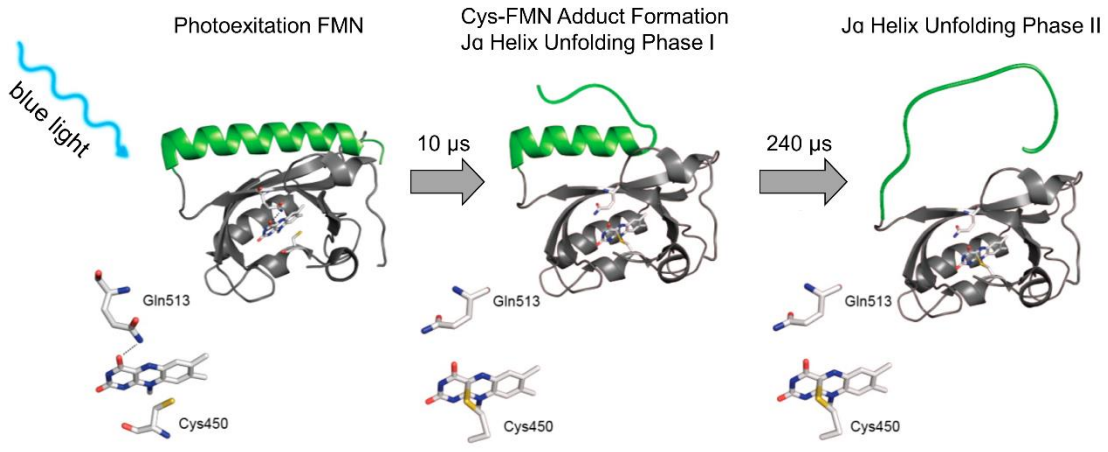

Figure 8: Mechanism of the blue light activation of AsLOV2 domain. By excitation with blue light the cofactor FMN changed from a singlet to a triplet state and forms a covalent bind with the Cys450 of the protein. This binding leads to a conformation change and is unwinding the Jα-helix shown in green. This unfolding that allows SspB to interact with iLID. This image was adopted from Konold et al. 2016.[127]

The binding affinity of iLID to the wild type SspB peptide, called Micro changes from 800 nM under blue light to 47 µM in the dark. A point mutation in the SspB at the arginine 73 to a glutamine, called Nano, change the binding affinity from 130 nM under blue light to 4.7 µM in the dark. The interaction between iLID and its binding partners can be activate within seconds with blue light and reverses in the dark within a few minutes.[107,130]

The photoswitchable protein iLID has been used to photoregulate various cell functions. As a proof of concept, iLID anchored protein has been used to recruit different Micro and Nano fusion proteins upon blue light illumination.[107,131] In other examples, the migration of cells has been directed into the illumination area by locally recruiting the guanine nucleotide exchange factor to the cell membrane and the downstream activation of Rac and Cdc42. Similarly, the migration of cells has been directed away from the illuminated area by activating the kinase RhoA.[107,132,133]

1.6.2 nMag and pMag protein pair

The proteins nMag and pMag originate from the photoreceptor Vivid from *Neurospora crassa*, which homodimerizes under blue light and dissociates into its monomers in the dark. Vivid is part of the light oxygen voltage (LOV) domains.[134,135] Similar to the LOV2 domain described above, upon blue light illumination the cofactor flavin adenine dinucleotide (FAD) forms a bond with the cysteine 108 (Cys108). This bond leads to a conformational change in the N-terminal α-helix and the dimerization. As for the LOV2 domain this processes reverses in the dark.[136]

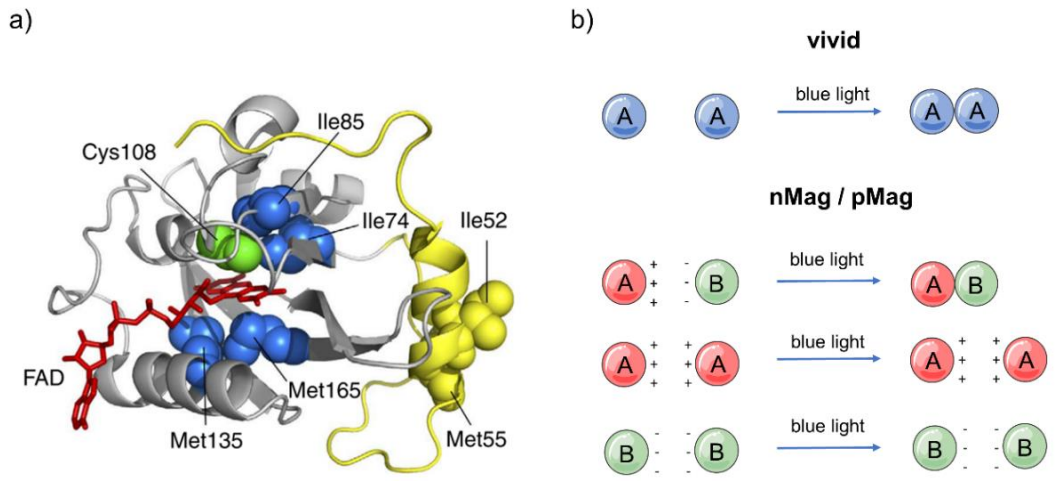

Figure 9: Vivid structure and the binding scheme of nMag pMag. a) the Vivid structure and key amino acid residues. The cofactor FAD shown in red interacts with the Cys108, shown in green, upon the illumination of blue light. The Ncap, amino acids from the first Ile47 to Asn56, shown in yellow. Other relevant amino acids related to photoactivation are shown in blue. b) Binding scheme of nMag/pMag resulting from changing amino acids from Vivid. Vivid homodimerize upon the illumination of blue light. Through changes in the amino acid residues pMag charged positive and nMag negative. The different attraction and repulsion forces are necessary to achieve a blue light induced heterodimerisation. Adapted from Kawano et al. 2015.[137]

Kawano et al. engineered the blue light dependent homodimerizer vivid into a heterodimerizer by introducing oppositely charged amino acids at the dimerization interphase (Figure 9).[137] Specifically, the nonpolar amino acids Ile52 and Met55 were either exchanged for the positively charged amino acid arginine to create a positively charged protein, positive magnet (pMag), or to the negatively charged amino acid aspartic acid (Asp52) and the sterically favorable glycine (Gly55) to create a negatively charged protein, negative magnet (nMag) (Table 1).[137] Beside the native dimerization, these mutations resulted in additional electrostatic attraction between nMag and pMag and repulsion between nMag and nMag as well as pMag and pMag. Thus, favoring the heterodimerization and diminishing the homodimerization.[137]

The dark reversion kinetics of the Vivid derived proteins nMag and pMag can be tuned by changing further amino acids within the PAS core. For this function, the four amino acids Ile74, Ile85, Met135 and Met165 were exchanged and resulted in off kinetics from

seconds to hours ($t_{1/2}$) (Table 1). The fasted dissociation of the protein pair in the dark was shown by nMagFast2/ pMagFast2 ($t_{1/2}$ = 25 s, k_{off}= 2.8 x 10^{-2} s^{-1}), followed by nMagFast1/ pMagFast1 ($t_{1/2}$ = 4.2 min, k_{off} = 2.7 x 10^{-3} s^{-1}), nMag/ Mag ($t_{1/2}$ = 1.8 h, k_{off}= 1.1 x 10^{-4} s^{-1}). The longest dissociation time in the dark was determined for nMagHigh1/ pMagHigh1 ($t_{1/2}$ = 4.7 h, k_{off} = 4.1 x 10^{-5} s^{-1}).[137] It should be noted, that despite the different dark reversion kinetics all versions of nMag and pMag interact with each other under blue light. The activation with blue light for all heterodimerizers is within seconds but the dissociation depends on the particular mutations.

Different combinations of magnet protein pairs were used inside the cell for recruiting proteins to the cell membrane and activate gene expression.[138,139] Most recently, the nMagHigh1 and pMag protein pair was used for light controlled genome editing platform by engineering CRISPR-Cas9 interaction to be blue light dependent.[140] Moreover, these photoswitchable proteins were also expressed on the surface of *E. coli* bacteria to regulate their surface adhesions and biofilm formation.[141]

Table 1: Engineering of Vivid, adapted from Kawano et al. 2015.

	Amino acid residues						
Name	52	55	74	85	135	165	$t_{1/2}$
Vivid	Ile	Met	Ile	Ile	Met	Met	2.0 h
nMag	Asp	Gly	Ile	Ile	Met	Met	1.8 h
nMagFast1	Asp	Gly	Ile	**Val**	Met	Met	4.2 min
nMagFast2	Asp	Gly	**Val**	**Val**	Met	Met	25 sec
nMagHigh1	Asp	Gly	Ile	Ile	**Ile**	**Ile**	4.7 h
pMag	Arg	Arg	Ile	**Val**	Met	Met	1.8 h
pMagFast1	Arg	Arg	**Val**	**Val**	Met	Met	4.2 min
pMagFast2	Arg	Arg	Ile	Ile	Met	Met	25 sec
pMagHigh1	Arg	Arg	Ile	Ile	**Ile**	**Ile**	4.7 h

1.7 Motivation and aim of this thesis

The bottom-up assembly of a spatially ordered tissue made from cellular building blocks based on the principles of self-assembly is a highly promising and powerful approach to tissue engineering, and an extreme synthetic and biological challenge at the same time.[142] To build multicellular structures requires more than simply putting together a solution with the right composition of cells; it requires specific interactions between the cells and spatial organization of these building blocks into hierarchical structures, which determines how cells work together as a tissue.[20,21] The bottom-up approach to tissue assembly parallels observations seen during tissue formation in biology, where no template or scaffold is needed and cell-cell interactions are a major driving force that determines their organization.[19] Remarkably, even dissociated cells from different tissues are able to self-aggregate and self-sort again into multicellular structures that resemble their tissues of origin.[143,144] Moreover, increasing possibilities in organoid[145] and stem cell culture[143,144] as well as programmable multicellular structures with synthetic cell to cell signaling[145] speaks for the massive potential of the living cells to self-organize into complex functional architectures and controlling them using synthetic biology.[101]

Going forward it is indispensable to understand how cells as the basic building blocks of tissues self-assemble. This requires controlling the interactions between cellular building blocks and understand to what extent the principles of self-assembly and self-sorting defined for nonliving colloidal particles apply to cells.[146] Such insight would allow building up multicellular architectures with predictable and programmable organization and understand the limits of multicellular structures that can be generated solely based on self-assembly and where further biological signals are required.[142] As model building blocks for materials, colloids provide a valuable framework for the self-assembly of micron sized objects such as the cells.[147] For colloidal systems, the interactions between colloids are the major driving force behind self-assembly and different architectures can

self-assemble depending on the kinetic and thermodynamic parameters for the interactions between the colloids. [148] While the compact and spherical structures at the thermodynamic equilibrium form under reaction limited cluster aggregation, lose and ramified assemblies in kinetically trapped states form under diffusion limited cluster aggregation.[72,75,76] This puts forward the importance of not just controlling the interactions between the colloidal/ cellular building blocks but also their dynamics. Cell-cell interactions have been controlled by modifying the surfaces of cells with complementary DNA strands[149], biotin/streptavidin [93], clickable functional groups[92,98] and supramolecular interaction[92,150] partners. Yet, most of these interactions are not reversible and provide no control over the dynamics of the cell-cell interactions. Moreover, the important role of the cell-cell interaction dynamics for the final multicellular structure has not been considered in these studies. This is in contrast to native cadherin family based cell-cell adhesions, which have fast exchange rates and form thermodynamically controlled multicellular structures.[44] Therefore, the question of what kind of tissue structures can be generated by employing only the principles of self-assembly and controlling cell-cell interactions to achieve diffusion or reaction limited assembly, remains unanswered.

Another concept where the principles of colloids and cells connect to one another is their self-sorting/sorting-out behavior in multicomponent mixtures.[47,49] Observations *in vivo* and *in vitro* in multicellular systems led to the differential adhesion hypothesis, which postulates that if two populations of cells are mixed the cells sort-out to reach a final organization that approaches a state with minimal internal free energy and maximum total cell-cell interactions.[151] Such self-sorting under thermodynamic control is only possible provided that the cell-cell interactions are dynamic and this criteria is indeed satisfied for native cadherin based cell-cell interactions.[44] Consequently, in mixtures of dissociated cells that express different type or levels of cadherins, the cells sort-out to form self-isolated, enveloped and intermixed multicellular structures depending on their

preference to bind to cells of the same or opposite type.[44,152] Yet, also other mechanisms of self-sorting that rely on local cell signaling or contractile properties of cells have also been proposed and add to the complexity of multicellular systems.[153] Similarly, multicolloidal mixtures self-sort into families of colloids based on multiple molecularly orthogonal homophilic and heterophilic interactions between different types of colloids.[66,69,70] For example, mixtures of four distinct colloids self-sort into two families of colloidal aggregates using two orthogonal heterodimerization pairs by virtue of a behavior named social self-sorting.[66,70]

In this thesis, I employed concepts known from colloidal self-assembly and self-sorting and explore how far these can be used in the context of multicellular structures (Figure 11). In the first part of this thesis, I established different photoswitchable cell-cell interactions for this purpose, which can be triggered under blue light illumination and turned off in the dark with different dynamics (Figure 10). Controlling the cell-cell interaction with light comes with the unique advantage of high spatiotemporal resolution and turning on the cell-cell adhesions remotely using low intensity biocompatible light without interfering with other cellular processes. Most importantly, regulation with light allows tuning cell-cell interaction dynamically by using pulses of light.

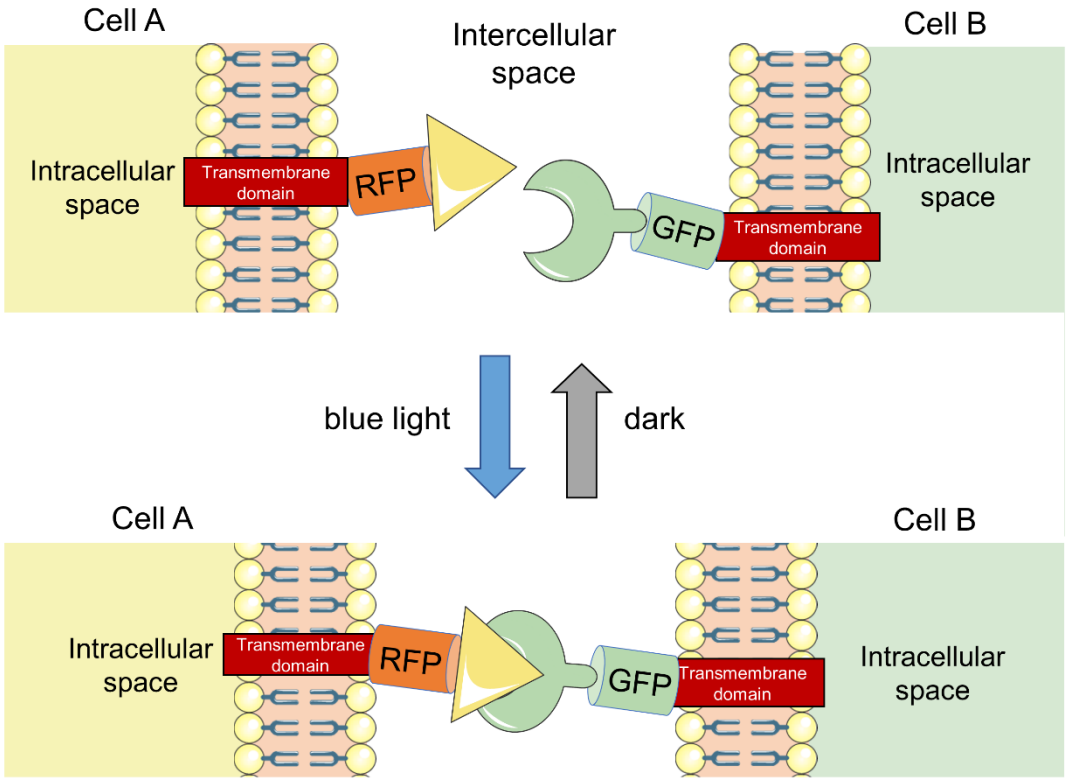

Figure 10: Schematic representation of light induced cell-cell contacts by using photoswitchable proteins on the cell surface. The transmembrane domain anchors the protein construct in the cell membrane, followed by a fluorescence and a photoswitchable protein. By the illumination with blue light the photoswitchable proteins heterodimerize and connect two cells.

In the second part of this thesis, these unique features enabled us to investigate how the thermodynamics and kinetics of the interactions between the cellular building blocks impact the multicellular assemblies and achieve self-assembly under kinetic and thermodynamic control as has been described for colloidal systems.

In the third part of this thesis, combining different orthogonal cell-cell interactions allowed us to not only self-assemble but also self-sort mixtures of four different cell types into separate preferential assemblies.

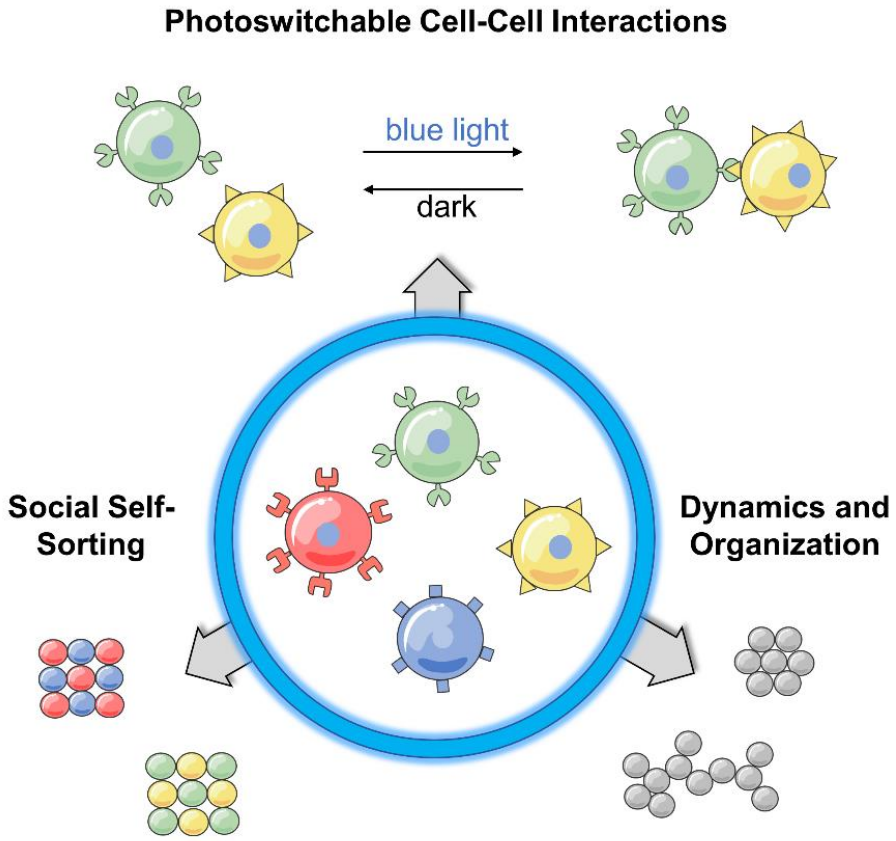

Figure 11: Schematic representation of objectives. Blue light self-assembly, variable organizational structures and social self-sorting. The cells expressing the photoswitchable protein on the cell surface are able to self-assembly through the illumination of light with their specific interaction partner and vice versa in dark.

2 Materials and methods

The following material, methods, results and discussion have been published as:

The importance of cell-cell interaction dynamics in bottom-up tissue engineering: Concepts of colloidal self-assembly in the fabrication of multicellular architectures.

Authors: **Mueller M.**, Rasoulinejad S., Garg S. and Wegner S. V. Wegner.

Nano Letters, 2019, doi:

The methods were developed in close cooperation with Samaneh Rasoulinejad and have been used in following publications:

Independent and Reversible Blue and Red Light Controlled Self-sorting Multicellular Structures

Authors: Rasoulinejad S., **Mueller M.,** and Wegner S. V., submitted (2019).

Blue Light Switchable Cell–Cell Interactions Provide Reversible and Spatiotemporal Control Towards Bottom-Up Tissue Engineering

Authors Yüz S. G., Rasoulinejad S., **Mueller M.,** Wegner A. E., and Wegner, S. V.

Advanced Biosystems. doi: 10.1002/adbi.201800310

Contributions

I performed all experiments except for the immunostaining of the photoswitchable proteins on the cell surface (Method 2.2.9 Immunostaining, Figure 14), which was performed by Sukant Garg. Methods used in this thesis were established in close collaboration with Samaneh Rasoulinejad and Seraphine V. Wegner supervised the thesis.

2.1 Materials

2.1.1 General laboratory equipment

Name	Company
Blue light panel	Abrillo
Electroporator Micro Pulser	Bio-Rad
Centrifuge Avanti J-26x XP	Beckman Coulter
Centrifuge 200	Carl Roth
Centrifuge Micro Star 17	VWR
Cell counting machine	Bio-Rad
Gel electrophoresis	Bio-Rad
Incubator Shaker series Innova 44	New Brunswick
Incubator cell culture C200	Labotect
Milli-Q Synthesis water purification system	Merck
Nano Drop 8-sample Spectrophometer	Peqlab Biotechnology
Pipettboy accu-jet pro	Brand
Plate Reader Tecan Spark	Tecan Group Ltd.
Transmission filter	Alt Intech
Safety Cabinet	Bioair
Scale EMB 1000-2	Kern
Vacusafe comfort	IBS Integra biosciences
Vortex Genie touch mixer	Scientific Industries
Waterbath	Memmert

2.1.2 Microscopes

Name	Company
CKX41 light microscope	Olympus
DMi8 fluorescence microscope	Leica
SP8 confocal microscope	Leica

2.1.3 Software

Name	Version
ImageJ (Fiji)	V1.51w
Mendeley	1.19.14
Microsoft Office	2016
Origin Pro	2017

2.1.4 Bacteria and cell lines

Name	Version
MDA-MB.231	ATTCC
DH5α	Thermo Fisher Scientific

2.1.5 Antibodies

Name	Company	Ref number
Anti-myc antibody rabbit monoclonal	Thermo Fisher Scientific	700648
Alexa fluor 488 goat anti rabbit	Thermo Fisher Scientific	A27034
Alexa fluor 555 goat anti rabbit	Thermo Fisher Scientific	A27039

2.1.6 Chemicals

Name	Company	Ref number
Ampicillin sodium salt	Carl Roth	HP62.2
Agar Agar	Carl Roth	5210.2
Bovine Serum Albumin (BSA)	Sigma Aldrich	A2153
Complete Protease Inhibitor cocktail tablets	Hoffmann La Roche	11697498001
Ethylenediaminetetraacetic acid (EDTA)	Sigma Aldrich	E5134
Flavin Adenine Dinucletide (FAD)	Sigma Aldrich	F8384
Flavin Mononucleotide (FMN)	Sigma Aldrich	F2253
Dimethyl sulfoxide (DMSO)	Sigma Aldrich	D2650
G418 geneticin Solution	Hoffmann La Roche	04727894001
Glycerol	Sigma Aldrich	G5516-500ML
Hepes 1 M	Thermo Fisher Scientific	15630056
Luria-Bertani media	Carl Roth	X968.3
Opti-MEM media	Thermo Fisher Scientific	31985-062
Paraformaldehyd (PFA)	Chem Cruz	SC-281692
PCR purification Kit	Qiagen	28104
Phosphat buffered saline (PBS)	Sigma Aldrich	D8537
Penicillin Streptomycin (PS)	Jena BioScience	ML-105XL
Triton X	Sigma Aldrich	X100
Tryphan blue solution	Sigma Aldrich	T8154

2.1.7 Biochemicals

Name	Company	Ref number
Accutase	Thermo Fisher Scientific	A111051
Cell Tracker green plasma membrane stain	Thermo Fisher Scientific	C2925
Cell Tracker deep red plasma membrane stain	Thermo Fisher Scientific	C34565
Dublecco's modified eagle medium (DMEM)	Thermo Fisher Scientific	10565018
DMEM F12 no phenolred	Thermo Fisher Scientific	21041025
DNA Ladder 1 kb	BioZol	DNA1000
dNTPS mix	Qiagen	201900
Dpn1 restriction enzyme	New England Biolabs	R0176S
Fetal Bovine Serum (FBS)	Sigma Aldrich	F2442
Fluoshield mountain media	Abcam	Ab104139
Gibson Assembly Master Mix	New England Biolabs	E2611S
Hoechst 33342	Invitrogen	H3570
Lipofectamin 3000 Reagent	Thermo Fisher Scientific	L3000001
Phusion HF DNA Polymerase	New England Biolabs	M0530S
Phusion HF Buffer	New England Biolabs	
QIAprep Spin Miniprep Kit	Qiagen	27106
QIAquick PCR Purification Kit	Qiagen	28104
Quantum Alexa Fluor 488 MESF	Bang Laboratories inc	488 A
Site directed mutagenesis Kit	Agilent	200523

2.1.8 Primer sequences

Primer name	Primer sequence 5’ to 3’
GFP pDisplay Fwd	gacaaagtgt gtaattatga cccgggatcc gcggctgcag
GFP pDisplay Rev	ctgcagccgc ggatcccggg tcataattac acactttgtc
pDisplay GFP Fwd	gggcccagcc ggccagatct gtgagcaagg gcgaggagct g
pDisplay GFP Rev	cagctcctcg cccttgctca cagatctggc cggctgggcc c
mCherry pDisplay Fwd	gcatggacga gctgtacaag cccgggaatc cgcggctgca g
mcherry pDisplay Rev	ctgcagccgc ggattcccgg gcttgtacag ctcgtccatg c
pDisplay mCherry Fwd	ggcccagccg gccagatctg tgagcaaggg cgaggagg
pDisplay mCherry Rev	cctcctcgcc cttgctcaca gatctggccg gctgggccc
pDisplay iLID Fwd	gccagaaact ccccggatcc agatctggcc ggctgggc
pDisplay iLID Rev	gcccagccgg ccagatctgg atccggggag tttctggc
iLID mCherry Fwd	cgaacgacga aaattacttt gtgagcaagg gcgaggagg
iLID mCherry Rev	cctcctcgcc cttgctcaca aagtaatttt cgtcgttcg
Nano GFP Rev	ctcgcccttg ctcacagatc taccaatatt cagctcgtca tag
Nano GFP Fwd	ctatgacgag ctgaatattg gtagatctgt gagcaagggc gag
pDisplay Nano Rev	cgtttcgggg agctggatcc ggccggctgg gccccagc
pDisplay Nano Fwd	gctggggccc agccggccgg atccagctcc ccgaaacg
pDisplay Mag Fwd	gattatgctg gggcccagcc ggccatgcac acactatatg ctc
pDisplay Mag Rev	gagcatatag tgtgtgcatg gccggctggg ccccagcata atc
Mag GFP Fwd	gcgagaccga aggcggtagc agatctgtga gcaagggcga g
Mag GFP Rev	ctcgcccttg ctcacagatc tgctaccgcc ttcggtctcg c

2.1.9 Plasmids

Name	Company	Ref number
pCRY2FL(deltaNLS)-mCherryN1	Addgene	26871
pCIBN(deltaNLS)-pmGFP	Addgene	26871
pDisplay vector	Invitrogen	V66020
pQE-80L iLID (C530M)	Addgene	60408
pQE-80L MBP-SspB Nano	Addgene	60409

2.2 Methods

2.2.1 Preparing electrocompetent DH5α bacteria

The transformation of plasmid DNA into DH5 α *E. coli* bacteria, electrocompetent bacteria were prepared as follows: 2 L distilled water, 100 mL of 10% glycerol in water and 1 L of Luria-Bertani (LB) media were prepared and autoclaved. 10 mL of LB media were inoculated as starter culture in a 50 mL Falcon tube containing appropriate antibiotics. The bacteria were grown overnight at 37 °C at 200 rpm and the next day the starter culture was transferred into a 2 L Erlenmeyer flask containing 1 L LB-media. The bacteria were grown at 37 °C, 200 rpm until an OD of 600 was reached. The prepared solutions, bottles and the centrifuge were cooled down to 4 °C. The bacteria were transferred to ice and cooled for 30 min. Afterwards the bacteria were separated into two high speed 500 mL centrifuge bottles and spun down at 6000 x g at 4 °C for 10 min. The supernatant was removed, and the cell pellet washed twice with 400 mL cold distilled water. After the second wash the bacteria were resuspended in 50 mL 10% glycerol and centrifuged at 6000 x g at 4 °C for 15 min. The supernatant was discarded. The pellet was resuspended in a total volume of 3 mL of 10% glycerol. The electrocompetent bacteria were aliquoted into 145 µL samples in 1.5 mL Eppendorf tubes and frozen immediately in liquid nitrogen. The stocks were stored afterwards at -80 °C.

2.2.2 Starting bacteria culture

10 mL of sterile LB-media containing the antibiotic ampicillin (50 µ/mL) was used for inoculating the bacteria. The media was incubated overnight at 37 °C and shaking at 200 rpm. To prepare a glycerol stock, 500 µL of the bacteria culture with 500 µL of 80% glycerol were mixed in to a 1.5 mL Eppendorf tube and stored at -80 °C.

2.2.3 Transformation with electroporation into DH5α bacteria

The cloned constructs were transformed into electrocompetent DH5α bacteria. The electroporation cuvette was cooled down to 4 °C and the LB-media prewarmed to 37 °C. 49.5 µL of electrocompetent DH5 α bacteria were mixed with 0.5 µL of the according DNA plasmid by pipetting. The mixture was added into a 0.1 mL electroporation cuvette. An electric pulse of 1.8 kV was given, and the solution immediately transferred to 450 µL LB medium in an 1.5 ml Eppendorf tube. The sample was incubated for 1 h at 37 °C. Afterwards the bacteria suspension was plated on a LB agar plate containing the appropriate antibiotic and incubated overnight at 37 °C.

2.2.4 Plasmid purification

The plasmid purification was done with the QIAprep Spin Minikit from Qiagen. According to the standard protocol a bacterial colony was picked with a sterile pipette tip from an agar plate and transferred into 10 mL LB media containing the appropriate antibiotic. The sample was incubated overnight at 37 °C and 180 rpm. The sample was spun down at 4,000 rpm at 4 °C for 10 min to obtain a separation of solid parts and solution. Afterwards the pellet was resuspended in 250 µL P1 Buffer and transferred to a 2 mL eppendorf tube. 250 µL of P2 Buffer were added to the suspension and mixed carefully by inverting the tube 4 to 6 times. 350 µL of N3 Buffer were added and the tube inverted for another 4 to 6 times. The sample was spun down for 10 min at 13,000 rpm, room temperature. Around 800 µL of the supernatant was transferred to a QIAprep 2.0 spin column and

centrifuged for 60 sec at 13,000 rpm, room temperature. The flow though was discarded and 750 µL PE Buffer added to the column. The sample was spun down for 60 sec at 13,000 rpm, room temperature. The flow though was discarded, and the sample again spun down. The column was placed into a sterile 1.5 mL Eppendorf collection tube and 50 µL of miliQ water added to eluate the plasmid DNA. After incubation of around 1 min at room temperature the sample was spun down for 60 s at 13,000 rpm, room temperature. The plasmid was collected in the 1.5 mL Eppendorf tube and the concentration determined by Nanodrop.

2.2.5 Polymerase chain reaction

To amplify the DNA and the adding of specific overhanging regions a polymerase chain reaction (PCR) was performed. For the PCR mix 0.5 µL of the template DNA was mixed with 2 µL dNTPS (10 mM solution), 5 µL forward primer (10 pmol), 5 µL reverse primer (10 pmol), 1 µL of Phusion HF polymerase and the Phusion HF buffer, topped to 100 µL with miliQ water. The PCR reaction conditions were set to 98 °C for 1 min, 98 °C for 30 sec, 30 sec of the annealing temperature according to primer length, 72 °C according to the length of the construct (1 min for 1000 bp). 72 °C for 10 min and stored at 4 °C. Steps 2 to 4 were repeated for 34 cycles. After the PCR, the sample was purified to remove primers, nucleotides and enzymes from the DNA with QIAquick PCR purification kit. To 100 µL of PCR product 500 µL of Buffer PB was added and the solutions were mixed. The sample was inserted into a QIAquick column tube with a 2 mL collection tube and centrifuged for 60 sec at 13,000 rpm, room temperature. The flow though was discarded and 750 µL of PE buffer added. The sample was spun down for 60 sec at 13,000 rpm, room temperature. The flow though was discarded again, and the sample centrifuged a second time to remove the residual wash buffer. The QIAquick column was transferred to a new 1.5 mL Eppendorf collection tube and 50 µL miliQ water was added to elute the

PCR product by another round of centrifugation for 1 min at 13,000 rpm, room temperature. The concentration of the PCR product was measured by Nanodrop.

2.2.6 Cloning

The DNA sequences coding for GFP or mCherrry were cloned between Ig κ leading sequence and C-terminal to the platelet-derived growth factor receptor (PDGFR) transmembrane of pDispay vector by using a Gibson's cloning kit following the manufacturer's protocol, to yield pDisplay-GFP and pDisplay-mCherry. DNA sequences coding for the photoswitchable proteins were amplified from following plasmids: pQE-80L iLID (C530M) (a gift from Brian Kuhlman), pQE-80L MBP-SspB Nano (a gift from Brian Kuhlman) and pMagHigh in pet21b (synthesized by Genescript). nMag, pMag and nMagHigh were generated from the pMagHigh-pet21b plasmid using a site-directed mutagenesis kit. Subsequently, the DNA sequences coding for the photoswitchable proteins pMag, pMagHigh and Nano were each cloned into the pDisplay-GFP, and nMag, nMagHigh and iLID were each cloned into mCherry-pDisplay between the Ig κ leader sequence and the fluorescence protein by using Gibson assembly following the standard protocol and primers listed in supporting information Table S1. The final plasmids were verified by sequencing (StarSEQ).

2.2.7 Cell culture

All cell lines were cultured in DMEM (Dulbecco's Modified Eagle Media, supplemented with 10% FBS (Fetal bovine serum, Sigma Aldrich) and 1% PS (Penicillin/Streptomycin) unless specified otherwise at 37 °C and 5% CO_2. Transfected cells were selected with 1800 µg/ml G418.

2.2.8 Preparation of stable cell lines

MDA-MB-231 cells were plated in a 6-well plate in total of 5 × 10^5 cells/well, cultured overnight and placed into fresh Opti-MEM the next day. For each well, 125 µL Opti-MEM and 3.75-7.5 µL Lipofectamine 3000 reagent were mixed in one tube and 250 µL Opti-MEM medium and 5 µg of plasmid with 10 µl P3000 reagent in a second tube. The two solutions were mixed together and incubated for 10 to 15 min at room temperature to form the DNA-lipid complex, before adding the solution on to the cells drop-by-drop. The next day, the culture medium was replaced with the regular culture medium containing 1800 µg/ml G418 for selection of transfected cells. When the cells in the 6-well plate reached confluence, the cells were detached using accutase and transfected cells were selectively and individually sorted into 96-well plate wells containing 200 µL of DMEM (containing 10% FBS, 1% PS, 2 mM EDTA (Ethylenediaminetetraacetic acid), and 25 mM HEPES (2-[4-(2-hydroxyethyl)piperazin-1-yl]ethanesulfonic acid)) using BD FACS Aria III 352 Cell sorter (Flow Cytometry Core Facility at the Institute of Molecular Biology (IMB), Mainz, Germany). To generate stable monoclonal cell lines, each clone was cultured separately with G418 selection starting from the second day and expanded into 6-well plates. GFP or mCherry protein expression in different clones was quantified based on the fluorescent protein tag using fluorescence microscopy and flow cytometry (Attune NxT acoustic Focusing Cytometer). Stable cell lines for each of the photoswitchable proteins with high protein expression were identified and used in further experiments (Table 2).

2.2.9 Immunostaining

Cells expressing different proteins at their surface were plated at 5x10^4 cells/well on glass coverslips in 12-well plates and cultured overnight. The adhered cells were rinsed with PBS (phosphate-buffered saline) once and incubated with 0.25 µg/mL recombinant monoclonal rabbit anti-Myc primary antibody diluted in 0.5 mL culture medium overnight

at 37°C. Subsequently, the cells were rinsed twice with PBS and fixed with pre-chilled methanol: acetone (1:1) on ice for 5 min. The fixed cells were washed with PBS for 10 min on a shaker at 150 rpm, blocked with serum albumin (2% BSA in PBST (PBS with 0.2% Triton-X)) for 60 min at 50 rpm, and then incubated with either 1 µg/mL superclonal™ recombinant Alexa fluor 488 goat-anti-rabbit or Alexa fluor 555 goat-anti-rabbit IgG secondary antibodies in blocking solution for 60 min at room temperature at 50 rpm. After washing with PBST (3 times, 10 min each), coverslips were incubated with 1 µg/mL Hoechst 33342 diluted in PBS for the nuclear staining for 10 min at room temperature at 50 rpm, washed with PBS for 10 min on a shaker at 150 rpm, mounted with 10 µL fluoroshield mounting medium, and visualized using a fluorescence microscope (Leica, DMi8) at 63× magnification.

2.2.10 Quantifying protein expression on the cell surface

Cells were plated 5 × 10^5 cells per t25-flask containing 5 mL of media and cultured overnight. The next day, the cells were washed with PBS and detached with 0.5 mL accutase for 5 min at room temperature. Cells were collected in a 1.5 mL Eppendorf tube with 1 mL DMEM media, pelleted at 500 × g for 5 min and resuspended in 500 µL PBS. The cells were counted, and 2.5 × 10^5 cells were incubated in 250 µL PBS containing 2 µL recombinant monoclonal rabbit anti-Myc primary antibody in the fridge on an orbital shaker at ca. 50 rpm for 45 min. The cells were washed once by adding 1 mL PBS and centrifuge at 500 × g for 5 min at 4 °C. The cell pellets were resuspended in 100 µL of PBS containing 2 µL of secondary Alexa fluor 488 goat-anti-rabbit antibody and incubated in the fridge on an orbital shaker at ca. 50 rpm for 60 min. Afterwards the cells were washed once with 1 mL PBS, resuspended in 200 µL PBS and measured with Axtune Flow Cytometry by using the BL1 laser. For quantification the Quantum Alexa Fluor 488 MESF kit was used following the manufactures protocol. The quantification was done using the QuickCal v. 2.4 software from Bangs Laboratories. For this, the

median of the fluorescence peak from each cell type was determined and converted into MESF (Molecules of Equivalent Soluble Fluorochrome) based on the calibration curve. To calculate the specific MESF of each cell type, the MESF for the same cell type (negative control) which was not incubated with antibodies and the MESF for MDA-MB-231 cells incubated with antibodies was subtracted.

2.2.11 Light source

Blue light LED light panel (463 nm, 14 W, 544 µW/cm^2) was used for all experiments. The light intensity was reduced to half with a white polycarbonate neutral density filter. For light pulsing a controllable power socket was used to switch the LED panel on and off.

2.2.12 Light dependent cell clustering and reversibility

Cells were grown to about 80% confluence in a T-flask and washed twice with PBS, followed by the addition of 1 mL and 0.5 mL accutase to T75- and T25-flasks, respectively. The cells were incubated for 5 min at room temperature and later collected in 5 mL DMEM. Cells were centrifuged at 100 rcf for 3 min, the supernatant was removed and the cell pellet was resuspended in 1 mL DMEM/F12 media without phenol red containing 10% FBS, 1% PS and 1800 µg/mL G418. The number of cells was counted using a cell counter. For experiments with monocultures, each cell line was diluted to 1 × 10^5 cells/mL in DMEM and 1 mL aliquots were added into 1.5 mL low protein binding tube. Similarly, for experiments with co-cultures of two cell lines, 5 × 10^4 cells/mL of each cell type were diluted into media and 1 mL aliquots were transferred into 1.5 mL low protein binding Eppendorf tube. In all experiments, the medium was supplemented with 25 mM HEPES, and 0.5 µM of the cofactor FAD (Flavin Adenine Dinucleotide) for nMag-, pMag-, nMagHigh- and pMagHigh-MDA and FMN (Flavin Mononucleotide) for the iLID- and Nano-MDA cells. Cell suspensions were either incubated in the dark or under blue

light using an LED panel with a neutral density filter at a light intensity of 272 µW/cm^2, on an orbital shaker at 20 rpm for 30 min. After the incubation in the dark or illumination, each 1 mL culture was transferred with a 1 mL pipette tip with a cut tip (to reduce shear forces) into 12-well plate wells containing 1 mL 4% paraformaldehyde (PFA). For each sample, bright field images were acquired using a 5x objective (field of view for one image was 4 mm²) and an area accounting to 25 or 64 fields of view was scanned using a tile scan on a Leica DMi8 microscope (1 cm^2 to 2.56 cm^2 per sample containing 25000 cells/cm^2).

Reversion of the clustering in the dark and clustering of cells under pulsed illumination were performed similarly with following modifications to the protocol above. For reversion of clustering, samples were first incubated for 30 minutes under blue light, followed by incubation in the dark and images were captured at regular intervals. Cells kept under continuous blue light illumination and in the dark were taken as the positive and negative controls, respectively and used to normalize the cluster areas. For clustering experiments under pulsed illumination, samples were incubated for 2 h in different light conditions: 120 min constant blue light illumination (120:0), 30 s blue light and 30 s dark (0.5 : 0.5)) (only for iLID-/Nano-MDA clusters). 1 min blue light and 1 min dark (1 : 1) (only for iLID-/Nano-MDA clusters), 5 min blue light and 5 min dark (5:5), 20 min blue light and 20 min dark (20:20), and 1 min blue light followed by 19 min dark (1:19).

2.2.13 Image analysis for cell clustering

All the image analysis was performed using Fiji-ImageJ 1.52d.[154] Bright field images acquired at the end of the cell clustering experiments, were background corrected for noise and differences in grey scale with the plugin “bioVoxxel” with a pseudo flat field correction. Single images acquired in the tile scan (25 (5×5) to 64 (8×8) images) were stitched together into a larger image (1 cm^2 to 2.56 cm^2) with the “Montage” plugin for

the cell clustering analysis and with the “Stitching”[155] plugin for fractal dimension analysis. To detect clusters of cells, objects >5000µm² (corresponding to a projected area of more than 20 cells) were detected using the “analyze particles” plugin. The following macro script was used for this image analysis:

```
run("Set Scale...", "distance=1024 known=1000 pixel= 1 = global");
run("Images to Stack", "name=Stack title=[] use");
run("Pseudo flat field correction", "blurring=50 stack");
close();
run("Make Montage...", "columns=8 rows=8 scale=1");
run("Sharpen");
run("Smooth");
run("Median...", "radius=8");
run("Gaussian Blur...", "sigma=2");
setAutoThreshold("Default dark");
setAutoThreshold("Default dark");
setOption("BlackBackground", false);
run("Convert to Mask");
setAutoThreshold("Default");
call("ij.plugin.frame.ThresholdAdjuster.setMode", "B&W");
run("Convert to Mask");
setAutoThreshold("Default dark");
run("Fill Holes");
run("Undo");
run("Convert to Mask");
setAutoThreshold("Default");
run("Convert to Mask");
run("Fill Holes");
waitForUser("Do something, then click OK.");
run("Analyze Particles...", "size=5000-Infinity
show=[Bare Outlines] display include add");
```

The areas of all recorded cell clusters were analyzed with OriginPro2019 for average area and the total number of the cell clusters in each sample. For analyzing the fractal dimension, all detected clusters were transferred to the Region-of-interest-Manager (ROI-Manager) in Fiji-ImageJ 1.52d. The fractal dimension of each detected cell cluster was analyzed using the plugin "Frac Lac"[80] For the fractal dimension analysis, the box counting method was used with 12 grids and standard ROI analysis settings. In the box counting method different grids were set over the binary image containing the cell aggregates. The average of fractal dimension (DB) for each cluster was calculated as the average of multiple box counting scans with varying grid orientations. The fractal dimension of the aggregation of iLID/Nano and nMagHigh/pMagHigh functionalized beads reported in an earlier study was analyzed similar to the cellular clusters (Table 4). Objects with an area bigger than 30 µm² (10 beads) were considered as cluster in the analysis. The statistical significance was calculated from at least two biological repetitions and 3 technical replicates in each repetition using OriginPro2019. Mann-Withney-U test was performed to analyze the statistical difference, and represented by p-values ns>0.05, **<0.05 and ***<0.001.

2.2.14 Social self-sorting with four cell types

For self-sorting experiments, each of the four different cell types were washed twice with PBS and detached with 1 mL accutase after a 5 min incubation at room temperature. Each cell type was collected in 5 mL DMEM and centrifuged by 100 rcf for 3 min at room temperature. The supernatant was removed followed by cell resuspension in 1 mL media (DMEM without phenol red containing 10% FBS, 1% PS, 1800 µg/mL G418) and the cell density was determined using a cell counter. For social self-sorting experiments, 2.5×10^4 cells/mL for each cell line with the same staining were mixed with 1 µL/mL of the Cell Tracker dye, i.e. nMag- and pMag-MDA (or nMagHigh- and pMagHigh-MDA) with Cell Tracker Green, and the iLID- and Nano-MDA with Cell Tracker Deep Red. Afterwards

the cells were incubated for 30 min at 37°C in an incubator and gently mixed every 10 min. Stained cells were spun down with centrifugation (100 rcf for 3 min) and resuspendend in the culture medium without phenol red containing 10% FBS, 1% PS, 0.5 µM FAD, 25 mM Hepes, 2 mM EDTA. In a total volume of 1 mL, 5×10^4 cells/mL from iLID-/Nano-MDA and 5×10^4 cells/mL from nMag-/pMag-MDA (or nMagHigh-/pMagHigh-MDA) were mixed to reach a total cell density of 1×10^5 cells/mL. Cell mixtures were then either incubated under blue light (272 µW/cm^2) or in the dark on an orbital shaker at 25 rpm overnight in an incubator at 37°C. Next day, these cells were carefully transferred into a 12-well plate wells containing 4% PFA as described earlier. From each sample, bright field images were acquired as described above through a 5× objective on a DMi8 Leica microscope for cell clustering analysis and a confocal fluorescence microscope (Leica, SP8) with 20× and 40× objectives in the Cell Tracker Green (excitation/emission 492/517) and Cell Tracker Deep Red (excitation/emission 630/650) channels to visualize the distribution of different prestained cell types.

2.2.15 Analyzing social self-sorting images

The images from the social self-sorting were analyzed by using imageJ and the plugin EzColocalisation.[156] The taken images with the confocal z-stack images that was described before where split into the single stacks of fluorescence channels (green and red fluorescence). The maximal intensity of the z-stack where combined in 1 image. Both channels, red and green fluorescence where loaded into the plugin EzColocalizsation and analyzed by colocalization with the settings threshold overlap score (TOS) linear matrix. The TOS value is 1 for complete colocalization, 0 for non-colocalization and -1 for anti-colocalization of the two fluorescence signals. The TOS metric matrix described the percentage of pixels in 10% steps (e.g. 10% red fluorescence describe the highest 10% of fluorescence signals of the fluorescence intensities that are colocalized with different percentage of the intensities at the other fluorescence channel.

3 Results and discussion

3.1 Photoswitchable cell-cell interactions

First, I focused on establishing different photoswitchable cell-cell interactions with different binding strengths, protein-protein interaction dynamics and reversion kinetics in the dark. For this purpose, I expressed different light dependent protein-protein interaction partners as synthetic adhesion receptors on the surfaces of the breast cancer cell line MDA-MB-231, which do not form strong native cell-cell adhesions and are commonly used to study the mesenchymal to epithelial transition.[157,158]

These blue light switchable protein-protein interactions differ substantially in their reversion rates in the dark, where the interaction of iLID/Nano reverses within a few minutes, the interaction of nMag/pMag reverses in about an hour and the interaction of nMagHigh/pMagHigh reverses over many hours. The different proteins were chosen due to the large range of dark reversion times they cover, their different protein-protein interaction dynamics, the tunability of their interactions with few point mutations (e.g. nMag/pMag vs. nMagHigh/pMagHigh) and their similar size, which presumably will lead to a similar expression level on the cell surface. To express these proteins on the cell surface each of genes coding for them were cloned into a pDisplay vector, which once the protein is expressed guides it to the cell membrane with an N-terminal murine Igκ-chain leader sequence and anchors it at the cell membrane with a C-terminal platelet derived growth factor receptor (PDGFR) transmembrane (TM) domain (Figure 12).

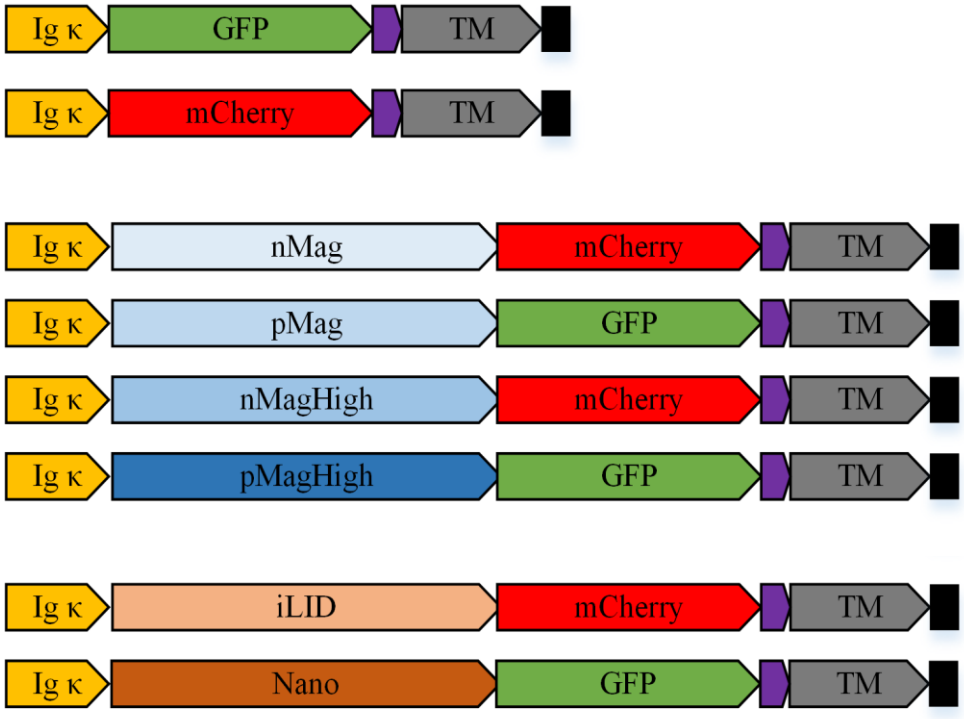

Figure 12: Schematic representation of DNA constructs. Open reading frame expressed with various the pDisplay plasmids. The fluorescence protein (GFP or mCherry) was cloned between the Ig κ leader sequence (yellow) and the Myc epitope (purple). Photoswitchable proteins were cloned between the fluorescence protein and the Ig κ leader sequence followed by a transmembrane domain (grey) and a stop codon (black).

In particular, I used three protein pairs that specifically heterodimerize with each other under blue light (450 nm) and dissociate from each other in the dark, named iLID and Nano (dark reversion rate 3.5×10^{-2} s^{-1}, $t_{1/2}$= 20 s)[107], nMag and pMag (dark reversion rate 1.1×10^{-4} s^{-1}, $t_{1/2}$= 1.8 h) and nMagHigh and pMagHigh (dark reversion rate 4.1×10^{-5} s^{-1}, $t_{1/2}$= 4.7 h).[137] Plasmids coding for different proteins were individually transfected into MDA-MB-231 cells and monoclonal stable monoclonal cell lines expressing these proteins at their surfaces were generated. The cell lines were named after the protein expressed at their surface; e.g. iLID expressing cells were named iLID-MDA. For each photoswitchable protein, a single clone with high protein expression was selected and the expression of each protein on the cell surface was confirmed by flow cytometry based on the signal of the fused fluorescent protein (Figure 13, Table 2).

Table 2 Fluorescence Intensities of the transfected clones, measured by flow cytometry.

Name	Fluorescence intensity	Laser
iLID mCherry-MDA 1	**85%**	**YL2**
iLID.mCherry-MDA 2	98%	YL2
iLID.mCherry-MDA 3	19%	YL2
iLID.mCherry-MDA 5	73%	YL2
iLID.mCherry-MDA 7	81%	YL2
Nano-GFP-MDA 2	**83%**	**BL1**
Nano-GFP-MDA 5	14%	BL1
Nano-GFP-MDA 7	26%	BL1
nMag-mCherry-MDA 3	**23%**	YL2
nMag-mCherry-MDA 5	**90%**	**YL2**
nMag-mCherry-MDA 8	16%	YL2
pMag-GFP-MDA 3	23%	BL1
pMag-GFP-MDA 5	**77%**	**BL1**
pMag-GFP-MDA 11	86%	BL1
nMagHigh mCherry-MDA 1	26%	YL2
nMagHigh mCherry-MDA 2	48%	YL2
nMagHigh mCherry-MDA 3	91%	YL2
nMagHigh mCherry-MDA 6	**50%**	**YL2**
pMagHigh GFP-MDA 1	28%	BL1
pMagHigh GFP-MDA 4	48%	BL1
pMagHigh GFP-MDA 9	**73%**	**BL1**
pMagHigh GFP-MDA 11	26%	BL1

All monoclonal cell lines showed at least 14% higher fluorescence signal compared to the control MDA-MB-231 cells (Table 2). One clone for each photoswitchable protein displaying cell type with a fluorescence signal at least 50% above the control cell line was selected. The selected cell lines iLID-MDA clone 1 (85%), Nano-MDA clone 2 (83%), nMag-MDA clone 5 (90%), pMag-MDA clone 5 (77%), nMagHigh clone 6 (50%) and pMagHigh clone 9 (73%) were used for further experiments. These cell lines are named

here on without the clone number and a clear shift of the fluorescence intensity is observed in the flow cytometry compare to the MDA-MB-231 control (Figure 13).

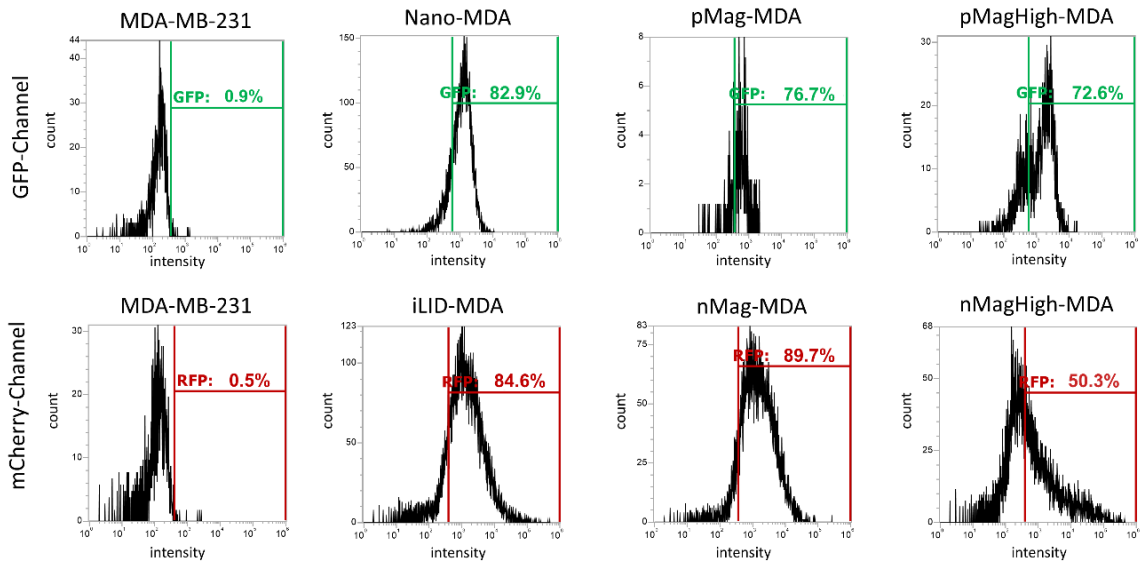

Figure 13: Florescence signal in flow cytometry for stable cell lines generated from MDA-MB-231 cells and expressing different photoswitchable and fluorescent proteins on the cell surface. The monoclonal stable cell lines, Nano-, pMag- and pMagHigh-MDA with a GFP fluorescent protein fusion expressed significantly higher GFP fluoresce than the parent MDA-MB231 cells. Likewise, the monoclonal stable cell lines, iLID-, nMag- and nMagHigh-MDA with a mCherry fluorescent protein fusion expressed significantly higher mCherry fluoresce than the controls. Only living cells, determined with the forward and side scatter, were quantified.

The Igκ-chain leader sequence signal peptide that guides the expressed protein into the secretory pathway is not specific for just the cell membrane and leads to display the protein on membranes inside the cell. To ensure the protein is not trapped intracellularly and indeed expressed on the outside of the cell, the immunostaining was done on unpermeabilized cells using the Myc-epitop between the fluorescence protein and the TM domain that is shown in a scheme in Figure 12. The Myc-epitop was detected with a primary anti-Myc-antibody and an additional fluorescently labeled secondary antibody against the primary antibody. To avoid cross-talk between the fluorescent protein and the fluorescently labeled secondary antibody, GFP and mCherry fused proteins were detected with Alexa fluor-555 and Alexa fluor 488 labeled secondary antibodies,

respectively. The microscopy images showed clear signal for all cell lines, which was mostly localized to the cell membrane (Figure 14). Even though some signal can also be seen within the cell, the pictures clearly show that the protein is expressed and located at the cell surface.

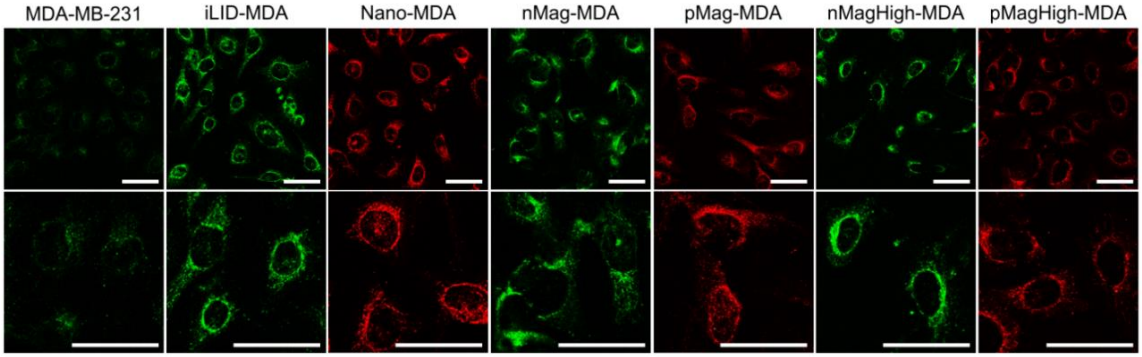

Figure 14: Immunostaining of proteins expressed on the cell surface. Live cells were stained with the primary anti-Myc antibody to detect only proteins expressed at the cell surface. Only the surface proteins were detected as the cells were not permeabilized before the removal of residual primary antibody, which were significantly higher for the stably transfected cells than the control. Scale bars are 20 µm.

To quantify the amount of protein expressed on the cell surface, quantitative flow cytometry was performed. For this purpose, the different cell types were stained with an anti-Myc antibody that are able to detect the Myc-epitop that is part of the displayed protein and a secondary antibody fusion construct with an Alexa fluor 488 fluorophore. The fluorescence detected for individual cells was compared to Alexa 488 labeled beads with known density and the molecules of equivalent soluble fluorchromes (MESF) were calculated for each cell type (Table 3). The quantitative flow cytometry measurements showed 6 x 10^3 to 5 x 10^4 photoswitchable proteins per cell on the cell membrane. This method provides an upper limit to the number of proteins as multiple secondary antibodies can bind to one primary antibody. The interaction between cells expressing complementary heterodimerizing proteins is limited by the protein with the lower expression levels on the cell surface (iLID-/Nano-MDA around 1.2 x 10^4 proteins per/cell, nMag-/pMag-MDA around 2.1 x 10^4 proteins/cell and nMagHigh-/pMagHigh-MDA 6.0 x

10^3 proteins/cell). The expression of the photoswitchable proteins on the cell surface was compared to the cadherins that have similarly overexpressed as adhesion molecules with 2 x 10^4 to 2.5 x 10^5 cadherins on the cell surface per cell.[159] Moreover, Duguay et al. analyzed the expression of different cadherins (E-/P-/N-cadherin) with around 2.4 to 15.8 x 10^4 E-cadherins per cell, which lead to a specific cell adhesion and sorting behavior.[49]

Table 3: Quantification of photoswitchable proteins on the cell surface.

Name	**Molecules of Equivalent Soluble Fluorchrome (MESF)**
iLID-MDA	1.2×10^4
Nano-MDA	5.0×10^4
nMag-MDA	2.1×10^4
pMag-MDA	4.6×10^4
nMagHigh-MDA	1.6×10^4
pMagHigh-MDA	6.0×10^3

In this thesis, I used MDA-MB-231 cells to demonstrate the concept, yet these genetically encoded photoswitchable proteins could be transfected and used to mediate cell-cell interactions between other cell types too. After confirming the expression of the photoswitchable proteins on the cell surface, I investigated if the photoswitchable proteins can mediate light-triggered cell-cell interactions, cells expressing complementary interaction partners (iLID-MDA and Nano-MDA, nMag-MDA and pMag-MDA, nMagHigh-MDA and pMagHigh-MDA) were incubated in suspension in the dark and under blue light illumination for 30 min. The mixed cultures of two complementary cell types aggregated significantly under blue light but remained scattered in the dark as observed in bright field images (Figure 15).

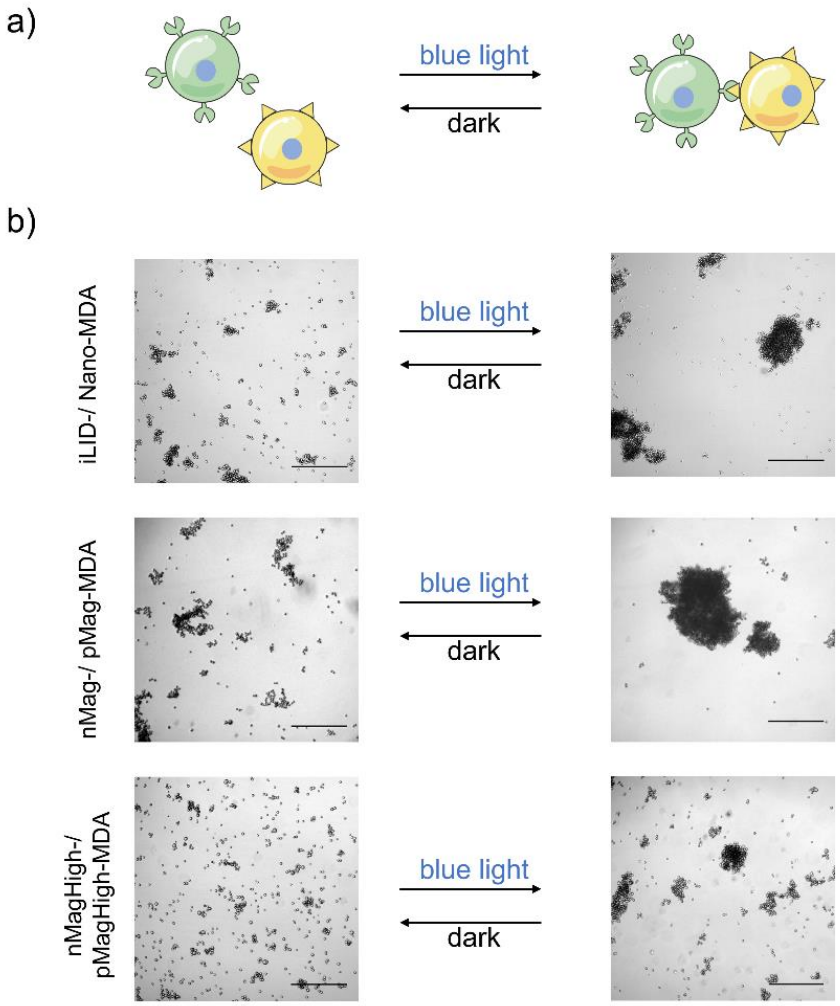

Figure 15: Blue light induced cell-cell interactions. a) Schematic principle of light induced cell-cell contacts by using photoswitchable proteins on the cell surface. b) Bright field images from iLID-/Nano-MDA, nMag-/pMag-MDA and nMagHigh-/pMagHigh-MDA expressing MDA-MB-231 cells that are kept in dark or illuminated with blue light. Scale bars are 500 µm.

The mixed cultures of two complementary cell types aggregated significantly under blue light but remained scattered in the dark as observed in bright field images (Figure 15). To quantify the cell aggregation, large areas of the samples were scanned (1 cm^2 to 2.56 cm^2 per sample containing about 25000 cells/cm^2), and cell aggregates with a two-dimensional projected area of larger than 5000 µm², i.e. contain at least 20 cells, were detected as clusters using automated image analysis. In each of the three co-cultures,

blue light resulted in the assembly of multicellular structures with a significantly higher mean cluster area than in the dark (Figure 16 a).

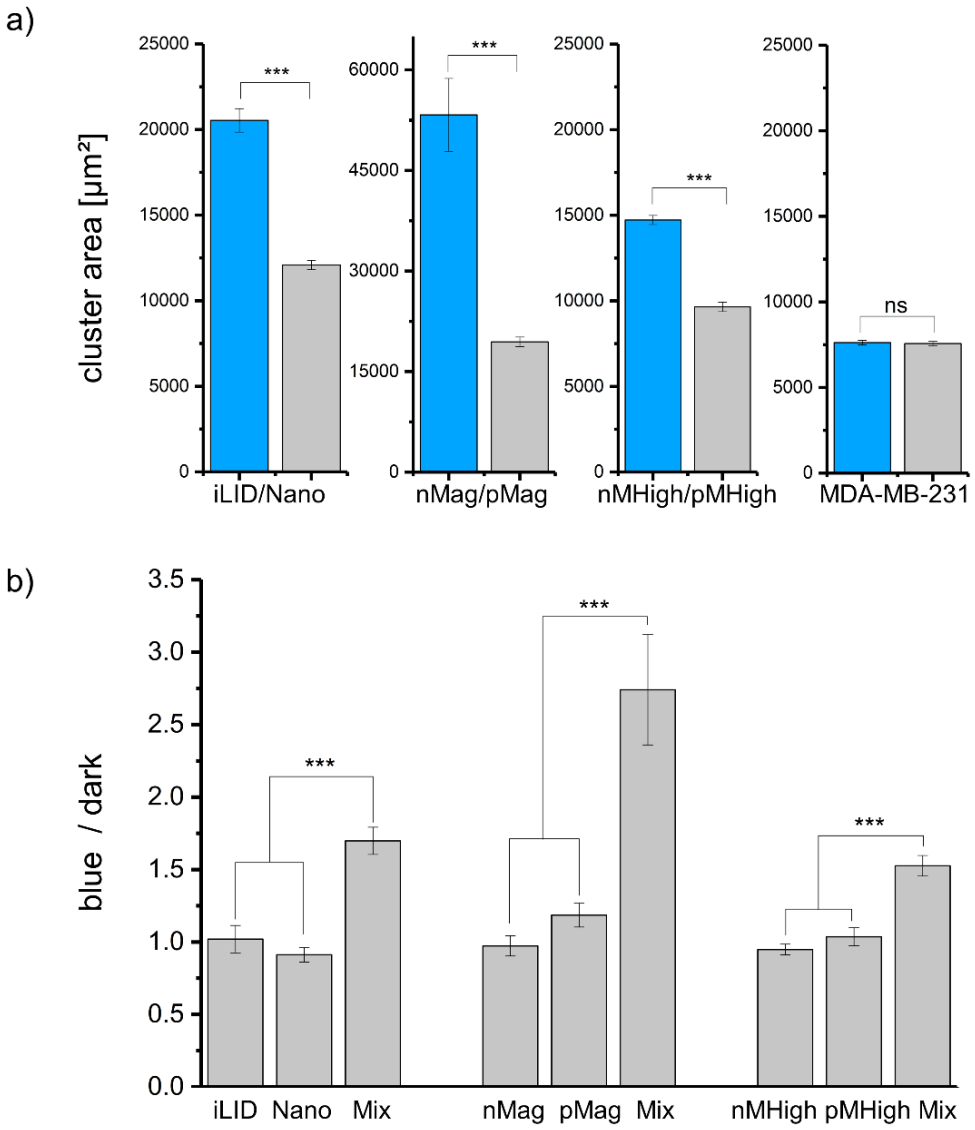

Figure 16: a) Graphical representation of light induced cell clustering as a result of 30~min illumination at 20 rpm. p value ***<0.001. b) Graphical representation of cluster-size ratio between blue light illuminated and dark, homo- and heterocultures.

In should be noted that this image analysis method underestimates the cluster size of the cell aggregates because the three-dimensional cell clusters are reduced to their 2-dimensional projected area. Yet, this reduction of 3D cell clusters to 2D objects is necessary due to technical reasons because 3D imaging and their analysis for so many

and large sample sizes is not plausible. The nMag-/pMag-MDA cells showed the largest cluster sizes upon illumination with blue light with an average cluster size of around 5 x 10^4 µm^2 followed by iLID-/Nano-MDA with around 2 x 10^4 µm^2 and nMagHigh-/pMagHigh-MDA with 1.5 x 10^4 µm^2. The cluster size differs for different photoswitchable cell-cell interactions under blue light around 3-fold. This difference is possibly due to the differences in protein expression on the cell surface (nMag-/pMag-MDA > iLID-/Nano-MDA > nMagHigh-/pMagHigh-MDA) and differences in interaction strength (Figure 16 b). On the contrary, the non-transfected MDA-MB-231 cells, used as a negative control, showed no significant clustering following this analysis and no difference in aggregation under illumination with blue light and in the dark.

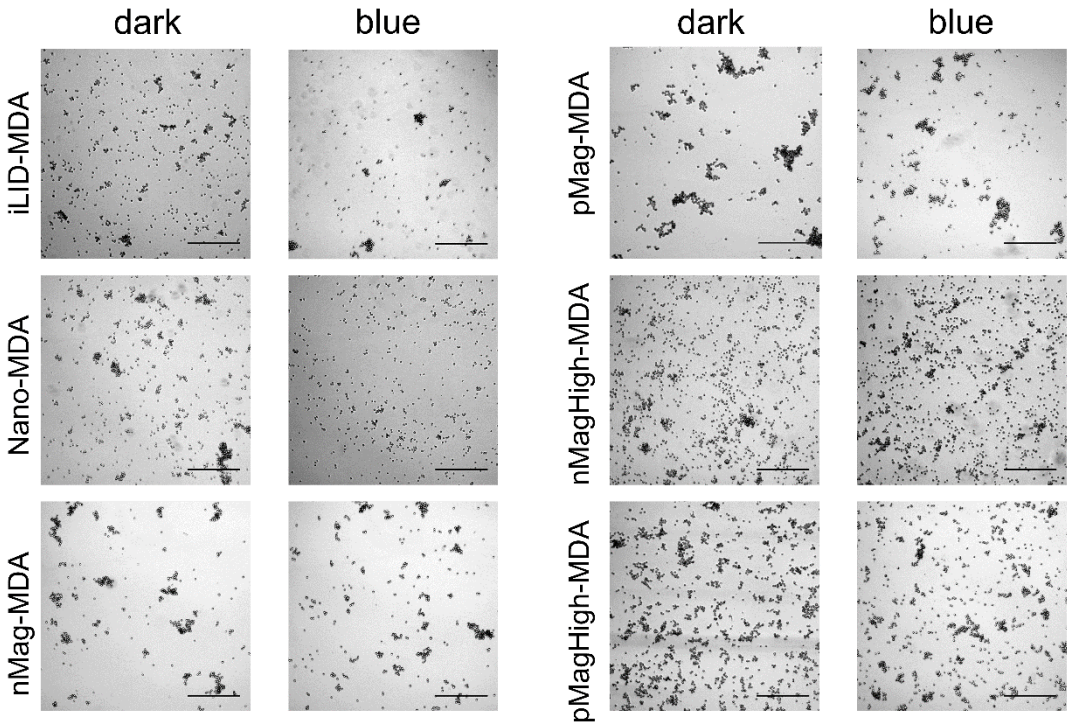

Figure 17: Bright field images of cell clustering in monocultures. The monocultures with 1x10^6 cells of each subtype were incubated at 20 rpm orbital shaking under blue light or dark and fixed with 4% paraformaldehyde. In monocultures the cells did not cluster significantly and the cell clustering did not change with blue light illumination. Scale bars are 500 µm.

After the light induced aggregation of cells, the question was of these interactions were indeed due to the specific heterodimerization of the protein pairs under blue light or if

homophilic interactions also contribute to the aggregation. Therefore, monocultures of each cell line were incubated under blue light and dark as described above (Figure 16 b, 17). For comparison, the ratio of the cell aggregation under blue light to the dark was determined for homo and hetero cultures. The blue to dark ratio was one for iLID-MDA and Nano-MDA cells individually showing that there is no light dependent change in aggregation in monocultures. On the other hand, this ration increased in the mixed cultures to around 1.7-fold. Similarly, nMag-MDA and pMag-MDA monocultures showed no specific blue light triggered interaction and a 2.7-fold increase in cluster area under blue light in the mixed sample. Likewise, the nMagHigh-MDA and pMagHigh-MDA cells showed no increase in aggregation under blue light in monocultures and 1.5-fold increase in aggregation under blue light in mixed cultures. Overall, it should be noted that there is some background aggregation of a single cell lines, but it is not significantly different under blue light and in the dark. Thus, the light depended interactions between cells are a result of the specific heterodimerization of the proteins expressed on the cell surface.

Triggering cell-cell interactions with blue light has the advantage of low cell toxicity compare to UV-light, which was used in the literature before.[92,160] To demonstrate that this is also the case under the here used experimental conditions and exclude the blue light toxicity towards MDA-MB-231 cells, cells were incubated under at 800 µW/cm^2 for 4 hours (compare to the used 272 µW/cm^2 in all presented experiments). These experiments showed no significant decrease in cell viability.[161] Thus the blue light is not

affecting the cell viability the cells can be treated with blue light and in the dark and the results can be compared with each other.

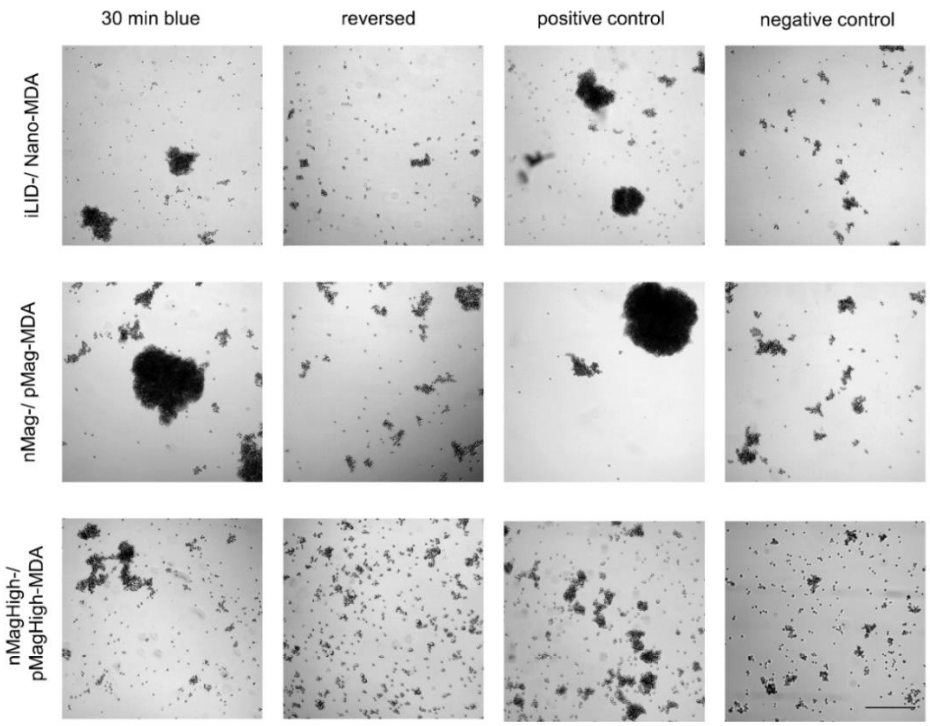

Figure 18: Bright field images of dark reversion after 30 min blue illumination, after reversion (iLID-/Nano-MDA, nMag-/pMag-MDA 90 min and nMagHigh-/pMagHigh-MDA cells 180 min dark after blue light illumination. The positive control shows the cell illuminated for the whole experiment in blue light and negative control in the dark. Scale bars are 500 µm.

The reversibility of cell-cell interactions is a key feature of cell-cell adhesions in biology and indispensable for the self-sorting following the differential adhesion hypothesis. The protein pairs iLID/Nano, nMag/pMag, and nMagHigh/pMagHigh, were selected due to their different reversion kinetics in the dark, (iLID/Nano $t_{1/2}$= 20 sec, nMag/pMag $t_{1/2}$= 1.8 h, nMagHigh/pMagHigh $t_{1/2}$= 4.7 h).[30] When cocultures of cells expressing complementary interaction partners were preaggregated for 30 min under blue light illumination and then placed in the dark all three aggregate types dissociated, yet with different time dependences (Figure 18, 19). The bright field images showed the aggregation of the cells after 30 min illumination with blue light and the bright field images after the reversion after 90 min in the dark for nMag-/pMag-MDA and iLID-Nano-MDA

and 180 min incubation in the dark for nMagHigh-/pMagHigh-MDA. The positive control was illuminated the whole experiment in blue light and the negative control kept in dark (Figure 18, 19).

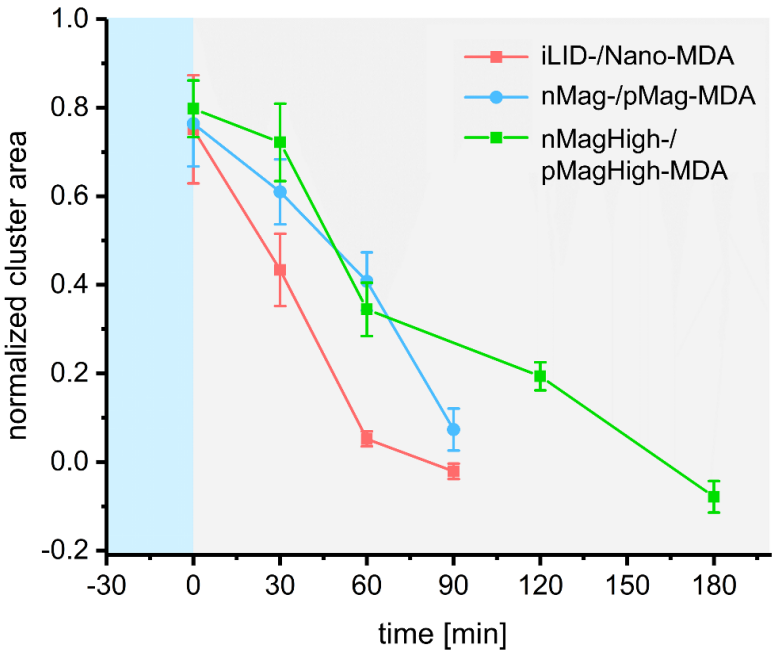

Figure 19: Reversion kinetics of iLID/Nano-MDA, nMag/pMag-MDA and nMagHigh/pMagHigh-MDA cells. The cells were preincubated for 30 min with blue light. Afterwards the cells were transferred into the dark and samples taken at different time points. The control was illuminated the whole experiment in blue light or dark (iLID/Nano-MDA and nMag/pMag-MDA for 90 min and nMagHigh/pMagHigh for 180 min). The cluster area was calculated between the positive control (value=1, that was kept the whole experiment in blue light) and the negative control (value=0, that was kept in the dark).

The aggregates in iLID-/Nano-MDA cocultures disassembled the fastest within 60 min, aggregates in nMag-/pMag-MDA cocultures disassembled within 90 min and in nMagHigh-/pMagHigh-MDA cocultures disassembled the slowest over 180 min. This trend corresponds to reversion time at the molecular level, which is iLID/Nano < nMag/pMag < nMagHigh/pMagHigh.[107,137] The disparity in the absolute values for the reversion for the cell-cell interactions to the protein level could potentially be due to multivalent protein-protein interactions between cells, processes that are coupled to the cell-cell interactions beyond the photoswitching and the display of the proteins on the extracellular cell surface.

3.2 Dynamic cell-cell interactions

The second striking difference between different photoswitchable protein pairs was the morphology of the multicellular aggregates formed (Figure 15). iLID-/Nano-MDA cocultures and nMag-/pMag-MDA cocultures formed compact aggregates with smooth edges after 30 min under blue light. On the other hand, in nMagHigh-/pMagHigh-MDA cocultures of under the same conditions formed lose and ramified aggregates with irregular shapes. Furthermore, iLID-/Nano-MDA and nMag-/pMag-MDA aggregates were also larger than nMagHigh-/pMagHigh-MDA aggregates.

These observations suggest that the kinetic and thermodynamic parameters of the cell-cell interactions play an important role in the self-assembly of multicellular structures. While iLID-/Nano-MDA and nMag-/pMag-MDA aggregates exemplify the RLCA dominated by thermodynamic control, aggregates of nMagHigh-/pMagHigh-MDA cells are examples of the DLCA and are mostly under kinetic control. This data also parallels reaction and diffusion limited cluster aggregation observed in colloidal polystyrene particles coated with iLID and Nano or nMagHigh and pMagHigh, respectively.[70] These observations directly correlate with the stronger protein-protein interaction between nMagHigh/pMagHigh and slower on/off rates compared to the weaker and more dynamics protein-protein interaction between nMag/pMag and iLID/Nano.

Next, I wanted to explore whether I could shift the self-assembled multicellular architectures from kinetically to thermodynamically controlled structures by altering the strength and dynamics of the cell-cell interactions. The photoswitchable cell-cell interactions provide a unique opportunity to address this question as protein-protein interaction strength and dynamics can be tuned using pulses of light.[162,163] For this purpose, I incubated different cocultures under blue light illumination with varying on and off times for a total of 2 h,(continuous 120 min on, 30 sec on/ 30 sec off (only for iLID-/Nano-MDA), 1min on/ 1 min off (only for iLID-/Nano-MDA), 5 min on/ 5 min off, 20 min

on/ 20 min off, 1 min on/ 19 min off), (Figure 20). The longer incubation period of 120 min was chosen to give the cells the possibility to rearrange and adapt within the clusters, compare to the before used incubation period of 30 min.

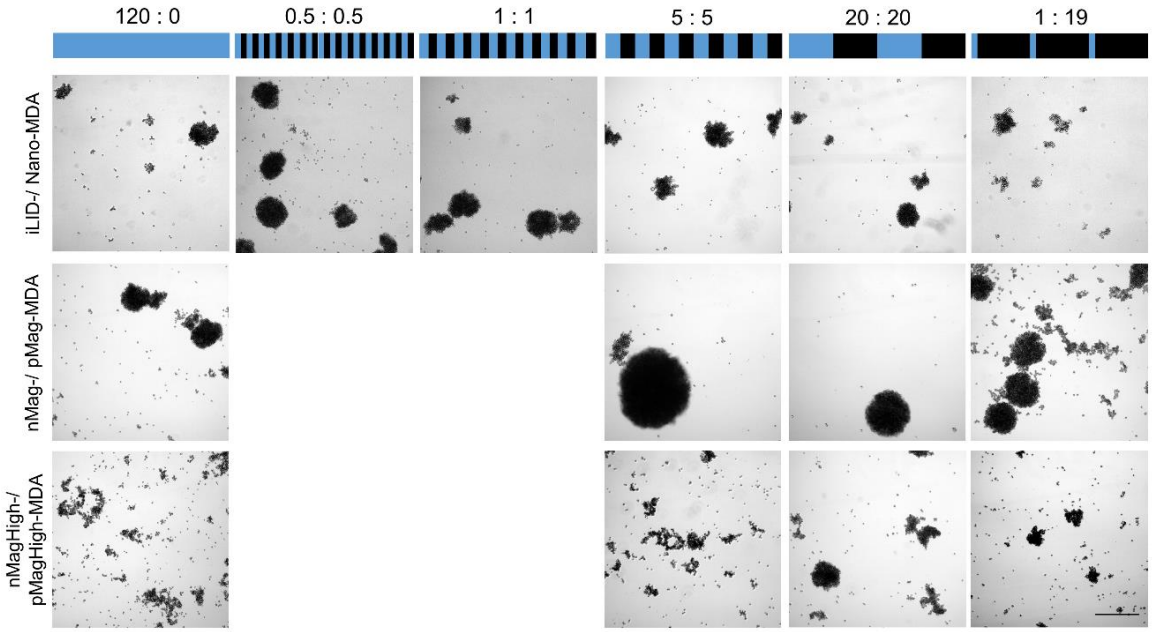

Figure 20: Variability of cell clustering efficiency with pulsing sequences of blue-light and dark incubation. The cells were incubated on an orbital shaker during pulsing While iLID-/Nano-MDA formed biggest clusters started in short pulsing sequences like 0.5 min blue light and 0.5 min dark (0.5 : 0.5) to 5 min blue light and 5 min dark (5 : 5), nMag-/pMag-MDA heterodimers formed biggest clusters at 5 min blue light and 5 min dark periods (5 : 5), nMagHigh-/pMagHigh-MDA biggest clustered at 20 min pulsing sequence (20 : 20). The different pulsing are represented in blue light [min] : dark[min], Scale bar = 500 µm.

I observed that different multicellular aggregates formed depending on the illumination frequency. Outstandingly, less total illumination but in pulses lead to an increase in cell aggregation for iLID-/Nano-MDA (0.5 min on/ 0.5 min off, 1 min on and off and 5 min on and off), nMag-/pMag-MDA cells (5 min on/ 5 min off, 20 min on/20 min off and 1 min on/ 19 min off) as well as nMagHigh-/pMagHigh-MDA cells (5 min on/ 5 min off and 20 min on/ 20 min off and 1 min on/ 19 min off) as also evident by the increase in the mean cluster area (Figure 21 a, c, e). The experiments were performed with the same number of cells; therefore the number of clusters were also analyzed (Figure 21 b, d, f). The number of clusters showed a decrease as the cluster area increased. This shows that at

this point smaller clusters fuse to form larger ones and in parallel decreasing the total number of clusters. For example, largest clusters of nMag-/pMag-MDA cells formed using 5 min pulsing periods where all cells assembled into around 8 clusters per cm^2. On the other hand, smallest clusters formed with nMagHigh/-pMagHigh-MDA cells under continuously illumination with an increase to around 100 clusters per cm^2.

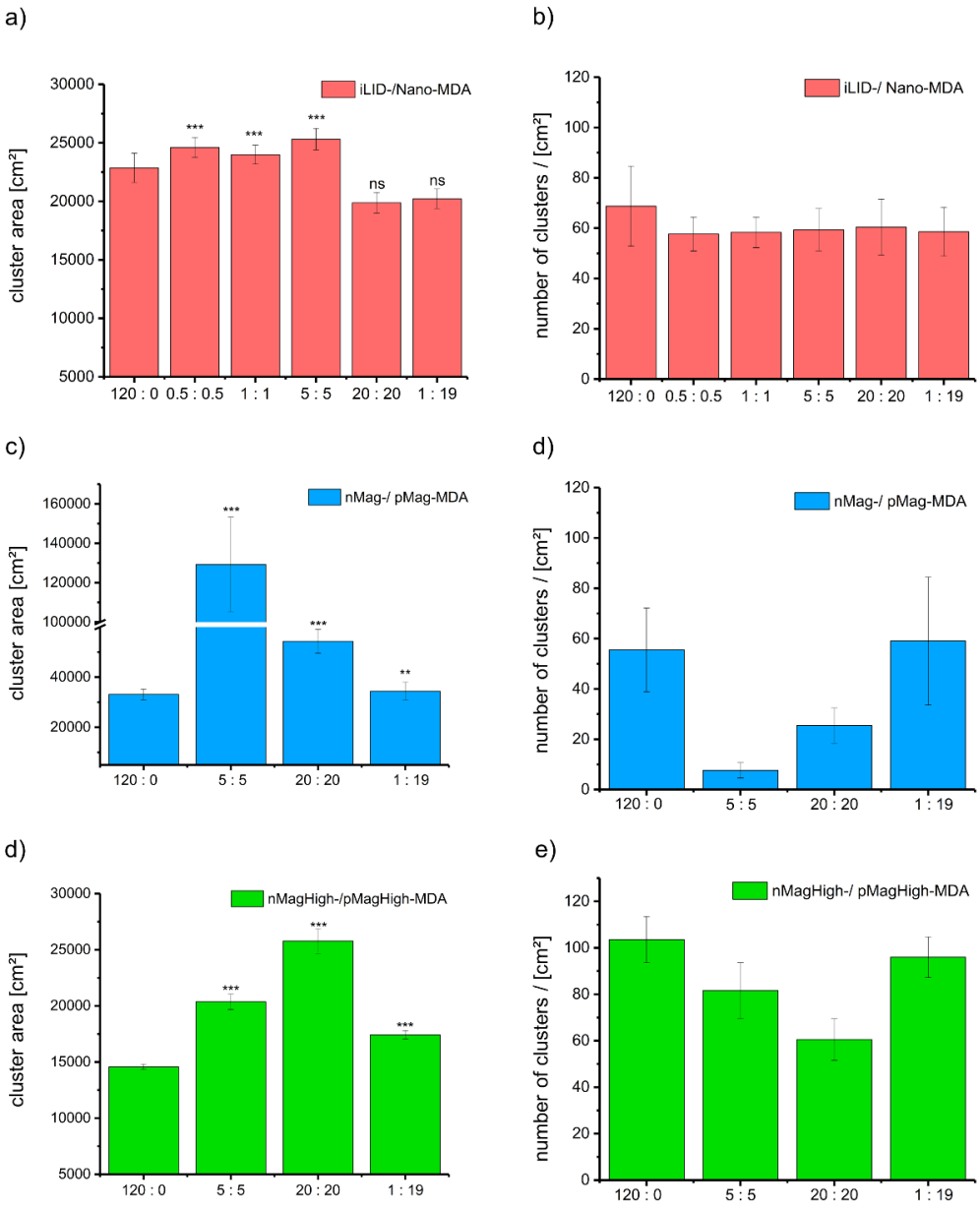

Figure 21: Graphical representation of the mean cluster area plotted against various pulsing sequences. The different pulsing are represented in blue light [min] : dark[min].

The increase in the area by pulsing light shows that pulsed illumination can lead to increased aggregation if the cell-cell interactions partially revert and cells can reposition themselves when the light is off such that upon reactivation with blue light cells can optimize their position and increase interactions with their neighbors. For this reason, longer pulsing periods (20 min on/ 20 min off) enhances aggregation for nMagHigh-/pMagHigh-MDA cells with slower dark reversion and a faster pulsing (5 min on/ 5 min off) enhances aggregation for nMag-/pMag-MDA and also 30 sec of pulsing increased the area of iLID-/Nano cells with faster dark reversion. iLID-/Nano-MDA cells, which have the fastest reversion time, pulsed illumination could not be increase the cell aggregation with longer dark periods than 5 min pulsing periods.

Longer off time (20 min on/ 20 min off) or less photoactivation (1 min on/ 19 min off) lead to a decrease in aggregation in all three photoswitchable cell-cell interaction pairs. This trend was best observed with nMag-/pMag-MDA cell aggregation, which increased with 5 min on/ 5 min off pulsing compared to continuous illumination, but decreased with lower pulsing frequency (20 min on/ 20 min off) although the total light dose was the same and even further if the photoactivation was decreased (1 min on/ 19 min off). The nMagHigh-/pMagHigh-MDA showed also a decrease of the cluster area with a 1 min blue light and 19 min dark periods that was different to the faster reversion of iLID-/Nano-MDA and nMag-/pMag-MDA that decreased the area of the cluster area at 20 min on and off pulsing. Thus, if the reversion of the cell-cell interactions in the dark is extensive or the reactivation with blue light is not sufficient, aggregates disassemble and the shorter the dark reversion time the photoswitchable protein the more pronounced this disassembly is. Taken together, this data shows that not only the cell-cell interaction strength but also their dynamics here modulated with pulsed illumination, are critical for the self-assembly of multicellular structures.

The second aspect that is closely related to the cell-cell interaction dynamics is the morphology of the multicellular assemblies, which vary from lose and ramified to compact and spherical going from DLCA to RLCA.[72] As observed above (Figure 20, 21), aggregation increases when cell-cell interaction are only partially reversed with pulsing, so that the cells could transiently reposition and strengthen their contact with neighboring cells. This could represent a shift from kinetically to thermodynamically controlled structures. To rationalize and quantify the relationship between morphology of the cluster and interaction dynamics, I determined the fractal dimension of the two dimensional contours of these multicellular aggregates as a measure of cluster shape complexity and size[78] (Figure 22, 23).

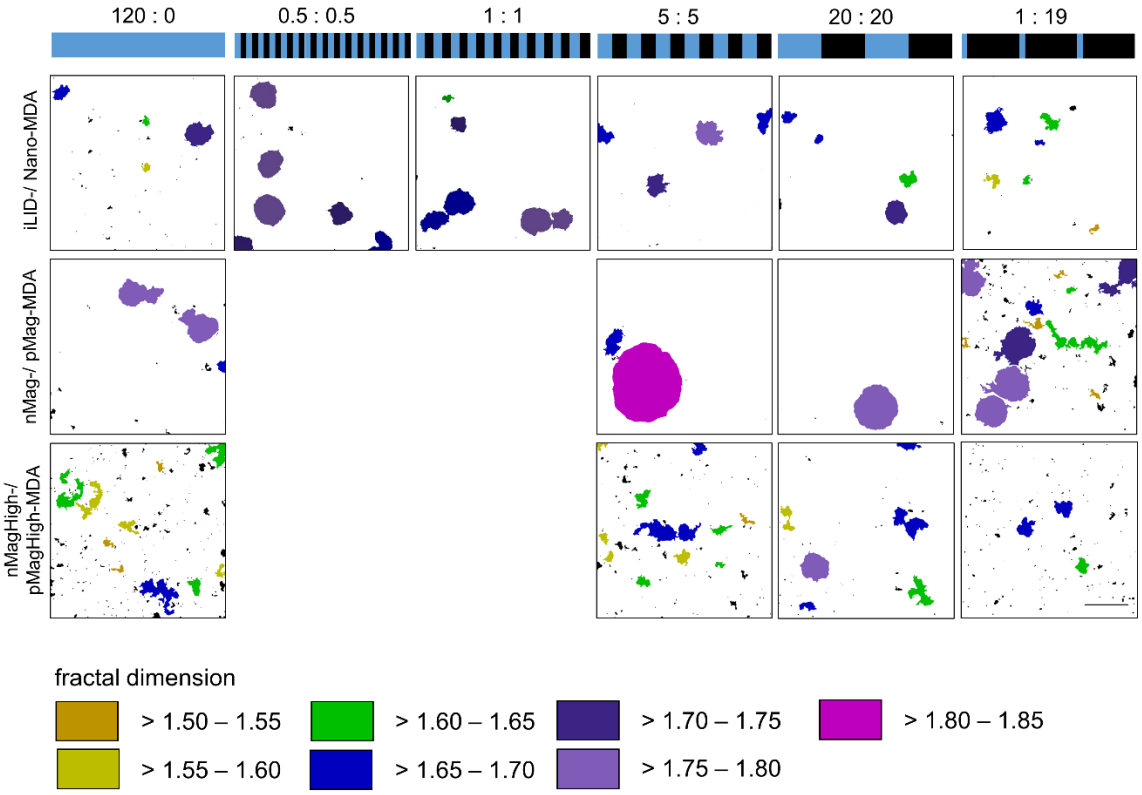

Figure 22: Exemplary fractal dimension analysis of cell clusters in the images shown in Figure 18. The fractal dimension of the cell clusters varies with different blue light illumination frequencies and the photoswitchable proteins on the cell displayed at the cell surface. Scale bar is 500 µm.

For comparison in colloidal systems, the fractal dimension increases from 1.46 for DLCA to 1.55 for RLCA for two dimensional aggregates.[164] For the cellular assemblies, I observed a significant range of the mean fractal dimensions from 1.595 for at nMagHigh-/pMagHigh-MDA cells under constant blue light dominated by DLCA to 1.651 for nMag-/pMag-MDA cells with 5 min pluses of blue light dominated by RLCA (Figure 23).

The individual clusters showed a higher variance from clusters with a fractal dimension of 1.5 to above 1.8 (Figure 22). Under constant activation, the fractal dimension was higher for assemblies based on protein-protein interactions with faster dynamics, (iLID/Nano and nMag/pMag), achieving thermodynamically driven structures. On the contrary, nMagHigh-/pMagHigh-MDA cells formed stronger and less dynamic interactions leading to kinetically trapped structures with lower fractal dimension. Pulsed photoactivation increases the dynamics of the cell-cell interactions; gives the cells an opportunity to rearrange and form a thermodynamically more stable structure, shifting the assembly from DLCA to RLCA as observed in both nMag-/pMag-MDA and nMagHigh-/pMagHigh-MDA cells. As shown in Figure 23, nMagHigh-/pMagHigh-MDA cells under constant blue light formed branched clusters with low fractal dimension of 1.595, which increased up to 1.61 as the time in the dark increased and the photoactivation time decreased. Likewise, for nMag-/pMag-MDA cell assemblies the fractal dimension increased when 5 min on/ 5 min off pulsing was used compared to continuous blue light illumination. Beyond 5 min on/ 5 min off pulsing, both the cluster size and fractal dimension reduced, suggesting excessive disassembly with increase in reversion time in the dark. Moreover, the pulsing frequency required to achieve more thermodynamically controlled assemblies i.e., RLCA, is closely connected to the reversion kinetics of the photoswitchable proteins. While 5 min on/ 5 min off pulsing was the best for the nMag/pMag pair with the faster dark reversion kinetics, the nMagHigh/pMagHigh interactions with slower kinetics required longer dark periods (ca.

20 min) and less photoactivation to release the kinetically trapped structures and transform them into more compact assemblies.

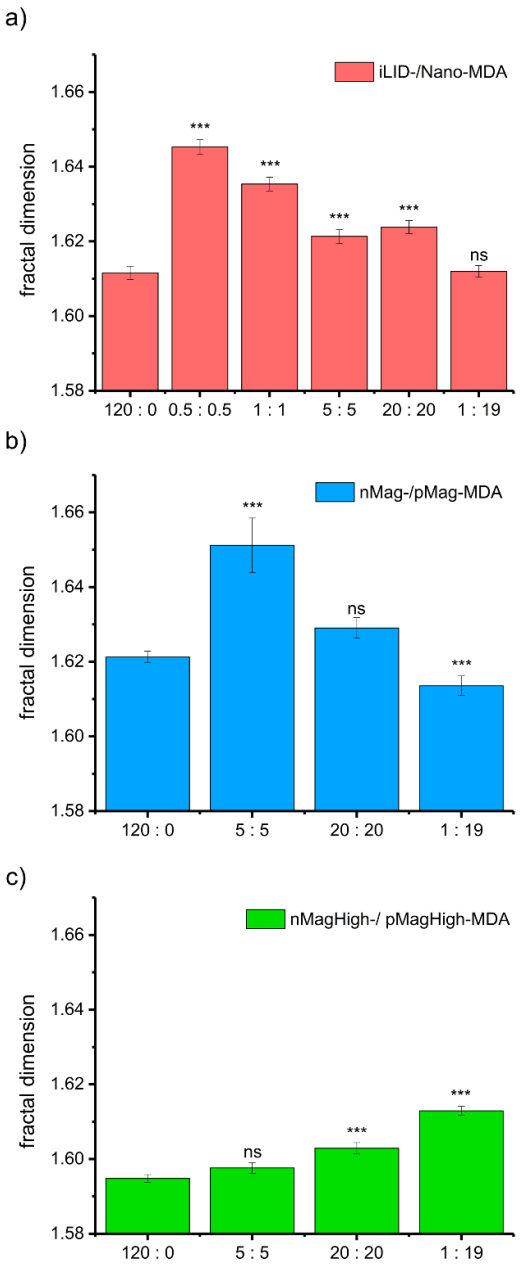

Figure 23: Graphical representation of the mean cluster area plotted against various pulsing sequences. The samples iLID/Nano-MDA, nMag/pMag-MDA and nMagHigh/pMagHigh-MDA were illuminated with blue light in different pulsing patterns, (blue light [min]: dark [min]).

The iLID-/Nano-MDA and nMag-/pMag-MDA cells showed the fractal dimension at the pulsing of 30 sec min pulsing and decreased until 5 min pulsing where it still showed a

significant higher fractal dimension to the constant illumination, iLID-/Nano also with 20 min pulsing area and fractal dimension decreased afterwards to the same fractal dimension they started at continuously illumination. The correlation of the highest area and fractal dimension could be explained by stable thermodynamically formed clusters that are able to interact with other cells rearrange and grow. Bigger clusters are also increase the possibility to meet other cells by diffusion. The decease of fractal dimension could be explained by the weak interaction between the cells when the aggregates getting to big and break apart, which could be seen in the nMag-/pMag-MDA cells at 1 min blue light and 19 min dark periods with a variance of cluster sizes and shape (Figure 20, 22). The fractal dimension also decreases significantly to a value lower to the continuously illumination of 120 min blue light. Compare to the faster dissociation of iLID-/Nano-MDA cells that decrease the fractal dimension to the value of constant illumination and not lower. This could be explained by the dynamics are not allowing to create bigger aggregates compare to the nMag-/pMag-MDA cells.

This range of cluster aggregation is between the DLCA and RLCA and shows the possibilities of tuning photoswitchable proteins on the cell surface to influence the organization of the cell aggregates, additionally there are numerous more options how these interactions can be modified by changing the experimental condition with pulsing light. Looking at a larger aspect the dependency of cell behavior on protein-protein interactions kinetics in multicellular structures can be describe in similar terms as colloid assembly and used in the design of bottom-up tissues.

3.3 Social self-sorting

In the third part of this thesis the specific light dependent interactions and dynamics of the induced cell-cell interactions are be used to achieve a social self-sorting of a four-component mixture of two distinct families.

Sorting-out/self-sorting is important mechanism in nature to form multicellular structures out of multiple cell types and organize them in subdomains, as observed during embryogenesis and *in vitro* reconstitution studies of different tissue types.[152] Achieving self-sorting in the context of bottom-up tissue engineering requires multiple orthogonal cell-cell interaction pairs with different interaction strengths, and each of these must be dynamic enough for cells to maximize the interactions with neighboring cells. If the cell-cell interactions are not dynamic enough, kinetically trapped architectures away from the thermodynamic optimum with no self-sorting form could form. To achieve sorting-out and multicellular structures with subdomains, I mixed four different cell types expressing two orthogonal protein pairs at their surface. In particular, I mixed iLID-/Nano-MDA expressing cells (each stained in red) with either nMag-/pMag-MDA or nMagHigh-/pMagHigh-MDA expressing cells (each stained in green), to check if their orthogonal specificity could result into self-sorting in a heterogeneous culture[70] (Figure 24). Cells expressing nMag, pMag, nMagHigh and pMagHigh were not combined as these proteins bind to one another.[137] In both of the four component mixtures, I observed light-dependent aggregation under continuous blue light illumination overnight (Figure 24 b), yet the aggregates differed in the organization of the different cell types. In the former mixture, iLID- and Nano-MDA cells (stained in red) clustered separately from the nMag- and pMag-MDA cells (stained in green), showing social sorting of the four cell types (Figure 24 b, right).

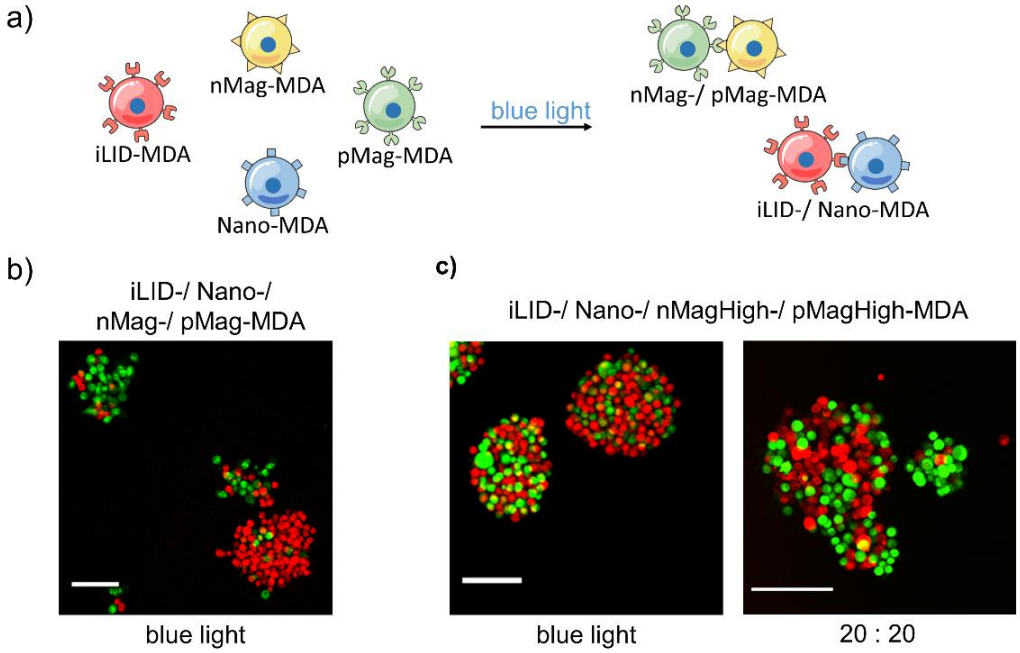

Figure 24: a) Schematic overview of social self-sorting of iLID-/Nano-MDA cells and nMag-/pMag-MDA cells into separate clusters under blue light. Confocal images of the prestained iLID-/Nano-MDA cells (shown in red) and nMag-/pMag-MDA cells (shown in green) in the dark and under blue light. b) Confocal images of the prestained iLID-/Nano-MDA cells (shown in red) and nMag-/pMag-MDA cells (shown in green) in the dark and under blue light. c) Confocal images of prestained iLID-/Nano-MDA cells (shown in red) and nMagHigh-/pMagHigh-MDA cells (shown in green) under constant and pulsed blue light (20 min on/20 min off). All scale bars are 100 µm.

On the other hand, in the mixture of iLID-, Nano-, nMagHigh- and pMagHigh-MDA cells, the green and red labelled cells were homogenously intermixed within the same multicellular structure and the four cell types aggregated together (Figure 24 c, left). For quantification of the area the cells were monitored with a bright field microscope, similar to the experiments above to analyze the area (Figure 25 a, c). The bright field images showed an increase in are at the illumination with blue light overnight compare to the dark sample. Interestingly, the pulsing of the iLID-/Nano-/nMagHigh-/pMagHigh-MDA cells showed an increase in area by the pulsing of blue light of 20 min on/off overnight (Figure 25 b, d).

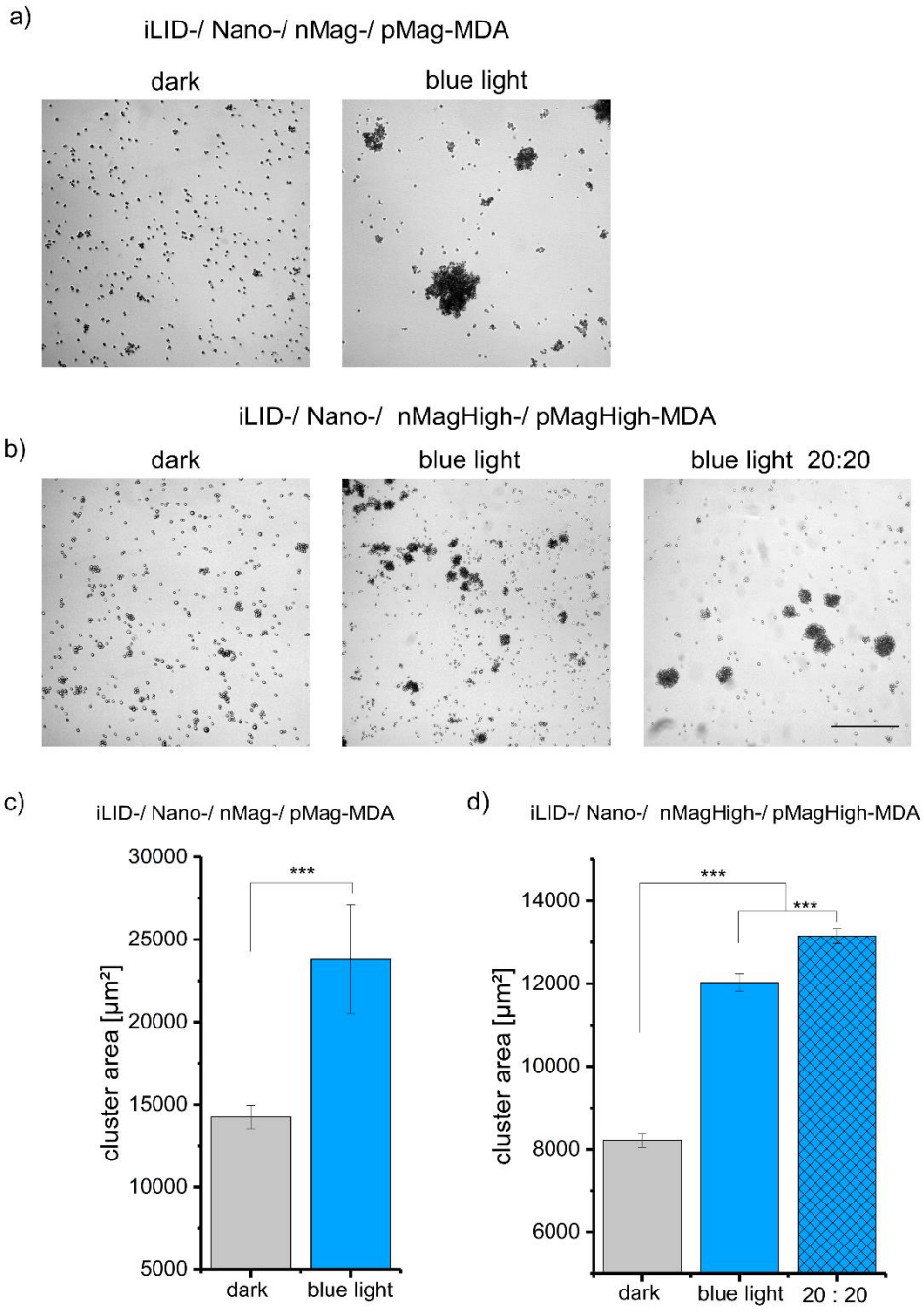

Figure 25: Bright Quantification of the mean cluster area for four cell type mixtures in d) b and e) c. Each experiment was performed in two biological replicates with technical triplicates. 64 images with a total area of 2.56 cm^2 were analyzed in each sample, each done in biological duplicated with 3 technical replicates. Error bars are the standard error of the mean cluster area, p-value < 0.001 represented as ***.

For quantification the images were analyzed by using colocalization of the fluorescence signals. The threshold overlap score (TOS) described the colocalization from complete colocalization (value 1) over noncolocalisation (value 0) to complete anticolocalization

(value -1), (Figure 26). The iLID-/Nano-/nMag-/pMag-MDA sample shown a smaller TOS value, meaning non colocalized by the illumination of blue light, followed by iLID-/Nano-/nMagHigh-/pMagHigh-MDA (20:20) and constant blue light illumination. The cells formed subunits within the same aggregate (Figure 24 c, right).

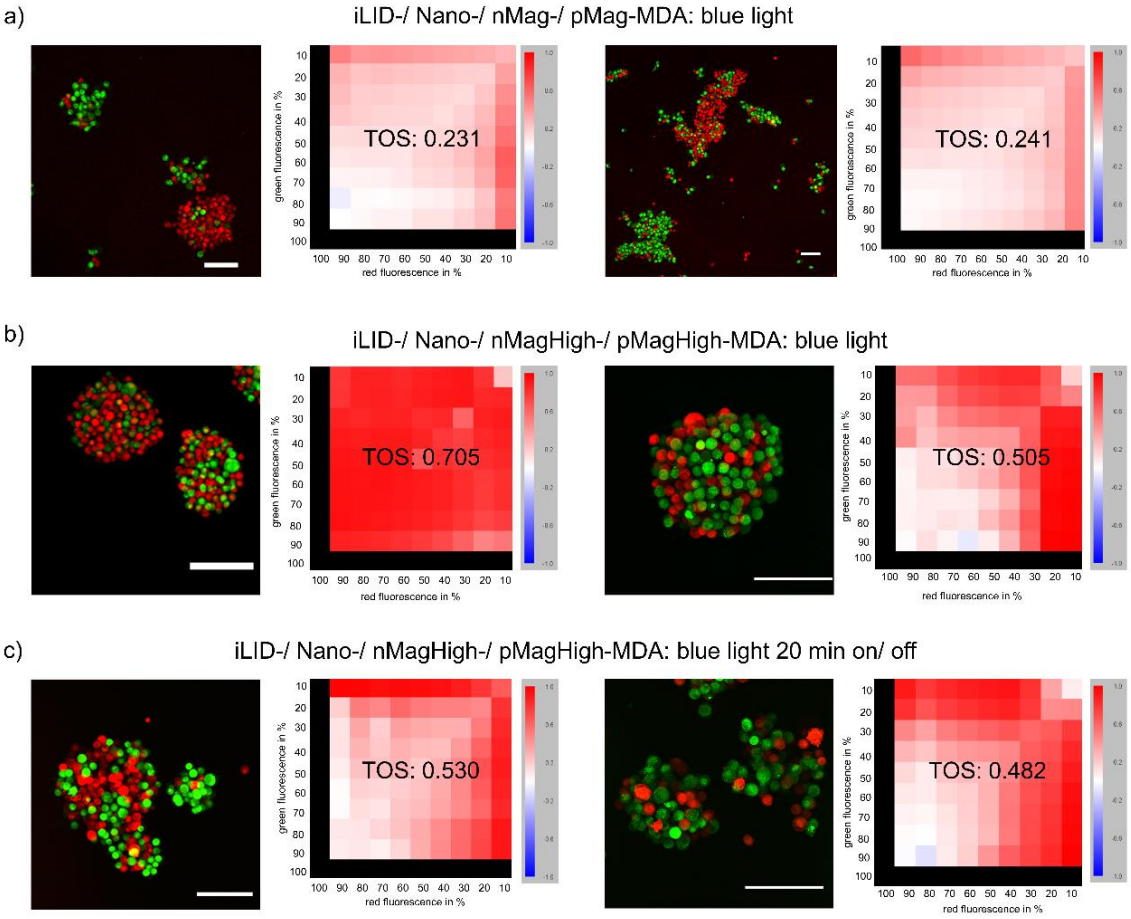

Figure 26: Analysing colocalization of social self-sorting. a) iLID/ Nano / nMag/ pMag-MDA illuminated with blue light. b**)** iLID/ Nano / nMagHigh/ pMagHigh-MDA illuminated with blue light. c) iLID/ Nano / nMagHigh/ pMagHigh-MDA illuminated with 20 min blue light pulses. Each pixel in the confocal z-stack image where analysed by the maximal intensity and split into green and red fluorescence. The colocalization of the pixels where analysed by using the metric matrix of the linear TOS values. The TOS value indicates a range from 1 complete colocalized, 0 noncolocalized and -1 complete anticolocalized. The metric matrix described the percentage of the highest intensity in 10% steps, meaning 10% are the highest intensity of pixels. Scale bars 100µm.

The fact that self-sorting, specifically social self-sorting [70] was observed combining the more dynamic cell-cell interaction pairs viz., iLID-/Nano-MDA and nMag-/pMag-MDA,

which favor thermodynamically controlled assemblies and not the nMagHigh/pMagHigh pair, which forms kinetically trapped structures, demonstrates also the importance of dynamics in self-sorting. In an attempt to increase the dynamics between the nMagHigh-/pMagHigh-MDA cells, 20 min on/ 20 min off pulsing was used to achieve self-sorting within the four-component mixture. The pulsing increased the area of the clusters, yet did not result in the complete self-sorting and only domains of green and red labeled Besides the significantly increased area of the cell aggregates by using light pulses, the social sorting could not be achieved with iLID-/Nano-MDA and nMagHigh-/pMagHigh-MDA cell (Figure 24 c, right). Indeed, the pulsing could not achieve a social sorting, so the aggregates are not completely intermixed and showed subdomains inside the aggregate. Additionally, single nMagHigh-/pMagHigh-MDA aggregates could be observed. These results showed the increase of the sorting out behavior of the different cell lines, but the interactions are not dynamic enough to result in completely separated social self-sorting.

4 Summary and outlook

In this thesis, I demonstrate the importance of cell-cell interaction dynamics in the assembly and self-sorting of multicellular structures from cells as building blocks under kinetic or thermodynamic control. Blue light triggered cell-cell interactions based on different photoswitchable protein interactions (iLID/Nano, nMag/pMag and nMagHigh/pMagHigh) with various binding strengths and dark reversion kinetics provide unique tools for modulating cell-cell interaction dynamics. Using different interaction pairs and the temporal control that light as a stimulus provides, I was able to assemble and tune multicellular structures from branched and ramified to compact and spherical. Moreover, in mixtures with four different cell types, I was able to achieve self-sorting provided that the cell-cell interactions were dynamic enough, as also postulated by the differential adhesion hypothesis. These finding showed that concepts of DLCA and RLCA aggregation as well as of self-sorting that are well-established for colloidal systems can also be applied to the self-assembly of cells into tissue like architectures. While to date cell-cell interactions have been controlled using chemical and genetic approaches, the importance of cell-cell interaction dynamics has not been considered. Most chemical approaches using DNA, clickable groups and biotin-streptavidin form strong interactions with low exchange rates and are hence expected to result in DLCA, which represent kinetically controlled branched structures. On the other hand, introducing different cadherins to the cell surface, which form highly dynamic protein-protein interactions, result in RLCA with round assemblies under thermodynamic control. In terms of dynamics, the photoswitchable cell-cell interactions based on different photoswitchable proteins offer a wide range of interaction dynamics and strengths, which can be modulated to achieve both kinetically and thermodynamically driven multicellular assemblies. In this respect bringing basic concepts of colloidal self-assembly to bottom-

up tissue engineering will help in the design of more predictable and complex micro-tissue structures.

The concept of self-sorting and the differences in interaction dynamics that lead to DLCA and RLCA have previously been demonstrated with polystyrene beads decorated with the photoswitchable proteins used in this study.

Chervyachkova et al. showed that like the cells used here iLID and Nano decorated beads form cluster with RLCA and nMagHigh and pMagHigh decorated particles form clusters with DLCA under blue light. Moreover, within mixtures of four bead types each decorated with one of these proteins social sorting was observed with iLID/Nano decorated beads forming separate assemblies than nMagHigh/pMagHigh decorated particles.[70]

Table 4: Cluster aggregation and fractal dimension of polystyrene particles by using different photoswitchable proteins on the surface of the beads.

Name	**Fractal dimension**	**area [µm²]**	**reference**
iLID-/Nano-beads	1.578	55.9	[70]
nMagHigh-/pMagHigh-beads	1.562	49.7	[70]

These observations with beads drove me to analyze the shape of the clusters formed with colloidal particles decorated with different photoswitchable proteins and compare their fractal dimensions to the results I achieved in this thesis with cells (Table 3). Similar to the cells, in the colloidal assemblies objects that were bigger than 30 μm^2, (correspond to the area of 10 beads) were considered as cluster. In this analysis, the iLID/Nano mediated aggregates showed a significantly higher fractal dimension of 1.578 compare to the fractal dimension of nMagHigh/pMagHigh mediated aggregates (p value < 0.001). Additionally, the average area of the clusters was significantly higher for iLID/Nano clusters (55.9 μm^2) compare to the area of nMagHigh-/pMagHigh clusters (49.7 μm^2) - (p value < 0.05). The analysis with the beads parallels the observation with the cells

displaying the same proteins at their surfaces. These results support the idea of the different binding interactions mediated by different photoswitchable proteins result in aggregates of different shapes. Therefore, this study drives the way to get one step further and demonstrates that observations with nonliving colloidal particles can also be transferred to cells.

The blue light switchable cell-cell interactions established here can further be used towards different purposes. To obtain different arrangements it would be of interest to use different stoichiometries of the two complementary cell types, which can lead to flower like or worm like assemblies. Moreover, the same photoswitchable interactions can be implemented onto other cell types that the here used MDA-MB-231 cells to combine cells with diverse functions. Additionally, in this thesis, I focused on the temporal control which light as an external trigger provides to induce cell-cell contacts but so far, the possibilities of spatial control were not exhausted. The spatial control could be also used to induce specific interaction limited to a certain region of interest. By using a microscope coupled to a digital mirror device, or a confocal microscope, it could be possible to illuminate such a certain area and induce controlled cell-cell contacts in a specific area and observe the behavior compare to the cells kept in the dark parallel.

The concepts of the photoswitchable cell-cell interactions, the importance of their dynamics and the self-sorting are transferrable to other types of cell-cell interactions that are mediated by other photoswitchable proteins. For example, Sentuerk et al. described recently asocial self-sorting behavior with colloidal particles using the proteins VVDHigh and Cph1, which homodimerize under blue and red light respectively. [69] Similarly, these proteins could be used to achieve asocial sorting in multicellular mixtures, complementary to the social sorting established here.

The here achieved social sorting could be coupled to the sorting out described in the DAH.[43] For example, in the enveloped arrangement requires low self-adhesion of one

cell and a high average adhesion between both cells in mixture. This could be achieved by using the different variants of the nMag/pMag proteins. The different cross interactions of nMagHigh to pMag and pMagHigh could be used to design such an enveloped assembly, with nMagHigh/pMagHigh expressing cells at the core and pMag-MDA cells together with nMagHigh-MDA cells to create an envelope. Therefore, the different cross interactions in the family of nMag-/pMag proteins and their different dynamics represents an interesting platform to self-assemble complex multicellular structures.

The question of how artificial cell-cell interactions influence the intracellular signaling pathways is another interesting aspect to address. The photoswitchable protein used here are anchored in the membrane of the cell but in contrast to the natural cell-cell adhesion proteins the cadherins do not have an intracellular domain that connects to the cytoskeleton and intracellular signaling networks. While the photoswitchable proteins are not involved in direct biochemical signaling pathways of the cell, the biophysical contract to the neighbors still has the potential to influence cell behavior. Thus, it would be interesting to study if the mechanical forces that are induced through the photoswitchable protein without a TM signal still change gene expression and cell behavior. Another possibility would be to add the intracellular domain of E-cadherins to the photoswitchable proteins to link to the actin cytoskeleton as well as the natural signaling pathway.

Bibliography

1. Langer, R. & Vacanti, J. P. Tissue Engineering. *Science* **260**, 920–926 (1993).

2. Rosso, F., Giordano, A., Barbarisi, M. & Barbarisi, A. From Cell-ECM Interactions to Tissue Engineering. *J. Cell. Physiol.* **199**, 174–180 (2004).

3. Athanasiou, K. A., Eswaramoorthy, R., Hadidi, P. & Hu, J. C. Self-Organization and the Self-Assembling Process in Tissue Engineering. *Annu. Rev. Biomed. Eng.* **15**, 115–136 (2013).

4. Breuls, R. G. M., Jiya, T. U. & Smit, T. H. Scaffold Stiffness Influences Cell Behavior: Opportunities for Skeletal Tissue Engineering. *Open Orthop. J.* **2**, 103–109 (2008).

5. Karimi, F., O'Connor, A. J., Qiao, G. G. & Heath, D. E. Integrin Clustering Matters: A Review of Biomaterials Functionalized with Multivalent Integrin-Binding Ligands to Improve Cell Adhesion, Migration, Differentiation, Angiogenesis, and Biomedical Device Integration. *Adv. Healthc. Mater.* **7**, 1–28 (2018).

6. Dhandayuthapani, B., Yoshida, Y., Maekawa, T. & Kumar, D. S. Polymeric scaffolds in tissue engineering application: A review. *Int. J. Polym. Sci.* **2011**, (2011).

7. Coenen, A. M. J., Bernaerts, K. V., Harings, J. A. W., Jockenhoevel, S. & Ghazanfari, S. Elastic materials for tissue engineering applications: Natural, synthetic, and hybrid polymers. *Acta Biomater.* **79**, 60–82 (2018).

8. Discher, D. E., Janmey, P. & Wang, Y. L. Tissue cells feel and respond to the stiffness of their substrate. *Science* **310**, 1139–1143 (2005).

9. Lv, H. *et al.* Mechanism of regulation of stem cell differentiation by matrix stiffness. *Stem Cell Res. Ther.* **6**, 1–11 (2015).

10. Li, S. Hydrolytic Degradation Characteristics of Aliphatic Polyesters Derived from Lactic and Glycolic Acids Suming. *J. Biomed. Mater. Res.* 342–353 (1998).

11. MacNeil, S. Progress and opportunities for tissue-engineered skin. *Nature* **445**, 874–880 (2007).

12. Vinatier, C. *et al.* Cartilage tissue engineering: towards a biomaterial-assisted mesenchymal stem cell therapy. *Curr. Stem Cell Res. Ther.* **4**, 318–329 (2009).

13. Hammouche, S., Hammouche, D. & McNicholas, M. Biodegradable bone regeneration synthetic scaffolds: in tissue engineering. *Curr. Stem Cell Res. Ther.* **7**, 134–142 (2012).

14. Cunha, C., Panseri, S. & Antonini, S. Emerging nanotechnology approaches in tissue engineering for peripheral nerve regeneration. *Nanomedicine Nanotechnology, Biol. Med.* **7**, 50–59 (2011).

15. Lawrence, B. D., Marchant, J. K., Pindrus, M. A., Omenetto, F. G. & Kaplan, D. L. Silk film biomaterials for cornea tissue engineering. *Biomaterials* **30**, 1299–1308 (2009).

16. Tiruvannamalai-Annamalai, R., Armant, D. R. & Matthew, H. W. T. A glycosaminoglycan based, modular tissue scaffold system for rapid assembly of perfusable, high cell density, engineered tissues. *PLoS One* **9**, (2014).

17. Iu, X. I. L. & Eter, P. X. M. A. Polymeric Scaffolds for Bone Tissue Engineering. *Ann. Biomed. Eng.* **32**, 477–486 (2004).

18. Elbert, D. L. Bottom-up tissue engineering. *Curr. Opin. Biotechnol.* **22**, 674–680 (2011).

19. Nichol, J. W. & Khademhosseini, A. Modular Tissue Engineering: Engineering Biological Tissues from the Bottom Up. *Soft Matter* **5**, 1312–1319 (2009).

20. M. S. Steinberg & Poole T. J. Strategies for specifying form and pattern: adhesion-guided multicellular assembly. *Philos. Trans. R. Soc. London Ser. B Biol. Sci.* **295**, 451–460 (1981).

21. Steinberg, M. S. Goal-Directedness in Embryonic Development. *Integr. Biol. Integr. Biol* 49–59 (1998).

22. Jakab, K. *et al.* Tissue engineering by self-assembly and bio-printing of living cells. *Biofabrication* **2**, 022001 (2010).

23. Haraguchi, Y. *et al.* Fabrication of functional three-dimensional tissues by stacking cell sheets in vitro. *Nat. Protoc.* **7**, 850–858 (2012).

24. Mironov, V., Boland, T., Trusk, T., Forgacs, G. & Markwald, R. R. Organ printing: Computer-aided jet-based 3D tissue engineering. *Trends Biotechnol.* **21**, 157–161 (2003).

25. Fedorovich, N. E., Wijnberg, H. M., Dhert, W. J. A. & Alblas, J. Distinct Tissue Formation by Heterogeneous Printing of Osteo- and Endothelial Progenitor Cells. *Tissue Eng. Part A* **17**, 2113–2121 (2011).

26. Lovett, M., Lee, K., Edwards, A. & Kaplan, D. L. Vascularization Strategies for Tissue Engineering. *Tissue Eng. Part B Rev.* **15**, 353–370 (2009).

27. Martin, I. *et al.* Bioreactor Cultivation Conditions Modulate the Composition and Mechanical Properties of Tissue-Engineered Cartilage. *J. Orthop. Res.* **17**, 130–138 (1999).

28. Aplin, A. E., Howe, A. K. & Juliano, R. L. Cell adhesion molecules, signal transduction and cell growth. *Curr. Opin. Cell Biol.* **11**, 737–744 (1999).

29. Hynes, R. O. Integrins: Bidirectional, allosteric signaling machines. *Cell* **110**, 673–687 (2002).

30. Wehrle-Haller, B. Assembly and disassembly of cell matrix adhesions. *Curr. Opin. Cell Biol.* **24**, 569–581 (2012).

31. Goldfinger, L. E. Integrin Signaling. *Encycl. Biol. Chem. Second Ed.* **285**, 441–445 (2013).

32. Takagi, J., Petre, B. M., Walz, T. & Springer, T. A. Global conformational earrangements in integrin extracellular domains in outside-in and inside-out signaling. *Cell* **110**, 599–611 (2002).

33. Nollet, F., Kools, P. & Van Roy, F. Phylogenetic analysis of the cadherin superfamily allows identification of six major subfamilies besides several solitary members. *J. Mol. Biol.* **299**, 551–572 (2000).

34. Gall, T. M. H. & Frampton, A. E. Gene of the month: E-cadherin (CDH1). *J. Clin. Pathol.* **66**, 928–932 (2013).

35. Shapiro, L. & Weis, W. I. Structure and biochemistry of cadherins and catenins. *Cold Spring Harb. Perspect. Biol.* **1**, 1–21 (2009).

36. Gumbiner, B. M. Regulation of cadherin-mediated adhesion in morphogenesis. *Nat. Rev. Mol. Cell Biol.* **6**, 622–634 (2005).

37. Klezovitch, O. & Vasioukhin, V. Cadherin signaling: keeping cells in touch. *F1000Research* **4**, 550 (2015).

38. Driesch, H. *The science and philosophy of the organism: The Gifford lectures delivered before the University of Aberdeen in the Year 1907 [-08]*. (A. and C. Black, 1908).

39. Holtfreter, J. Gewebeaffinitat, ein Mittel der embryonalen Formbildung. *Arch. Exp. Zellforsch.* **23**, 169–209 (1939).

40. Steinberg, M. S. Mechanism of Tissue Reconstruction by Dissociated Cells , II : Time-Course of Events inine Scene- Utilization of Nitrogen Compounds by Unicellular Algae. *Science* **137**, 762–763 (1962).

41. Steinberg, M. S. On the Mechanism of Tissue Reconstruction By Dissociated Cells, III. Free Energy Relations and the Reorganization of Fused, Heteronomic Tissue Fragments. *Proc. Natl. Acad. Sci.* **48**, 1769–1776 (1962).

42. Steinberg, M. S. On the Mechanism of Tissue Reconstruction by Dissociated cells, I. Population Kinetics, Differential Adhesiveness, and the Absence of Direct Migration. *Proc Natl Acad Sci USA* **48**, 1577–1582 (1962).

43. Steinberg, M. S. Reconstruction of Tissues by Dissociated Cells. *Science* **141**, 401–408 (1963).

44. Foty, R. A. & Steinberg, M. S. Differential adhesion in model systems. *Wiley Interdiscip. Rev. Dev. Biol.* **2**, 631–645 (2013).

45. Palsson, E. A 3-D model used to explore how cell adhesion and stiffness affect cell sorting and movement in multicellular systems. *J. Theor. Biol.* **254**, 1–13 (2008).

46. Shinbrot, T., Chun, Y., Caicedo-Carvajal, C. & Foty, R. Cellular morphogenesis in silico. *Biophys. J.* **97**, 958–967 (2009).

47. Katsamba, P. *et al.* Linking molecular affinity and cellular specificity in cadherin-mediated adhesion. *Proc. Natl. Acad. Sci.* **106**, 11594–11599 (2009).

48. Nose, A., Nagafuchi, A. & Takeichi, M. Expressed recombinant cadherins mediate cell sorting in model systems. *Cell* **54**, 993–1001 (1988).

49. Duguay, D., Foty, R. A. & Steinberg, M. S. Cadherin-mediated cell adhesion and tissue segregation: Qualitative and quantitative determinants. *Dev. Biol.* **253**, 309–323 (2003).

50. Steinberg, M. S. & Takeichi, M. Experimental specification of cell sorting, tissue spreading, and specific spatial patterning by quantitative differences in cadherin expression. *Proc. Natl. Acad. Sci. U. S. A.* **91**, 206–209 (1994).

51. Huang, X. *et al.* Interfacial assembly of protein-polymer nano-conjugates into stimulus-responsive biomimetic protocells. *Nat. Commun.* **4**, 1–9 (2013).

52. Trigg, E. B. & Winey, K. I. Nanoscale layers in polymers to promote ion transport. *Mol. Syst. Des. Eng.* **4**, 252–262 (2019).

53. Villringer, S. *et al.* Lectin-mediated protocell crosslinking to mimic cell-cell junctions and adhesion. *Sci. Rep.* **8**, 1–11 (2018).

54. Di Michele, L. & Eiser, E. Developments in understanding and controlling self assembly of DNA-functionalized colloids. *Phys. Chem. Chem. Phys.* **15**, 3115–3129 (2013).

55. Macfarlane, R. J. *et al.* Nanoparticle superlattice engineering with DNA. *Science* **334**, 204–208 (2011).

56. Wang, Y. *et al.* Synthetic Strategies Toward DNA-Coated Colloids that Crystallize. *J. Am. Chem. Soc.* **137**, 10760–10766 (2015).

57. Ap, A. *et al.* Organization Of Nanocrystal Molecules Using Dna. *Nature* **382**, 609–611 (1996).

58. Mirkin, C. A., Letsinger, R. L., Mucic, R. C. & Storhoff, J. J. A DNA-based method for rationally assembling nanoparticels into macroscopic materials. *Nature* **382**, 607–609 (1996).

59. J. D. Watson and F. H. C. Crick. A structure for deoxyribose nucleic acid. *J. Am. Coll. Cardiol.* **42**, 373–374 (1953).

60. Gerth, M. & Voets, I. K. Molecular control over colloidal assembly. *Chem.*

Commun. **53**, 4414–4428 (2017).

61. Manna, D., Udayabhaskararao, T., Zhao, H. & Klajn, R. Orthogonal Light-Induced Self-Assembly of Nanoparticles using Differently Substituted Azobenzenes. *Angew. Chemie - Int. Ed.* **54**, 12394–12397 (2015).

62. Klajn, R., Bishop, K. J. M. & Grzybowski, B. A. Light-controlled self-assembly of reversible and irreversible nanoparticle suprastructures. *Proc. Natl. Acad. Sci. U. S. A.* **104**, 10305–10309 (2007).

63. Zhang, L. *et al.* Light-triggered reversible self-assembly of gold nanoparticle oligomers for tunable SERS. *Langmuir* **31**, 1164–1171 (2015).

64. Zhang, Q., Dong, R., Chang, X., Ren, B. & Tong, Z. Spiropyran-Decorated SiO2-Pt Janus Micromotor: Preparation and Light-Induced Dynamic Self-Assembly and Disassembly. *ACS Appl. Mater. Interfaces* **7**, 24585–24591 (2015).

65. Chen, G. & Jiang, M. Cyclodextrin-based inclusion complexation bridging supramolecular chemistry and macromolecular self-assembly. *Chem. Soc. Rev.* **40**, 2254–2266 (2011).

66. Han, K. *et al.* Social Self-Sorting of Colloidal Families in Co-Assembling Microgel Systems. *Angew. Chemie - Int. Ed.* **56**, 2176–2182 (2017).

67. Han, K., Go, D., Hoenders, D., Kuehne, A. J. C. & Walther, A. Switchable supracolloidal coassembly of microgels mediated by host/guest interactions. *ACS Macro Lett.* **6**, 310–314 (2017).

68. Zhou, Y. *et al.* Reversible Janus particle assembly via responsive host-guest interactions. *Chem. Commun.* **51**, 2725–2727 (2015).

69. Sentürk, O. I., Chervyachkova, E., Ji, Y. & Wegner, S. V. Independent Blue and Red Light Triggered Narcissistic Self-Sorting Self-Assembly of Colloidal Particles. *Small* **1901801**, 1901801 (2019).

70. Chervyachkova, E. & Wegner, S. V. Reversible Social Self-Sorting of Colloidal Cell-Mimics with Blue Light Switchable Proteins. *ACS Synth. Biol.* **7**, 1817–1824 (2018).

71. Weitz, D. A., Huang, J. S., Lin, M. Y. & Sung, J. Dynamics of Diffusion-Limited

Kinetic Aggregation. *Phys. Rev. Lett.* **53**, 1657–1660 (1984).

72. Tang, S., Preece, J. M., McFarlane, C. M. & Zhang, Z. Fractal morphology and breakage of DLCA and RLCA aggregates. *J. Colloid Interface Sci.* **221**, 114–123 (2000).

73. Weitz D. A., S., H. J., Y., L. M. & J., S. Limits of the Fractal Dimension for Irreversible Kinetic Aggregation of Gold Coloids. *Phys. Rev. Lett.* **54**, 1416–1419 (1985).

74. Lin, M. Y. *et al.* Universality in colloid aggregation. *Nat.* · **339**, 360–362 (1989).

75. Jungblut, S., Joswig, J. O. & Eychmüller, A. Diffusion-Limited Cluster Aggregation: Impact of Rotational Diffusion. *J. Phys. Chem. C* **123**, 950–954 (2019).

76. Lin, M. Y. *et al.* Universal reaction-limited colloid aggregation. *Phys. Rev. A* **41**, 2005–2020 (1990).

77. Maye, M. M., Nykypanchuk, D., Van Der Lelie, D. & Gang, O. DNA-regulated micro- and nanoparticle assembly. *Small* **3**, 1678–1682 (2007).

78. Lazzari, S., Nicoud, L., Jaquet, B., Lattuada, M. & Morbidelli, M. Fractal-like structures in colloid science. *Adv. Colloid Interface Sci.* **235**, 1–13 (2016).

79. Mandelbrot, B. B. *The fractal geometry of nature*. **173**, (WH freeman New York, 1983).

80. Karperien, A. FracLac for ImageJ. *Charles Sturt University* (2013). Available at: https://imagej.nih.gov/ij/plugins/fraclac/FLHelp/Introduction.htm.

81. Meakin, P. Formation of fractal clusters and networks by irreversible diffusion-limited aggregation. *Phys. Rev. Lett.* **51**, 1119–1122 (1983).

82. Pierce, F., Sorensen, C. M. & Chakrabarti, A. Aggregation-fragmentation in a model of DNA-mediated colloidal assembly. *Langmuir* **21**, 8992–8999 (2005).

83. Logan, B. E. & Wilkinson, D. B. Fractal geometry of marine snow and other biological aggregates. *Limnol. Oceanogr.* **35**, 130–136 (1990).

84. Mukhopadhyay, P., Wu, A. & Isaacs, L. Social self-sorting in aqueous solution. *J. Org. Chem.* **69**, 6157–6164 (2004).

85. Vilanova, N., De Feijter, I., Teunissen, A. J. P. & Voets, I. K. Light induced assembly and self-sorting of silica microparticles. *Sci. Rep.* **8**, 1–9 (2018).

86. Higashi, N., Ochiai, T., Kanazawa, C. & Koga, T. Site-specific adsorption of gold nanoparticles coated with thermo-responsive peptides. *Polym. J.* **45**, 523–528 (2013).

87. Hamner, K. L. & Maye, M. M. Thermal aggregation properties of nanoparticles modified with temperature sensitive copolymers. *Langmuir* **29**, 15217–15223 (2013).

88. Stephan, M. T. & Irvine, D. J. Enhancing cell therapies from the outside in: Cell surface engineering using synthetic nanomaterials. *Nano Today* **6**, 309–325 (2011).

89. Dutta, D., Pulsipher, A., Luo, W. & Yousaf, M. N. Synthetic chemoselective rewiring of cell surfaces: Generation of three-dimensional tissue structures. *J. Am. Chem. Soc.* **133**, 8704–8713 (2011).

90. O'Brien, P. J., Luo, W., Rogozhnikov, D., Chen, J. & Yousaf, M. N. Spheroid and tissue assembly via click chemistry in microfluidic flow. *Bioconjug. Chem.* **26**, 1939–1949 (2015).

91. Koo, H. *et al.* Bioorthogonal Click Chemistry-Based Synthetic Cell Glue. *Small* **11**, 6458–6466 (2015).

92. Shi, P. *et al.* Spatiotemporal control of cell–cell reversible interactions using molecular engineering. *Nat. Commun.* **7**, 13088 (2016).

93. Sarkar, D. *et al.* Engineered cell homing. *Blood* **118**, 184–192 (2011).

94. Wang, B. *et al.* Multicellular assembly and light-regulation of cell-cell communication by conjugated polymer materials. *Adv. Mater.* **26**, 2371–2375 (2014).

95. De Bank, P. A. *et al.* Accelerated Formation of multicellular §-D Structures by Cell-to-Cell-Linking. *Biortechnology Bioeng.* **97**, 1460–1469 (2007).

96. Gartner, Z. J. & Bertozzi, C. R. Programmed assembly of 3-dimensional microtissues with defined cellular connectivity. *Proc. Natl. Acad. Sci. U. S. A.* **106**,

4606–4610 (2009).

97. Xiong, X. *et al.* DNA aptamer-mediated cell targeting. *Angew. Chemie - Int. Ed.* **52**, 1472–1476 (2013).

98. Luo, W., Pulsipher, A., Dutta, D., Lamb, B. M. & Yousaf, M. N. Remote Control of Tissue Interactions via Engineered Photo-switchable Cell Surfaces. *Sci. Rep.* **4**, 6313 (2015).

99. Jensen, P. R. & Hammer, K. Artificial promoters for metabolic optimization. *Biotechnol. Bioeng.* **58**, 191–195 (1998).

100. Cachat, E. *et al.* 2- and 3-Dimensional Synthetic Large-Scale De Novo Patterning By Mammalian Cells Through Phase Separation. *Sci. Rep.* **6**, 1–8 (2016).

101. Toda, S., Blauch, L. R., Tang, S. K. Y., Morsut, L. & Lim, W. A. Programming self-organizing multicellular structures with synthetic cell-cell signaling. *Science* **162**, eaat0271 (2018).

102. Morsut, L. *et al.* Engineering Customized Cell Sensing and Response Behaviors Using Synthetic Notch Receptors. *Cell* **11**, 780–791 (2016).

103. Fenno, L., Yizhar, O. & Deisseroth, K. The Development and Application of Optogenetics. doi:10.1146/annurev-neuro-061010-113817

104. Deisseroth, K. Optogenetics - Method of the Year. *Nat. Methods* **8**, 1–4 (2010).

105. Yazawa, M., Sadaghiani, A. M., Hsueh, B. & Dolmetsch, R. E. Induction of protein-protein interactions in live cells using light. *Nat. Biotechnol.* **27**, 941–947 (2009).

106. Sun, T., Zhang, B., Lin, J. & Ren, Y. Reversible photocontrol of oxidase activity by inserting a photosensitive domain into the oxidase. *Bioresour. Bioprocess.* **6**, 0–5 (2019).

107. Guntas, G. *et al.* Engineering an improved light-induced dimer (iLID) for controlling the localization and activity of signaling proteins. *Proc. Natl. Acad. Sci.* **112**, 112–117 (2015).

108. Kim, N. *et al.* Spatiotemporal control of fibroblast growth factor receptor signals by blue light. *Chem. Biol.* **21**, 903–912 (2014).

109. Shin, Y. *et al.* Spatiotemporal Control of Intracellular Phase Transitions Using Light-Activated optoDroplets. *Cell* **168**, 159--171.e14 (2017).

110. Zhou, X. X. *et al.* A Single-Chain Photoswitchable CRISPR-Cas9 Architecture for Light-Inducible Gene Editing and Transcription. *ACS Chem. Biol.* **13**, 443–448 (2018).

111. Mühlhäuser, W. W. D., Fischer, A., Weber, W. & Radziwill, G. Optogenetics - Bringing light into the darkness of mammalian signal transduction. *Biochim. Biophys. Acta - Mol. Cell Res.* **1864**, 280–292 (2017).

112. Ajith Karunarathne, W. K., O'Neill, P. R. & Gautam, N. Subcellular optogenetics - Controlling signaling and single-cell behavior. *J. Cell Sci.* **128**, 15–25 (2015).

113. Toettcher, J. E. The spatiotemporal limits of developmental Erk signaling. **40**, 185–192 (2018).

114. Chen, D., Gibson, E. S. & Kennedy, M. J. A light-triggered protein secretion system. *J. Cell Biol.* **201**, 631–640 (2013).

115. Wang, X., Chen, X. & Yang, Y. Spatiotemporal control of gene expression by a light-switchable transgene system. *Nat. Methods* **9**, 266–269 (2012).

116. Taslimi, A. *et al.* An optimized optogenetic clustering tool for probing protein interaction and function. *Nat. Commun.* **5**, 1–9 (2014).

117. Zoltowski, B. D., Motta-Mena, L. B. & Gardner, K. H. Blue light-induced dimerization of a bacterial LOV-HTH DNA-binding protein. *Biochemistry* **52**, 6653–6661 (2013).

118. Levskaya, A. *et al.* Engineering Escherichia coli to see light. *Nature* **438**, 441 (2005).

119. Kennedy, M. J. *et al.* Rapid blue-light-mediated induction of protein interactions in living cells. *Nat. Methods* **7**, 973–975 (2010).

120. Shimizu-Sato, S., Huq, E., Tepperman, J. M. & Quail, P. H. A light-switchable gene promoter system. *Nat. Biotechnol.* **20**, 1041–1044 (2002).

121. Halavaty, A. S. & Moffat, K. N- and C-terminal flanking regions modulate light-induced signal transduction in the LOV2 domain of the blue light sensor

phototropin 1 from Avena sativa. *Biochemistry* **46**, 14001–14009 (2007).

122. Harper, S. M. Structural Basis of a Phototropin Light Switch. *Science* **301**, 1541–1544 (2003).

123. Zhu, J. *et al.* Photoadduct Formation from the FMN Singlet Excited State in the LOV2 Domain of Chlamydomonas reinhardtii Phototropin. *J. Phys. Chem. Lett.* **7**, 4380–4384 (2016).

124. Harper, S. M., Christie, J. M. & Gardner, K. H. Disruption of the LOV-J$α$ helix interaction activates phototropin kinase activity. *Biochemistry* **43**, 16184–16192 (2004).

125. Swartz, T. E. *et al.* The Photocycle of a Flavin-binding Domain of the Blue Light Photoreceptor Phototropin. *J. Biol. Chem.* **276**, 36493–36500 (2001).

126. Zayner, J., Chloe, A. & Sosnick, T. R. The amino terminal helix modulates light activated conformational changes in AsLOV2. *J. Mol. Biol.* **419**, 61–74 (2012).

127. Konold, P. E. *et al.* Unfolding of the C-Terminal J$α$ Helix in the LOV2 Photoreceptor Domain Observed by Time-Resolved Vibrational Spectroscopy. *J. Phys. Chem. Lett.* **7**, 3472–3476 (2016).

128. Salomon, M., Christie, J. M., Knieb, E., Lempert, U. & Briggs, W. R. Photochemical and mutational analysis of the FMN-binding domains of the plant blue light receptor, phototropin. *Biochemistry* **39**, 9401–9410 (2000).

129. Lungu, O. I. *et al.* Designing Photoswitchable Peptides Using the AsLOV2 Domain. *Chem. Biol.* **19**, 507–517 (2012).

130. Lungu, O. I. *et al.* Designing Photoswitchable Peptides Using the AsLOV2 Domain. *Chem. Biol.* **19**, 507–517 (2012).

131. Seth P., Z. *et al.* Tuning the Binding Affinities and Reversion Kinetics of a Light Inducible Dimer Allows Control of Transmembrane Protein Localization Seth. *Physiol. Behav.* **176**, 139–148 (2017).

132. Zimmerman, S. P., Asokan, S. B., Kuhlman, B. & Bear, J. E. Cells lay their own tracks - optogenetic Cdc42 activation stimulates fibronectin deposition supporting directed migration. *J. Cell Sci.* **130**, 2971–2983 (2017).

133. O'Neill, P. R. *et al.* Membrane Flow Drives an Adhesion-Independent Amoeboid Cell Migration Mode. *Dev. Cell* **46**, 9-22.e4 (2018).

134. Loros, J. J. & Dunlap, J. C. Genetic and Molecular Analysis of Circadian Rhytmus in Neurospora. *Annu. Rev. Physiol.* **63**, 757–794 (2001).

135. Crosson, S., Rajagopal, S. & Moffat, K. The LOV domain family: Photoresponsive signaling modules coupled to diverse output domains. *Biochemistry* **42**, 2–10 (2003).

136. Zoltowski, B. D. *et al.* Conformational Switching in the Fungal Light Sensor. *Science* **36**, 1054–1058 (2007).

137. Kawano, F., Suzuki, H., Furuya, A. & Sato, M. Engineered pairs of distinct photoswitches for optogenetic control of cellular proteins. *Nat. Commun.* **6**, 1–8 (2015).

138. Biology, A. C. S. S. Assembly domain-based optogenetic system for the efficient control of cellular signaling. (2016). doi:10.1021/acssynbio.7b00022

139. Baumschlager, A., Aoki, S. K. & Khammash, M. Dynamic Blue Light-Inducible T7 RNA Polymerases (Opto-T7RNAPs) for Precise Spatiotemporal Gene Expression Control. *ACS Synth. Biol.* **6**, 2157–2167 (2017).

140. Nihongaki, Y., Otabe, T., Ueda, Y. & Sato, M. A split CRISPR–Cpf1 platform for inducible genome editing and gene activation. *Nat. Chem. Biol.* **15**, 882–888 (2019).

141. Chen, F. & Wegner, S. V. Blue Light Switchable Bacterial Adhesion as a Key Step toward the Design of Biofilms. *ACS Synth. Biol.* **6**, 2170–2174 (2017).

142. Liu, H. S. & Gartner, Z. J. Directing the assembly of spatially organized multicomponent tissues from the bottom-up. *Trends Biotechnol.* **22**, 1–7 (2012).

143. Harrison, S. E., Sozen, B., Christodoulou, N., Kyprianou, C. & Zernicka-Goetz, M. Assembly of embryonic and extraembryonic stem cells to mimic embryogenesis in vitro. *Science* **356**, (2017).

144. Rivron, N. C. *et al.* Blastocyst-like structures generated solely from stem cells. *Nature* **557**, 106–111 (2018).

145. Wan, A. C. A. Recapitulating Cell–Cell Interactions for Organoid Construction – Are Biomaterials Dispensable? *Trends Biotechnol.* **34**, 711–721 (2016).

146. Merindol, R. & Walther, A. Materials learning from life: Concepts for active, adaptive and autonomous molecular systems. *Chem. Soc. Rev.* **46**, 5588–5619 (2017).

147. Valignat, M. P., Theodoly, O., Crocker, J. C., Russel, W. B. & Chaikin, P. M. Reversible self-assembly and directed assembly of DNA-linked micrometer-sized colloids. *Proc. Natl. Acad. Sci. U. S. A.* **102**, 4225–4229 (2005).

148. Li, F., Josephson, D. P. & Stein, A. Colloidal assembly: The road from particles to colloidal molecules and crystals. *Angew. Chemie - Int. Ed.* **50**, 360–388 (2011).

149. Selden, N. S. *et al.* Chemically programmed cell adhesion with membrane-anchored oligonucleotides. *J. Am. Chem. Soc.* **134**, 765–768 (2012).

150. Shi, P. *et al.* Polyvalent Display of Biomolecules on the Live Cells. *Angew. Chemie Int. Ed.* 1–6 (2018). doi:10.1002/anie.201712596

151. Foty, R. A. & Steinberg, M. S. The differential adhesion hypothesis: A direct evaluation. *Dev. Biol.* **278**, 255–263 (2005).

152. Foty, R. A. & Steinberg, M. S. Cadherin-mediated cell-cell adhesion and tissue segregation in relation to malignancy. *Int. J. Dev. Biol.* **48**, 397–409 (2004).

153. Canty, L., Zarour, E., Kashkooli, L., François, P. & Fagotto, F. Sorting at embryonic boundaries requires high heterotypic interfacial tension. *Nat. Commun.* **8**, (2017).

154. Schneider, C. A., Rasband, W. S. & Eliceiri, K. W. NIH Image to ImageJ: 25 years of image analysis. *Nat. Methods* **9**, 671–675 (2012).

155. Preibisch, S., Saalfeld, S. & Tomancak, P. Globally optimal stitching of tiled 3D microscopic image acquisitions. *Bioinformatics* **25**, 1463–1465 (2009).

156. Stauffer, W., Sheng, H. & Lim, H. N. EzColocalization: An ImageJ plugin for visualizing and measuring colocalization in cells and organisms. *Sci. Rep.* **8**, 1–13 (2018).

157. Chao, Y. L., Shepard, C. R. & Wells, A. Breast carcinoma cells re-express E-

cadherin during mesenchymal to epithelial reverting transition. *Mol. Cancer* **9**, 1–18 (2010).

158. Nieman, M. T., Prudoff, R. S., Johnson, K. R. & Wheelock, M. J. of their E-Cadherin Expression. **147**, 631–643 (1999).

159. Youssef, J., Nurse, A. K., Freund, L. B. & Morgan, J. R. Quantification of the forces driving self-assembly of three-dimensional microtissues. *Proc. Natl. Acad. Sci. U. S. A.* **108**, 6993–6998 (2011).

160. Gartner, Z. J. & Bertozzi, C. R. Programmed assembly of 3-dimensional microtissues. **106**, 1–5 (2009).

161. Yüz, S. G., Rasoulinejad, S., Mueller, M., Wegner, A. E. & Wegner, S. V. Blue Light Switchable Cell-Cell Interactions Provide Reversible and Spatiotemporal Control Towards Bottom-Up Tissue Engineering. *Adv. Biosyst.* **1800310**, 1800310 (2019).

162. Aoki, K. *et al.* Stochastic ERK activation induced by noise and cell-to-cell propagation regulates cell density-dependent proliferation. *Mol. Cell* **52**, 529–540 (2013).

163. Melendez, J. *et al.* Real-time optogenetic control of intracellular protein concentration in microbial cell cultures. *Integr. Biol. Integr. Biol* **366**, 366–372 (2014).

164. Meakin, P. Diffusion-controlled aggregation on two-dimensional square lattices: Results from a new cluster-cluster aggregation model. *Phys. Rev. B* **29**, 2930–2942 (1984).

Appendix

Nucleotide and amino acid sequences, ORF

pDisplay GFP TM

DNA sequence 5’ to 3’

TTGGTACCGAGCTCGGATCCACTAGTAACGGCCGCCAGTGTGCTGGAATTCGGCTTGGGGATAT
CCACCATGGAGACAGACACACTCCTGCTATGGGTACTGCTGCTCTGGGTTCCAGGTTCCACTGG
TGACTATCCATATGATGTTCCAGATTATGCTGGGGCCCAGCCGGCCAGATCTGTGAGCAAGGGC
GAGGAGCTGTTCACCGGGGTGGTGCCCATCCTGGTCGAGCTGGACGGCGACGTAAACGGCCACA
AGTTCAGCGTGTCCGGCGAGGGCGAGGGCGATGCCACCTACGGCAAGCTGACCCTGAAGTTCAT
CTGCACCACCGGCAAGCTGCCCGTGCCCTGGCCCACCCTCGTGACCACCCTGACCTACGGCGTG
CAGTGCTTCAGCCGCTACCCCGACCACATGAAGCAGCACGACTTCTTCAAGTCCGCCATGCCCG
AAGGCTACGTCCAGGAGCGCACCATCTTCTTCAAGGACGACGGCAACTACAAGACCCGCGCCGA
GGTGAAGTTCGAGGGCGACACCCTGGTGAACCGCATCGAGCTGAAGGGCATCGACTTCAAGGAG
GACGGCAACATCCTGGGGCACAAGCTGGAGTACAACTACAACAGCCACAACGTCTATATCATGG
CCGACAAGCAGAAGAACGGCATCAAGGTGAACTTCAAGATCCGCCACAACATCGAGGACGGCAG
CGTGCAGCTCGCCGACCACTACCAGCAGAACACCCCCATCGGCGACGGCCCCGTGCTGCTGCCC
GACAACCACTACCTGAGCACCCAGTCCGCCCTGAGCAAAGACCCCAACGAGAAGCGCGATCACA
TGGTCCTGCTGGAGTTCGTGACCGCCGCCGGGATCACTCTCGGCATGGACGAGCTGTATAAGGG
TAAAAAGAAGAAAAAGAAGTCAAAGACAAAGTGTGTAATTATGACCCGGGATCCGCGGCTGCAG
GTCGACGAACAAAAACTCATCTCAGAAGAGGATCTGAATGCTGTGGGCCAGGACACGCAGGAGG
TCATCGTGGTGCCACACTCCTTGCCCTTTAAGGTGGTGGTGATCTCAGCCATCCTGGCCCTGGT
GGTGCTCACCATCATCTCCCTTATCATCCTCATCATGCTTTGGCAGAAGAAGCCACGTTAG

pDisplay mCherry TM

DNA sequence 5’ to 3’

TTGGTACCGAGCTCGGATCCACTAGTAACGGCCGCCAGTGTGCTGGAATTCGGCTTGGGGATAT
CCACCATGGAGACAGACACACTCCTGCTATGGGTACTGCTGCTCTGGGTTCCAGGTTCCACTGG
TGACTATCCATATGATGTTCCAGATTATGCTGGGGCCCAGCCGGCCAGATCTGTGAGCAAGGGC

GAGGAGGATAACATGGCCATCATCAAGGAGTTCATGCGCTTCAAGGTGCACATGGAGGGCTCCG
TGAACGGCCACGAGTTCGAGATCGAGGGCGAGGGCGAGGGCCGCCCCTACGAGGGCACCCAGAC
CGCCAAGCTGAAGGTGACCAAGGGTGGCCCCCTGCCCTTCGCCTGGGACATCCTGTCCCCTCAG
TTCATGTACGGCTCCAAGGCCTACGTGAAGCACCCCGCCGACATCCCCGACTACTTGAAGCTGT
CCTTCCCCGAGGGCTTCAAGTGGGAGCGCGTGATGAACTTCGAGGACGGCGGCGTGGTGACCGT
GACCCAGGACTCCTCCCTGCAGGACGGCGAGTTCATCTACAAGGTGAAGCTGCGCGGCACCAAC
TTCCCCTCCGACGGCCCCGTAATGCAGAAGAAGACCATGGGCTGGGAGGCCTCCTCCGAGCGGA
TGTACCCCGAGGACGGCGCCCTGAAGGGCGAGATCAAGCAGAGGCTGAAGCTGAAGGACGGCGG
CCACTACGACGCTGAGGTCAAGACCACCTACAAGGCCAAGAAGCCCGTGCAGCTGCCCGGCGCC
TACAACGTCAACATCAAGTTGGACATCACCTCCCACAACGAGGACTACACCATCGTGGAACAGT
ACGAACGCGCCGAGGGCCGCCACTCCACCGGCGGCATGGACGAGCTGTACAAGCCCGGGAATCC
GCGGCTGCAGGTCGACGAACAAAAACTCATCTCAGAAGAGGATCTGAATGCTGTGGGCCAGGAC
ACGCAGGAGGTCATCGTGGTGCCACACTCCTTGCCCTTTAAGGTGGTGGTGATCTCAGCCATCC
TGGCCCTGGTGGTGCTCACCATCATCTCCCTTATCATCCTCATCATGCTTTGGCAGAAGAAGCC
ACGTTAG

pDisplay iLID mCherry TM

DNA sequence 5’ to 3’

TTGGTACCGAGCTCGGATCCACTAGTAACGGCCGCCAGTGTGCTGGAATTCGGCTTGGGGATAT
CCACCATGGAGACAGACACACTCCTGCTATGGGTACTGCTGCTCTGGGTTCCAGGTTCCACTGG
TGACTATCCATATGATGTTCCAGATTATGCTGGGGCCCAGCCGGCCAGATCTGGATCCGGGGAG
TTTCTGGCAACCACACTGGAACGGATCGAGAAAAATTTCGTGATTACTGATCCGAGACTGCCTG
ACAACCCAATCATTTTTGCGAGCGATTCCTTCCTGCAGCTGACAGAATATTCTCGGGAAGAGAT
CCTGGGGCGCAATTGCCGTTTTCTGCAGGGACCCGAGACAGACCGTGCCACTGTTCGGAAAATC
AGAGATGCTATTGACAACCAGACTGAAGTGACCGTTCAGCTGATCAATTATACCAAGAGCGGCA
AGAAGTTCTGGAACGTGTTCCACCTGCAGCCGATGCGCGATTATAAGGGCGACGTCCAGTACTT
CATTGGCGTGCAGCTGGATGGCACCGAACGTCTTCATGGCGCCGCTGAGCGTGAGGCGGTCATG
CTGATCAAAAAGACAGCCTTTCAGATTGCTGAGGCAGCGAACGACGAAAATTACTTTGTGAGCA
AGGGCGAGGAGGATAACATGGCCATCATCAAGGAGTTCATGCGCTTCAAGGTGCACATGGAGGG
CTCCGTGAACGGCCACGAGTTCGAGATCGAGGGCGAGGGCGAGGGCCGCCCCTACGAGGGCACC
CAGACCGCCAAGCTGAAGGTGACCAAGGGTGGCCCCCTGCCCTTCGCCTGGGACATCCTGTCCC
CTCAGTTCATGTACGGCTCCAAGGCCTACGTGAAGCACCCCGCCGACATCCCCGACTACTTGAA
GCTGTCCTTCCCCGAGGGCTTCAAGTGGGAGCGCGTGATGAACTTCGAGGACGGCGGCGTGGTG
ACCGTGACCCAGGACTCCTCCCTGCAGGACGGCGAGTTCATCTACAAGGTGAAGCTGCGCGGCA

CCAACTTCCCCTCCGACGGCCCCGTAATGCAGAAGAAGACCATGGGCTGGGAGGCCTCCTCCGA
GCGGATGTACCCCGAGGACGGCGCCCTGAAGGGCGAGATCAAGCAGAGGCTGAAGCTGAAGGAC
GGCGGCCACTACGACGCTGAGGTCAAGACCACCTACAAGGCCAAGAAGCCCGTGCAGCTGCCCG
GCGCCTACAACGTCAACATCAAGTTGGACATCACCTCCCACAACGAGGACTACACCATCGTGGA
ACAGTACGAACGCGCCGAGGGCCGCCACTCCACCGGCGGCATGGACGAGCTGTACAAGCCCGGG
AATCCGCGGCTGCAGGTCGACGAACAAAAACTCATCTCAGAAGAGGATCTGAATGCTGTGGGCC
AGGACACGCAGGAGGTCATCGTGGTGCCACACTCCTTGCCCTTTAAGGTGGTGGTGATCTCAGC
CATCCTGGCCCTGGTGGTGCTCACCATCATCTCCCTTATCATCCTCATCATGCTTTGGCAGAAG
AAGCCACGTTAG

Amino acid sequence

MVPSSDPLVTAASVLEFGLGISTMETDTLLLWVLLLWVPGSTGDYPYDVPDYAGAQPARSGSGE
FLATTLERIEKNFVITDPRLPDNPIIFASDSFLQLTEYSREEILGRNCRFLQGPETDRATVRKI
RDAIDNQTEVTVQLINYTKSGKKFWNVFHLQPMRDYKGDVQYFIGVQLDGTERLHGAAEREAVM
LIKKTAFQIAEAANDENYFVSKGEEDNMAIIKEFMRFKVHMEGSVNGHEFEIEGEGEGRPYEGT
QTAKLKVTKGGPLPFAWDILSPQFMYGSKAYVKHPADIPDYLKLSFPEGFKWERVMNFEDGGVV
TVTQDSSLQDGEFIYKVKLRGTNFPSDGPVMQKKTMGWEASSERMYPEDGALKGEIKQRLKLKD
GGHYDAEVKTTYKAKKPVQLPGAYNVNIKLDITSHNEDYTIVEQYERAEGRHSTGGMDELYKPG
NPRLQVDEQKLISEEDLNAVGQDTQEVIVVPHSLPFKVVVISAILALVVLTIISLIILIMLWQK
KPR

pDisplay Nano GFP TM

DNA sequence 5’ to 3’

TTGGTACCGAGCTCGGATCCACTAGTAACGGCCGCCAGTGTGCTGGAATTCGGCTTGGGGATAT
CCACCATGGAGACAGACACACTCCTGCTATGGGTACTGCTGCTCTGGGTTCCAGGTTCCACTGG
TGACTATCCATATGATGTTCCAGATTATGCTGGGGCCCAGCCGGCCGGATCCAGCTCCCCGAAA
CGCCCTAAGCTGCTGCGTGAATATTACGATTGGCTGGTTGATAACAGCTTTACCCCATATCTGG
TGGTGGATGCCACATACCTGGGCGTGAACGTGCCCGTGGAGTATGTGAAAGACGGTCAGATCGT
GCTGAATCTGTCTGCAAGTGCGACCGGCAACCTGCAACTGACAAATGATTTTATCCAGTTCAAC
GCCCGCTTTAAGGGCGTGTCTCGTGAACTGTATATCCCGATGGGTGCCGCTCTGGCCATTTACG
CTCGCGAGAACGGCGATGGTGTGATGTTCGAACCAGAAGAAATCTATGACGAGCTGAATATTGG
TAGATCTGTGAGCAAGGGCGAGGAGCTGTTCACCGGGGTGGTGCCCATCCTGGTCGAGCTGGAC
GGCGACGTAAACGGCCACAAGTTCAGCGTGTCCGGCGAGGGCGAGGGCGATGCCACCTACGGCA

AGCTGACCCTGAAGTTCATCTGCACCACCGGCAAGCTGCCCGTGCCCTGGCCCACCCTCGTGAC
CACCCTGACCTACGGCGTGCAGTGCTTCAGCCGCTACCCCGACCACATGAAGCAGCACGACTTC
TTCAAGTCCGCCATGCCCGAAGGCTACGTCCAGGAGCGCACCATCTTCTTCAAGGACGACGGCA
ACTACAAGACCCGCGCCGAGGTGAAGTTCGAGGGCGACACCCTGGTGAACCGCATCGAGCTGAA
GGGCATCGACTTCAAGGAGGACGGCAACATCCTGGGGCACAAGCTGGAGTACAACTACAACAGC
CACAACGTCTATATCATGGCCGACAAGCAGAAGAACGGCATCAAGGTGAACTTCAAGATCCGCC
ACAACATCGAGGACGGCAGCGTGCAGCTCGCCGACCACTACCAGCAGAACACCCCCATCGGCGA
CGGCCCCGTGCTGCTGCCCGACAACCACTACCTGAGCACCCAGTCCGCCCTGAGCAAAGACCCC
AACGAGAAGCGCGATCACATGGTCCTGCTGGAGTTCGTGACCGCCGCCGGGATCACTCTCGGCA
TGGACGAGCTGTATAAGGGTAAAAAGAAGAAAAAGAAGTCAAAGACAAAGTGTGTAATTATGAC
CCGGGATCCGCGGCTGCAGGTCGACGAACAAAAACTCATCTCAGAAGAGGATCTGAATGCTGTG
GGCCAGGACACGCAGGAGGTCATCGTGGTGCCACACTCCTTGCCCTTTAAGGTGGTGGTGATCT
CAGCCATCCTGGCCCTGGTGGTGCTCACCATCATCTCCCTTATCATCCTCATCATGCTTTGGCA
GAAGAAGCCACGTTAG

Amino acid sequence

MVPSSDPLVTAASVLEFGLGISTMETDTLLLWVLLLWVPGSTGDYPYDVPDYAGAQPAGSSSPK
RPKLLREYYDWLVDNSFTPYLVVDATYLGVNVPVEYVKDGQIVLNLSASATGNLQLTNDFIQFN
ARFKGVSRELYIPMGAALAIYARENGDGVMFEPEEIYDELNIGRSVSKGEELFTGVVPILVELD
GDVNGHKFSVSGEGEGDATYGKLTLKFICTTGKLPVPWPTLVTTLTYGVQCFSRYPDHMKQHDF
FKSAMPEGYVQERTIFFKDDGNYKTRAEVKFEGDTLVNRIELKGIDFKEDGNILGHKLEYNYNS
HNVYIMADKQKNGIKVNFKIRHNIEDGSVQLADHYQQNTPIGDGPVLLPDNHYLSTQSALSKDP
NEKRDHMVLLEFVTAAGITLGMDELYKGKKKKKKSKTKCVIMTRDPRLQVDEQKLISEEDLNAV
GQDTQEVIVVPHSLPFKVVVISAILALVVLTIISLIILIMLWQKKPR

pDisplay nMag mCherry TM

DNA sequence 5’ to 3’

TTGGTACCGAGCTCGGATCCACTAGTAACGGCCGCCAGTGTGCTGGAATTCGGCTTGGGGATAT
CCACCATGGAGACAGACACACTCCTGCTATGGGTACTGCTGCTCTGGGTTCCAGGTTCCACTGG
TGACTATCCATATGATGTTCCAGATTATGCTGGGGCCCAGCCGGCCATGCACACACTATATGCT
CCCGGAGGGTATGATATAATGGGATACCTAGATCAAATAGGCAACCGTCCGAACCCGCAAGTGG
AGCTGGGCCCGGTGGACACCAGCTGCGCGCTGATCCTGTGCGACCTGAAGCAGAAAGATACCCC
GATTGTGTACGCGAGCGAGGCGTTCCTGTACATGACCGGTTATAGCAACGCGGAAGTTCTGGGC

CGTAACTGCCGTTTTCTGCAAAGCCCGGATGGTATGGTGAAGCCGAAAAGCACCCGTAAGTATG
TTGACAGCAACACCATCAACACCATGCGTAAAGCGATCGATCGTAACGCGGAAGTGCAGGTTGA
AGTGGTTAACTTCAAGAAAAACGGCCAACGTTTCGTGAACTTTCTGACCATGATTCCGGTTCGT
GATGAGACCGGCGAATATCGTTATAGCATGGGTTTTCAATGCGAGACCGAAGGCGGTAGCAGAT
CTGTGAGCAAGGGCGAGGAGGATAACATGGCCATCATCAAGGAGTTCATGCGCTTCAAGGTGCA
CATGGAGGGCTCCGTGAACGGCCACGAGTTCGAGATCGAGGGCGAGGGCGAGGGCCGCCCCTAC
GAGGGCACCCAGACCGCCAAGCTGAAGGTGACCAAGGGTGGCCCCCTGCCCTTCGCCTGGGACA
TCCTGTCCCCTCAGTTCATGTACGGCTCCAAGGCCTACGTGAAGCACCCCGCCGACATCCCCGA
CTACTTGAAGCTGTCCTTCCCCGAGGGCTTCAAGTGGGAGCGCGTGATGAACTTCGAGGACGGC
GGCGTGGTGACCGTGACCCAGGACTCCTCCCTGCAGGACGGCGAGTTCATCTACAAGGTGAAGC
TGCGCGGCACCAACTTCCCCTCCGACGGCCCCGTAATGCAGAAGAAGACCATGGGCTGGGAGGC
CTCCTCCGAGCGGATGTACCCCGAGGACGGCGCCCTGAAGGGCGAGATCAAGCAGAGGCTGAAG
CTGAAGGACGGCGGCCACTACGACGCTGAGGTCAAGACCACCTACAAGGCCAAGAAGCCCGTGC
AGCTGCCCGGCGCCTACAACGTCAACATCAAGTTGGACATCACCTCCCACAACGAGGACTACAC
CATCGTGGAACAGTACGAACGCGCCGAGGGCCGCCACTCCACCGGCGGCATGGACGAGCTGTAC
AAGCCCGGGAATCCGCGGCTGCAGGTCGACGAACAAAAACTCATCTCAGAAGAGGATCTGAATG
CTGTGGGCCAGGACACGCAGGAGGTCATCGTGGTGCCACACTCCTTGCCCTTTAAGGTGGTGGT
GATCTCAGCCATCCTGGCCCTGGTGGTGCTCACCATCATCTCCCTTATCATCCTCATCATGCTT
TGGCAGAAGAAGCCACGTTAG

Amino acid sequence

MVPSSDPLVTAASVLEFGLGISTMETDTLLLWVLLLWVPGSTGDYPYDVPDYAGAQPAMHTLYA
PGGYDIMGYLDQIGNRPNPQVELGPVDTSCALILCDLKQKDTPIVYASEAFLYMTGYSNAEVLG
RNCRFLQSPDGMVKPKSTRKYVDSNTINTMRKAIDRNAEVQVEVVNFKKNGQRFVNFLTMIPVR
DETGEYRYSMGFQCETEGGSRSVSKGEEDNMAIIKEFMRFKVHMEGSVNGHEFEIEGEGEGRPY
EGTQTAKLKVTKGGPLPFAWDILSPQFMYGSKAYVKHPADIPDYLKLSFPEGFKWERVMNFEDG
GVVTVTQDSSLQDGEFIYKVKLRGTNFPSDGPVMQKKTMGWEASSERMYPEDGALKGEIKQRLK
LKDGGHYDAEVKTTYKAKKPVQLPGAYNVNIKLDITSHNEDYTIVEQYERAEGRHSTGGMDELY
KPGNPRLQVDEQKLISEEDLNAVGQDTQEVIVVPHSLPFKVVVISAILALVVLTIISLIILIML
WQKKPR

pDisplay pMag GFP TM

DNA sequence 5’ to 3’

TTGGTACCGAGCTCGGATCCACTAGTAACGGCCGCCAGTGTGCTGGAATTCGGCTTGGGGATAT
CCACCATGGAGACAGACACACTCCTGCTATGGGTACTGCTGCTCTGGGTTCCAGGTTCCACTGG
TGACTATCCATATGATGTTCCAGATTATGCTGGGGCCCAGCCGGCCATGCACACACTATATGCT
CCCGGAGGGTATGATATAATGGGATACCTACGTCAAATACGCAACCGTCCGAACCCGCAAGTGG
AGCTGGGCCCGGTGGACACCAGCTGCGCGCTGATCCTGTGCGACCTGAAGCAGAAAGATACCCC
GATTGTGTACGCGAGCGAGGCGTTCCTGTACATGACCGGTTATAGCAACGCGGAAGTTCTGGGC
CGTAACTGCCGTTTTCTGCAAAGCCCGGATGGTATGGTGAAGCCGAAAAGCACCCGTAAGTATG
TTGACAGCAACACCATCAACACCATGCGTAAAGCGATCGATCGTAACGCGGAAGTGCAGGTTGA
AGTGGTTAACTTCAAGAAAAACGGCCAACGTTTCGTGAACTTTCTGACCATGATTCCGGTTCGT
GATGAGACCGGCGAATATCGTTATAGCATGGGTTTTCAATGCGAGACCGAAGGCGGTAGCAGAT
CTGTGAGCAAGGGCGAGGAGCTGTTCACCGGGGTGGTGCCCATCCTGGTCGAGCTGGACGGCGA
CGTAAACGGCCACAAGTTCAGCGTGTCCGGCGAGGGCGAGGGCGATGCCACCTACGGCAAGCTG
ACCCTGAAGTTCATCTGCACCACCGGCAAGCTGCCCGTGCCCTGGCCCACCCTCGTGACCACCC
TGACCTACGGCGTGCAGTGCTTCAGCCGCTACCCCGACCACATGAAGCAGCACGACTTCTTCAA
GTCCGCCATGCCCGAAGGCTACGTCCAGGAGCGCACCATCTTCTTCAAGGACGACGGCAACTAC
AAGACCCGCGCCGAGGTGAAGTTCGAGGGCGACACCCTGGTGAACCGCATCGAGCTGAAGGGCA
TCGACTTCAAGGAGGACGGCAACATCCTGGGGCACAAGCTGGAGTACAACTACAACAGCCACAA
CGTCTATATCATGGCCGACAAGCAGAAGAACGGCATCAAGGTGAACTTCAAGATCCGCCACAAC
ATCGAGGACGGCAGCGTGCAGCTCGCCGACCACTACCAGCAGAACACCCCCATCGGCGACGGCC
CCGTGCTGCTGCCCGACAACCACTACCTGAGCACCCAGTCCGCCCTGAGCAAAGACCCCAACGA
GAAGCGCGATCACATGGTCCTGCTGGAGTTCGTGACCGCCGCCGGGATCACTCTCGGCATGGAC
GAGCTGTATAAGGGTAAAAAGAAGAAAAAGAAGTCAAAGACAAAGTGTGTAATTATGACCCGGG
ATCCGCGGCTGCAGGTCGACGAACAAAAACTCATCTCAGAAGAGGATCTGAATGCTGTGGGCCA
GGACACGCAGGAGGTCATCGTGGTGCCACACTCCTTGCCCTTTAAGGTGGTGGTGATCTCAGCC
ATCCTGGCCCTGGTGGTGCTCACCATCATCTCCCTTATCATCCTCATCATGCTTTGGCAGAAGA
AGCCACGTTAG

Amino acid sequence

MVPSSDPLVTAASVLEFGLGISTMETDTLLLWVLLLWVPGSTGDYPYDVPDYAGAQPAMHTLYA
PGGYDIMGYLRQIRNRPNPQVELGPVDTSCALILCDLKQKDTPIVYASEAFLYMTGYSNAEVLG
RNCRFLQSPDGMVKPKSTRKYVDSNTINTMRKAIDRNAEVQVEVVNFKKNGQRFVNFLTMIPVR

DETGEYRYSMGFQCETEGGSRSVSKGEELFTGVVPILVELDGDVNGHKFSVSGEGEGDATYGKL
TLKFICTTGKLPVPWPTLVTTLTYGVQCFSRYPDHMKQHDFFKSAMPEGYVQERTIFFKDDGNY
KTRAEVKFEGDTLVNRIELKGIDFKEDGNILGHKLEYNYNSHNVYIMADKQKNGIKVNFKIRHN
IEDGSVQLADHYQQNTPIGDGPVLLPDNHYLSTQSALSKDPNEKRDHMVLLEFVTAAGITLGMD
ELYKGKKKKKKSKTKCVIMTRDPRLQVDEQKLISEEDLNAVGQDTQEVIVVPHSLPFKVVVISA
ILALVVLTIISLIILIMLWQKKPR

pDisplay nMagHigh mCherry TM

DNA sequence 5’ to 3’

TTGGTACCGAGCTCGGATCCACTAGTAACGGCCGCCAGTGTGCTGGAATTCGGCTTGGGGATAT
CCACCATGGAGACAGACACACTCCTGCTATGGGTACTGCTGCTCTGGGTTCCAGGTTCCACTGG
TGACTATCCATATGATGTTCCAGATTATGCTGGGGCCCAGCCGGCCATGCACACACTATATGCT
CCCGGAGGGTATGATATAATGGGATACCTAGATCAAATAGGCAACCGTCCGAACCCGCAAGTGG
AGCTGGGCCCGGTGGACACCAGCTGCGCGCTGATCCTGTGCGACCTGAAGCAGAAAGATACCCC
GATTGTGTACGCGAGCGAGGCGTTCCTGTACATGACCGGTTATAGCAACGCGGAAGTTCTGGGC
CGTAACTGCCGTTTTCTGCAAAGCCCGGATGGTATGGTGAAGCCGAAAAGCACCCGTAAGTATG
TTGACAGCAACACCATCAACACCATTCGTAAAGCGATCGATCGTAACGCGGAAGTGCAGGTTGA
AGTGGTTAACTTCAAGAAAAACGGCCAACGTTTCGTGAACTTTCTGACCATCATTCCGGTTCGT
GATGAGACCGGCGAATATCGTTATAGCATGGGTTTTCAATGCGAGACCGAAGGCGGTAGCAGAT
CTGTGAGCAAGGGCGAGGAGGATAACATGGCCATCATCAAGGAGTTCATGCGCTTCAAGGTGCA
CATGGAGGGCTCCGTGAACGGCCACGAGTTCGAGATCGAGGGCGAGGGCGAGGGCCGCCCCTAC
GAGGGCACCCAGACCGCCAAGCTGAAGGTGACCAAGGGTGGCCCCCTGCCCTTCGCCTGGGACA
TCCTGTCCCCTCAGTTCATGTACGGCTCCAAGGCCTACGTGAAGCACCCCGCCGACATCCCCGA
CTACTTGAAGCTGTCCTTCCCCGAGGGCTTCAAGTGGGAGCGCGTGATGAACTTCGAGGACGGC
GGCGTGGTGACCGTGACCCAGGACTCCTCCCTGCAGGACGGCGAGTTCATCTACAAGGTGAAGC
TGCGCGGCACCAACTTCCCCTCCGACGGCCCCGTAATGCAGAAGAAGACCATGGGCTGGGAGGC
CTCCTCCGAGCGGATGTACCCCGAGGACGGCGCCCTGAAGGGCGAGATCAAGCAGAGGCTGAAG
CTGAAGGACGGCGGCCACTACGACGCTGAGGTCAAGACCACCTACAAGGCCAAGAAGCCCGTGC
AGCTGCCCGGCGCCTACAACGTCAACATCAAGTTGGACATCACCTCCCACAACGAGGACTACAC
CATCGTGGAACAGTACGAACGCGCCGAGGGCCGCCACTCCACCGGCGGCATGGACGAGCTGTAC
AAGCCCGGGAATCCGCGGCTGCAGGTCGACGAACAAAAACTCATCTCAGAAGAGGATCTGAATG
CTGTGGGCCAGGACACGCAGGAGGTCATCGTGGTGCCACACTCCTTGCCCTTTAAGGTGGTGGT
GATCTCAGCCATCCTGGCCCTGGTGGTGCTCACCATCATCTCCCTTATCATCCTCATCATGCTT
TGGCAGAAGAAGCCACGTTAG

Amino acid sequence

MVPSSDPLVTAASVLEFGLGISTMETDTLLLWVLLLWVPGSTGDYPYDVPDYAGAQPAMHTLYA
PGGYDIMGYLDQIGNRPNPQVELGPVDTSCALILCDLKQKDTPIVYASEAFLYMTGYSNAEVLG
RNCRFLQSPDGMVKPKSTRKYVDSNTINTIRKAIDRNAEVQVEVVNFKKNGQRFVNFLTIIPVR
DETGEYRYSMGFQCETEGGSRSVSKGEEDNMAIIKEFMRFKVHMEGSVNGHEFEIEGEGEGRPY
EGTQTAKLKVTKGGPLPFAWDILSPQFMYGSKAYVKHPADIPDYLKLSFPEGFKWERVMNFEDG
GVVTVTQDSSLQDGEFIYKVKLRGTNFPSDGPVMQKKTMGWEASSERMYPEDGALKGEIKQRLK
LKDGGHYDAEVKTTYKAKKPVQLPGAYNVNIKLDITSHNEDYTIVEQYERAEGRHSTGGMDELY
KPGNPRLQVDEQKLISEEDLNAVGQDTQEVIVVPHSLPFKVVVISAILALVVLTIISLIILIML
WQKKPR

pDisplay pMagHigh GFP TM

DNA sequence 5’ to 3’

TTGGTACCGAGCTCGGATCCACTAGTAACGGCCGCCAGTGTGCTGGAATTCGGCTTGGGGATAT
CCACCATGGAGACAGACACACTCCTGCTATGGGTACTGCTGCTCTGGGTTCCAGGTTCCACTGG
TGACTATCCATATGATGTTCCAGATTATGCTGGGGCCCAGCCGGCCATGCACACACTATATGCT
CCCGGAGGGTATGATATAATGGGATACCTACGTCAAATACGCAACCGTCCGAACCCGCAAGTGG
AGCTGGGCCCGGTGGACACCAGCTGCGCGCTGATCCTGTGCGACCTGAAGCAGAAAGATACCCC
GATTGTGTACGCGAGCGAGGCGTTCCTGTACATGACCGGTTATAGCAACGCGGAAGTTCTGGGC
CGTAACTGCCGTTTTCTGCAAAGCCCGGATGGTATGGTGAAGCCGAAAAGCACCCGTAAGTATG
TTGACAGCAACACCATCAACACCATTCGTAAAGCGATCGATCGTAACGCGGAAGTGCAGGTTGA
AGTGGTTAACTTCAAGAAAAACGGCCAACGTTTCGTGAACTTTCTGACCATCATTCCGGTTCGT
GATGAGACCGGCGAATATCGTTATAGCATGGGTTTTCAATGCGAGACCGAAGGCGGTAGCAGAT
CTGTGAGCAAGGGCGAGGAGCTGTTCACCGGGGTGGTGCCCATCCTGGTCGAGCTGGACGGCGA
CGTAAACGGCCACAAGTTCAGCGTGTCCGGCGAGGGCGAGGGCGATGCCACCTACGGCAAGCTG
ACCCTGAAGTTCATCTGCACCACCGGCAAGCTGCCCGTGCCCTGGCCCACCCTCGTGACCACCC
TGACCTACGGCGTGCAGTGCTTCAGCCGCTACCCCGACCACATGAAGCAGCACGACTTCTTCAA
GTCCGCCATGCCCGAAGGCTACGTCCAGGAGCGCACCATCTTCTTCAAGGACGACGGCAACTAC
AAGACCCGCGCCGAGGTGAAGTTCGAGGGCGACACCCTGGTGAACCGCATCGAGCTGAAGGGCA
TCGACTTCAAGGAGGACGGCAACATCCTGGGGCACAAGCTGGAGTACAACTACAACAGCCACAA
CGTCTATATCATGGCCGACAAGCAGAAGAACGGCATCAAGGTGAACTTCAAGATCCGCCACAAC
ATCGAGGACGGCAGCGTGCAGCTCGCCGACCACTACCAGCAGAACACCCCCATCGGCGACGGCC
CCGTGCTGCTGCCCGACAACCACTACCTGAGCACCCAGTCCGCCCTGAGCAAAGACCCCAACGA

GAAGCGCGATCACATGGTCCTGCTGGAGTTCGTGACCGCCGCCGGGATCACTCTCGGCATGGAC
GAGCTGTATAAGGGTAAAAAGAAGAAAAAGAAGTCAAAGACAAAGTGTGTAATTATGACCCGGG
ATCCGCGGCTGCAGGTCGACGAACAAAAACTCATCTCAGAAGAGGATCTGAATGCTGTGGGCCA
GGACACGCAGGAGGTCATCGTGGTGCCACACTCCTTGCCCTTTAAGGTGGTGGTGATCTCAGCC
ATCCTGGCCCTGGTGGTGCTCACCATCATCTCCCTTATCATCCTCATCATGCTTTGGCAGAAGA
AGCCACGTTAG

Amino acid sequence

MVPSSDPLVTAASVLEFGLGISTMETDTLLLWVLLLWVPGSTGDYPYDVPDYAGAQPAMHTLYA
PGGYDIMGYLRQIRNRPNPQVELGPVDTSCALILCDLKQKDTPIVYASEAFLYMTGYSNAEVLG
RNCRFLQSPDGMVKPKSTRKYVDSNTINTIRKAIDRNAEVQVEVVNFKKNGQRFVNFLTIIPVR
DETGEYRYSMGFQCETEGGSRSVSKGEELFTGVVPILVELDGDVNGHKFSVSGEGEGDATYGKL
TLKFICTTGKLPVPWPTLVTTLTYGVQCFSRYPDHMKQHDFFKSAMPEGYVQERTIFFKDDGNY
KTRAEVKFEGDTLVNRIELKGIDFKEDGNILGHKLEYNYNSHNVYIMADKQKNGIKVNFKIRHN
IEDGSVQLADHYQQNTPIGDGPVLLPDNHYLSTQSALSKDPNEKRDHMVLLEFVTAAGITLGMD
ELYKGKKKKKKSKTKCVIMTRDPRLQVDEQKLISEEDLNAVGQDTQEVIVVPHSLPFKVVVISA
ILALVVLTIISLIILIMLWQK